500 million years of punctuated addition of juvenile crust during extension in the Goochland Terrane, central Appalachian Piedmont Province

Aaron J. Martin[1], Irene Kadel-Harder[2], Brent E. Owens[3], Kouki Kitajima[4], Scott D. Samson[5], Sanjeet K. Verma[1]

[1]División de Geociencias Aplicadas, IPICYT, CP 78216, San Luis Potosí, S.L.P., MEXICO

Martin is corresponding author. E-mail: aaron.martin@ipicyt.edu.mx

[2]Department of Geological and Atmospheric Sciences, Iowa State University, Ames, IA 50011, USA

[3]Department of Geology, College of William and Mary, Williamsburg, VA 23187, USA

[4]Department of Geoscience, The University of Wisconsin, Madison, WI 53706, USA

[5]Department of Earth Sciences, Syracuse University, Syracuse, NY 13244, USA

Total words in main text: 15020

0. ABSTRACT

The Goochland Terrane is an enigmatic crustal block in the Appalachian Piedmont Province of central Virginia, USA. Sparse exposures of terminal Mesoproterozoic and late Neoproterozoic igneous rocks in the central Goochland Terrane offer the opportunity to investigate both the continental affinity of the terrane during the Proterozoic Eon and the timing and mechanisms of crustal growth. We apply multiple geochemical tools to these rocks: tectonic discrimination using whole rock major and trace element abundances; whole rock Sm-Nd isotopes; O, U-Pb, and Lu-Hf isotope analyses of spots in zircon; and measurement of O isotopes in multi-grain quartz separates. Eruption of the Sabot Amphibolite protolith is difficult to date, but we tentatively assign an age of 552±11 Ma. Goochland Terrane continental crust first separated from the mantle prior to ca. 1050-1010 Ma intrusion of the Montpelier Anorthosite and the State Farm Gneiss protolith. The granitic magma that became the State Farm Gneiss protolith could have been derived entirely from partial melting of this initial Goochland Terrane crust. In contrast, the magmas that became the Montpelier Anorthosite, Neoproterozoic granitoid, and the Sabot Amphibolite were mixtures of mantle melt and preexisting Goochland Terrane crust. This production of juvenile continental crust occurred during continental extension and, eventually, rifting. The timing and compositions of terminal Mesoproterozoic magmatism in the Goochland Terrane closely match those in the nearby Blue Ridge Province. Although the compositions of the Neoproterozoic magmas in the two regions are similar, intrusion and possibly eruption occurred about 10 M.y. later in the Goochland Terrane.

KEYWORDS

juvenile continental crust; extension-related magmatism; zircon; isotopes; Proterozoic Eon

1. INTRODUCTION

The timing of and tectonic setting during production of continental crust remain important research issues globally despite decades of post-plate tectonics revolution investigation of these subjects (Armstrong, 1968; Moorbath, 1975; Reymer and Schubert, 1986; Patchett and Chase, 2002; Stern and Scholl, 2010; Condie et al., 2011; Cawood et al., 2013). Critical questions include the following. What is the relative importance of generation of continental crust in different tectonic settings such as magmatic arcs or extensional domains (e.g., Stern and Scholl, 2010)? Both globally and in any one location, is continental crust created continuously or episodically (e.g., Patchett and Chase, 2002; Condie et al., 2011)?

The Goochland Terrane is a fault-bounded crustal block in the Appalachian Piedmont Province of Virginia, eastern USA (Figs. 1, 2). Unlike younger neighboring rocks, geologists commonly interpret the Goochland Terrane as a sliver of Mesoproterozoic continental crust because the oldest exposed rocks in the terrane intruded near the end of this era (Aleinikoff et al., 1996; Owens and Tucker, 2003) and because whole rock Nd isotope model ages for extraction of these intrusive rocks from the depleted mantle are approximately 1400 Ma (Owens and Samson, 2004). Nearly all of the Mesoproterozoic and Neoproterozoic rocks in the Goochland Terrane are meta-igneous, affording us an opportunity to investigate the timing and mechanisms of pre-Cambrian growth of this fragment of continental crust.

In this paper we use whole rock major and trace element abundances combined with oxygen, samarium-neodymium, lutetium-hafnium, and uranium-lead isotope analyses to elucidate magmatic sources of Goochland Terrane continental crust. We then discuss implications for the magmatic and tectonic development of the Goochland Terrane, especially the mechanisms and timing of addition of continental crust.

2. GEOLOGIC SETTING

Geologists use distinctions originally based on physiography to divide the central and southern Appalachian Orogen into tectonic provinces (Hatcher, 1989). From west to east these include the Blue Ridge, Piedmont, and Coastal Plain provinces (Fig. 1B). The Blue Ridge Province consists of Middle and Late Mesoproterozoic intrusive rocks that formed and were metamorphosed due to amalgamation of Rodinia as well as Neoproterozoic felsic intrusions and sedimentary and volcanic strata formed during breakup of Rodinia (Aleinikoff et al., 1995; Tollo et al., 2004; 2017). The Goochland Terrane is part of the Piedmont Province. Dominated by metasedimentary rocks, the Piedmont Province is the formerly deepest and most outboard part of the Paleozoic Appalachian Orogen currently exposed (Hibbard et al., 2006). The Neoproterozoic and Paleozoic Piedmont Province rocks constitute a collage of fault-bounded terranes of varying origin (Horton et al., 1989). The rocks in some terranes, such as the Westminster Terrane, intruded or were deposited on the eastern edge of Laurentia (Martin et al., 2015). Others, such as the rocks that compose Carolinia, intruded and were deposited on the periphery of Gondwana (Pollock et al., 2012). The Goochland Terrane is now located at the northeastern end of Carolinia (Fig. 1A), and several authors tentatively concluded that like Carolinia, the Goochland Terrane may have been exotic to Laurentia prior to possible accretion during the Paleozoic Era (Horton et al., 1989; Rankin, 1994; see also Hibbard and Samson, 1995; Keppie et al., 1996). The arguments in favor of an exotic origin were differences in structure and stratigraphy between the Goochland Terrane and known

Laurentian outliers in the Piedmont Province. In contrast, Farrar (1984), Aleinikoff et al. (1996), and Glover et al. (1997) linked the Goochland Terrane to Laurentia during Proterozoic and Paleozoic time. Overlapping compositions and intrusion ages of latest Mesoproterozoic anorthosite and felsic rocks in the Goochland Terrane and the Blue Ridge Province, as well as the comparable latest Mesoproterozoic metamorphism of the rocks in these two regions, formed the bases for this linkage. Bartholomew and Tollo (2004) likewise concluded that the Goochland Terrane was part of Laurentia during Proterozoic time, placing the Goochland Terrane farther north than its current position during pre-Cambrian time because of similar Neoproterozoic igneous rocks in the Goochland Terrane on the one hand and Pennsylvania, New Jersey, and New York on the other.

The oldest rock units in the Goochland Terrane are a granitic gneiss that intruded at ca. 1050-1010 Ma, called the State Farm Gneiss, and the 1045±10 Ma Montpelier Anorthosite (Fig. 2; Table 1; Aleinikoff et al., 1996; Owens and Tucker, 2003). The composition of the Montpelier Anorthosite is unusual compared to other massif anorthosite on Earth in three ways: (1) Montpelier is one of the two most potassic anorthosite bodies found on Earth, (2) it is the only known anorthosite in which the barium concentration exceeds the strontium concentration, and (3) quartz is common (Owens and Dymek, 2016). A suite of granitic magmas intruded the State Farm Gneiss at ca. 660 to 580 Ma (Owens and Tucker, 2003). This suite has not been formally named, so we follow Owens and Tucker (2003) in referring to these rocks as Neoproterozoic granitoid.

The Sabot Amphibolite mostly crops out near the State Farm Gneiss (Fig. 2). Dominated by meta-mafic rocks with minor intercalated meta-felsic layers, the Sabot Amphibolite nowhere intrudes the State Farm Gneiss; in individual outcrops the Sabot Amphibolite rests on the Mesoproterozoic gneiss with apparent concordance between the compositional layering in the State Farm Gneiss and the base of the Sabot Amphibolite. Glover (1989) reported a low-angle discordance between the base of the Sabot Amphibolite and compositional layering in the underlying State Farm Gneiss at the regional scale. Weakly-deformed pegmatite dikes intruded both the State Farm Gneiss and the Sabot Amphibolite, but the Sabot Amphibolite does not host other intrusions. These outcrop- and map-scale observations lead us to the interpretation that the Sabot Amphibolite is a meta-volcanic sequence deposited atop the State Farm Gneiss (see also Goodwin, 1970). The eruption age is difficult to determine both because meta-basaltic rocks typically yield little zircon related to eruption and also due to the intense deformation and metamorphism of the Sabot Amphibolite. The eruption age was unknown prior to the current study but here we suggest it may be ca. 550 Ma based on U/Pb isotopic dating of zircon from an intercalated felsic layer.

The most widely exposed unit in the Goochland Terrane is the Maidens Gneiss, which consists of intercalated sedimentary and igneous rocks, metamorphosed to granulite facies followed by amphibolite facies (Farrar, 1984). The igneous crystallization age of at least some of the Maidens Gneiss igneous rocks is ca. 400 Ma (Owens et al., 2010). There are many small amphibolite bodies within the area nominally mapped as Maidens Gneiss in Figure 2. We take these amphibolite bodies to be structurally dismembered parts of the Sabot Amphibolite based on their locations close to the Sabot Amphibolite and the Mesoproterozoic rocks as well as their compositional similarity to the Sabot Amphibolite.

3. METHODS

3.1 Sabot Amphibolite whole rock major and trace element abundances

Owens collected all samples. Major, minor, and some trace element abundances were analyzed by X-ray fluorescence at Washington University in Saint Louis using methods described by Couture et al. (1993) and Couture and Dymek (1996) (marked in Table S1). Other trace element abundances were analyzed by instrumental neutron activation analysis at Washington University following the techniques described by Korotev (1987). A few trace elements in two samples were analyzed by inductively coupled plasma mass spectrometry at Activation Laboratories, Ltd., Ontario, Canada (marked in Table S1). We use cut-offs of 45, 52, and 63 weight percent SiO_2 to classify rocks as ultramafic, mafic, intermediate, or felsic.

3.2 Sabot Amphibolite whole rock neodymium isotopes

Owens collected all samples except sample 1994, which was collected by Samson. Samples 1994 and SA-001 were collected from mafic parts of the Sabot Amphibolite, which also contains minor intercalated felsic layers at this outcrop. Nd and Sm isotope analyses were performed at Syracuse University following the procedures in Samson et al. (1995) with the modification that the ^{149}Sm-^{150}Nd tracer solution was added to the powdered sample prior to dissolution. The measured ^{143}Nd/^{144}Nd ratio was corrected for mass bias using ^{146}Nd/^{144}Nd=0.7219. The uncertainty on the initial εNd value of a rock measured in the Syracuse laboratory is better than 0.4 epsilon units (Samson et al., 1995). We used the isotopic compositions of the chondritic uniform reservoir from Bouvier et al. (2008) to calculate εNd values. Depleted mantle values were taken from DePaolo (1981).

3.3 Zircon sample collection and processing

Martin collected all samples except Mont1, which was collected by Owens. We separated and mounted zircon in the laboratories in the Department of Geology at the University of Maryland. Zircon was isolated from each sample by first crushing the rock using a mortar and pestle, then removing the silt- and clay-size grains by hand-panning in water, removing magnetic grains with a Frantz magnetic barrier separator, and removing less-dense grains in methylene iodide. We picked zircon crystals by hand, then cast the grains in an epoxy disk together with shards or loose grains of standard zircon crystals. After the epoxy hardened, we ground and polished the disks by hand to expose the interiors of the grains. Prior to isotope analysis, the grains were imaged using backscattered electrons and cathodoluminescence in the JEOL JXA-8900R electron probe microanalyzer at the University of Maryland. The images were used to avoid multiple cathodoluminescence zones, cracks, and inclusions during selection of spots for isotope analysis. We report all uncertainties at the 2-sigma level.

3.4 Oxygen isotopes in spots in zircon

After polishing and imaging the zircon grains, we analyzed oxygen isotopes in spots in the zircon using the CAMECA IMS 1280 secondary ion mass spectrometer (SIMS) housed in the WiscSIMS laboratory at the University of Wisconsin Madison. The analyses were conducted over two consecutive days. We followed the mount preparation and analytical procedures described in Kita et al. (2009), Valley and Kita (2009), and Wang et al. (2014). The primary beam consisted of Cs^{+} ions focused to a beam diameter of 15 μm. Secondary ions for ^{16}O, ^{18}O, and $^{16}O^{1}H$ were collected simultaneously by three Faraday cup detectors. Ratios of $^{16}O^{1}H/^{16}O$ (hereafter called OH/O) in the sample zircon were corrected for background by subtracting the measured ratio in bracketing standard zircon, which was assumed to be anhydrous (Wang et al., 2014). Zircon standard KIM-5, with a $\delta^{18}O$ value of 5.09±0.12‰ VSMOW (Valley, 2003), was included in the epoxy mounts with the Goochland Terrane zircon. We corrected for instrumental mass fractionation by bracketing four analyses of spots in KIM-5 before and after every fifteen analyses of spots in Goochland Terrane zircon. Reported precisions are the two standard deviation values around the means of the measured $\delta^{18}O$ values of the eight bracketing analyses of KIM-5 for each block of fifteen Goochland Terrane analyses. We report and discuss all results relative to VSMOW.

3.5 Uranium/lead isotope dating of spots in zircon from Sabot Amphibolite sample Sabot1

Zircon from a felsic layer in the Sabot Amphibolite, extracted from sample Sabot1, was analyzed in the Arizona LaserChron Center at the University of Arizona to determine the eruption age of this meta-volcanic unit (Fig. 2; Table 1). Gehrels and Pecha (2014) discussed the analytical methods in detail; here we provide a brief summary. Material was ablated from the polished surface of zircon crystals using a Photon Machines Analyte G2 Excimer laser with a beam diameter of 10 μm. Despite declining analytical precision with decreasing laser beam diameter, we used a 10 μm-diameter spot to permit targeting distinct cores or rims with minimal overlap of different cathodoluminescence domains and to avoid inclusions and cracks. A flow of helium carried the ablated zircon into the plasma source of a Nu high resolution inductively coupled plasma mass spectrometer, which was fitted with a flight tube wide enough to measure uranium, thorium, and lead isotopes simultaneously. All measurements were made in static mode using discrete dynode ion counters. Each analysis comprised three parts: background measurement via a 15-second integration on peaks with the laser off, fifteen 1-second integrations with the laser firing, and a 30-second delay to purge the previous sample. The depths of the resulting ablation pits were approximately 15 µm.

Data reduction was performed offline using an Excel program written at the Arizona LaserChron Center. A common lead correction was applied to the ^{204}Pb signal assuming an initial lead composition from Stacey and Kramers (1975). We corrected for mass fractionation of isotopes during analysis using bracketing analyses of standard zircon "Sri Lanka," which has an accepted age of 563.5±3.2 Ma (Gehrels et al., 2008). We calculated concentrations of uranium and thorium in the sample zircon based on analyses of the Sri Lanka standard zircon, which contains approximately 518 ppm uranium and 68 ppm thorium.

3.6 Uranium/lead and hafnium isotopes in spots in zircon from other samples

U/Pb and Hf isotopes in zircon from all samples except Sabot 1 were analyzed in the GeoAnalytical Lab at Washington State University using the laser ablation split stream technique (Table 1). Analyses took place during two separate sessions on two consecutive days. We followed the measurement and data reduction procedures detailed in Fisher et al. (2014), which we briefly summarize here. The polished surface of each zircon grain was ablated using a NewWave 213 nm Nd:YAG laser. The laser diameter was 40 µm for samples 511001, 511005, and Mont1 and 30 µm for samples 511004 and 512001. We also used a 30 µm beam for ten spots in zircon from sample 511001 and six spots in zircon from sample 511005 (marked in Table S2). The laser spots were centered on the pits created by the oxygen isotope analyses. The ablated zircon was carried out of the sample cell in a stream of He, which was then split into two separate paths. One stream entered a

ThermoScientific Element2 single collector high resolution inductively coupled plasma mass spectrometer for measurement of uranium and lead isotopes. The second stream passed into a ThermoScientific Neptune multi-collector inductively coupled plasma mass spectrometer for measurement of lutetium, ytterbium, and hafnium isotopes. Analyses of shards or loose grains of at least two different zircon standards bracketed every 12 analyses of unknown zircon.

Each analysis consisted of background measurement on peaks for 30 s with the laser off followed by 65 s of ablation. The first 6 s of ablation were marked by increasing signal intensities, so the first 6 s of data were not included in the U/Pb date calculation. The next 30 s of data were used to calculate the U/Pb dates. U/Pb data were reduced offline using an in-house Excel program. Repeated measurements of reference zircon R33 and Temora yielded concordia ages of 420±5 and 422±6 Ma, respectively (Table S2, Fig. S1), within uncertainty of the accepted crystallization ages (Black et al., 2004). Hf data were reduced offline using Iolite software following the methods described by Fisher et al. (2014). We removed from further consideration any Hf analysis with a duration of less than 20 s. Repeated measurements of reference zircon FC1, R33, and Temora produced mean $^{176}Hf/^{177}Hf$ ratios of 0.282163±53, 0.282754±37, and 0.282663±41, respectively (Table S2), all of which are within uncertainty of the accepted values (Woodhead and Hergt, 2005; Fisher et al., 2014).

We calculated the ratio $^{176}Hf/^{177}Hf$ at the interpreted time of zircon crystallization using the measured and corrected $^{176}Hf/^{177}Hf$ and $^{176}Lu/^{177}Hf$ values and the ^{176}Lu decay constant of 1.867×10^{-11} year^{-1} (Scherer et al., 2001; Soderlund et al., 2004). Epsilon Hf values were calculated using the isotopic compositions of the chondritic uniform reservoir given by Bouvier et al. (2008). The depleted mantle reservoir for hafnium follows a linear evolution starting with separation from the chondritic uniform reservoir at 3800 Ma to an εHf value of +16 today (Vervoort et al., 2016). Present-day values for the depleted mantle reservoir are $^{176}Hf/^{177}Hf$ = 0.283238 and $^{176}Lu/^{177}Hf$ = 0.039755 (Goodge et al., 2017).

3.7 Uranium/lead data analysis and presentation

We prepared concordia and weighted mean diagrams using Isoplot version 4.15 (Ludwig, 2008). The weighted means were calculated with weighting according to the square of the internal uncertainties. The total uncertainty on the determination of the eruption age of the protolith for sample Sabot1 was calculated by quadratic addition of the measurement (internal) and systematic (external) uncertainties.

3.8 Oxygen isotopes in multi-grain quartz separates

In this study, we compare the oxygen isotope composition of coexisting quartz and zircon to test for post-intrusive or post-eruptive isotopic alteration of the quartz. We isolated quartz from the portion of each sample that floated in methylene iodide during zircon separation. These low-density grains were mostly quartz and plagioclase, which are difficult to distinguish optically. To make the quartz and plagioclase appear different under the stereographic microscope, we bathed the separate in concentrated tetrafluoroboric acid at room temperature for ten minutes, which did not affect the appearance of the quartz but caused an opaque white crust to grow on the surfaces of the plagioclase. We then picked quartz grains by hand. Sample Mont1 did not yield sufficient quartz for analysis.

We analyzed oxygen isotopes in approximately 1-2 mg of quartz from each of the four remaining samples at the University of Wisconsin Madison using the rapid heating, defocused beam method for laser fluorination described by Spicuzza et al. (1998). This technique utilizes a defocused CO_2 laser beam to heat the quartz aliquot in an atmosphere of BrF_5. Oxygen isotopes were analyzed with a Finnigan MAT 251 mass spectrometer. Repeated analyses of the UWG-2 garnet standard before and after the analyses of the Goochland Terrane quartz were used to correct the raw quartz analyses using the accepted UWG-2 $\delta^{18}O$ value of 5.8‰ SMOW (Valley et al., 1995). The two standard deviation value around the mean of the eight analyses of UWG-2 throughout the single day of analysis of Goochland Terrane quartz was ±0.17‰. We take this value as the uncertainty of the quartz O isotope measurements (Table S3). We report and discuss all results relative to VSMOW.

4. RESULTS

4.1 Geochemical classification and tectonic setting

Figure 3 shows thin section photomicrographs of each sample. Table S1 contains element abundances for the Sabot Amphibolite samples and figure 4 shows that the mafic Sabot Amphibolite samples are mostly basalt and basaltic andesite (57-42 weight percent SiO_2), whereas the felsic sample is rhyolite (75 weight percent SiO_2). Owens and Tucker (2003) found that the composition of the State Farm Gneiss ranges from granite to quartz monzodiorite (77-56 weight percent SiO_2) and the compositions of the Neoproterozoic granitoid range from granite to syenite (77-60 weight percent SiO_2).

We used the discrimination schemes described in Agrawal et al. (2008), Verma and Verma (2013), and Verma et al. (2013) to help provide information about the tectonic setting during generation of these magmas. Most of the felsic and intermediate samples from the State Farm Gneiss plot in the within-plate field (combined continental rift and ocean island field), although in some discrimination diagrams some samples fall in the combined island arc and continental arc field (Tables S4, S5; Fig. 5). Most Neoproterozoic granitoid samples, both felsic and intermediate, plot in the combined continental rift and ocean island field (Tables S6, S7; Fig. 5). The mafic samples from the Sabot Amphibolite mostly fall in the mid-ocean ridge field; a few samples plot in the continental rift field (Table S8; Fig. 5C). Figure 5 shows only three of the many possible discrimination diagrams; tables S4-S8 tabulate the results of all the discriminations.

4.2 Sample Sabot1 field relations and uranium/lead isotopic dates in spots in zircon

Near the location of samples 512001 and Sabot1, multiple felsic layers are intercalated with the more abundant mafic layers typical of the Sabot Amphibolite (Fig. 6). The felsic layers have thicknesses of 0.3-4 m whereas the mafic layers are 3-5 m thick. At least some of the felsic layers appear to be composites made up of thinner felsic layers with thicknesses of 5-10 cm (Fig. 6B). The contacts between the mafic and felsic layers are parallel to the foliation in the rocks; the felsic layers nowhere cut across the mafic layers. These contacts are sharp and planar at the mesoscopic scale seen in the field (Figs. 6A, 6B), but the contacts undulate at the microscopic scale in thin section (Fig. 6C). At the microscopic scale, some contacts show interfingering of layers with the two compositions (Fig. 6D).

The eruption age of the volcanic protolith of the Sabot Amphibolite was unknown prior to the current study, so our work on this unit first focused on determining the age of volcanic eruption via U/Pb dating of spots in zircon obtained from a felsic layer (sample Sabot1). Cathodoluminescence images of zircon revealed complex zoning in most grains, with most displaying different cathodoluminescence responses from core and rim domains (Fig. 7). In some grains, inclusions are more abundant in cores than rims (Fig. 7A). Figure

8 and Table S9 present the results of 35 spot analyses in 23 grains from sample Sabot1. Figure 9 shows that all analyses older than ca. 500 Ma came from zircon core domains and that grain cores mostly have lower U/Th ratios than grain rims. Figure 9 also shows that analyses that yielded $^{206}Pb/^{238}U$ dates younger than ca. 453 Ma ranged to higher U/Th ratios and had a higher mean U/Th ratio compared to older analyses.

4.3 Whole rock neodymium isotopes

Table S10 presents the results of the Sm-Nd isotope analyses of the Sabot Amphibolite whole rock samples. Figure 10 shows these data as well as the whole rock Nd isotope data from the older Proterozoic units in the Goochland Terrane (Owens and Samson, 2004). The εNd values for the Sabot Amphibolite at the time of eruption (550 Ma) ranged from +6.3 to +1.5. The two most positive Sabot samples fall within the range of values for the depleted mantle at 550 Ma, considering uncertainties. All the Sabot Amphibolite analyses yielded initial values more positive than the initial εNd values for the older Proterozoic rocks. Initial εNd values for the 1040 Ma Montpelier Anorthosite, 1030 Ma State Farm Gneiss, and 600 Ma Neoproterozoic granitoid were +1.1 to +0.7, +1.2 to -0.2, and +0.6 to -0.3, respectively. None of the initial εNd values from these older Proterozoic units were near depleted mantle values at the time of intrusion.

4.4 Uranium/lead and hafnium isotopes in spots in zircon

Tables S2 and S3 and Figures 11 and 12 present the results of the laser ablation split stream analyses of spots in zircon. Figure 13 shows images of zircon grains from each sample with $\delta^{18}O$ values, U/Pb dates, and εHf values from the indicated spots.

All analyzed zircon from Montpelier Anorthosite sample Mont1 had low uranium contents, from 53-10 ppm (see also Aleinikoff et al., 1996). Consequently, the ^{207}Pb signals during many of our analyses were insufficient to reliably determine crystallization dates, and we successfully determined dates from only five spots. All five analyses are strongly discordant, with Proterozoic $^{206}Pb/^{207}Pb$ dates and ca. 300 Ma $^{206}Pb/^{238}U$ dates (Fig. 11A; Tables S2, S3). εHf values at 1040 Ma, the approximate time of intrusion, ranged from +12.9 to +1.4 (Tables S2, S3; Fig. 12). The three most positive εHf values were near the depleted mantle value at 1040 Ma.

All but three analyses from State Farm Gneiss sample 511005 are concordant; the three discordant analyses plot only slightly off concordia (Tables S2, S3; Fig. 11B). Most of the analyses give dates between 1050 and 1000 Ma, near the published intrusion age of ca. 1050-1010 Ma (Owens and Tucker, 2003). Spot 30 in the core of grain big_20 is concordant and, at ca. 990 Ma, slightly younger than most other analyses. The U concentration and U/Th ratio of this grain are much higher than all other analyses from this sample. We interpret this crystal to be of metamorphic origin. We use 1030 Ma to calculate εHf values from all other spots; these values ranged from +2.7 to -1.5 at this time (Tables S2, S3; Fig. 12). These near-chondritic values were about 10 εHf units less than the depleted mantle value at 1030 Ma.

The U/Pb isotope data from Neoproterozoic granitoid sample 511004 define two age groups (Tables S2, S3; Fig. 11C). The first group consists of the two analyses from the core of grain 22, which plot near concordia and have $^{206}Pb/^{207}Pb$ dates of ca. 1130 and 1108 Ma. The U concentrations of these two spots are lower than the concentrations in all other analyzed grains from this sample. We interpret the core of grain 22 to be a xenocryst inherited from Late Mesoproterozoic igneous rocks such as the State Farm Gneiss. Owens and Tucker (2003) also argued for inheritance of Mesoproterozoic zircon in this granitoid body. The Montpelier Anorthosite is not a viable source for the zircon xenocryst because the sample 511004 grain 22 core U concentrations of 368 and 190 ppm are much higher than the U concentrations in zircon from the Montpelier Anorthosite. In contrast, the grain 22 core U contents are similar to those in zircon from the State Farm Gneiss. We use an age of 1035 Ma to calculate the εHf values for these two spots. The εHf values at 1035 Ma were +1.7 and +1.2, consistent with derivation from the State Farm Gneiss or a similar source. The second age group consists of all other analyses from this sample. Many of these analyses are concordant with dates between 680 and 620 Ma. Discordant analyses plot slightly off concordia with most $^{206}Pb/^{207}Pb$ dates between 700 and 620 Ma. Owens and Tucker (2003) interpreted the $^{206}Pb/^{207}Pb$ date of ca. 654 Ma from a single concordant zircon analysis from this granitoid body to date intrusion. Using this previous dating as a guide, we interpret all Group 2 analyses to result from zircon crystallization at ca. 654 Ma followed by minor lead loss from many of the grains. εHf values of these analyses at 650 Ma ranged from +6.0 to +0.8 (Fig. 12).

The U/Pb isotope data from Neoproterozoic granitoid sample 511001 similarly define two age groups (Tables S2, S3; Fig. 11D). The first group includes the three concordant analyses from three separate grains that yielded $^{206}Pb/^{207}Pb$ dates between 1091 and 1005 Ma. This group also contains the discordant analyses that yielded $^{206}Pb/^{207}Pb$ dates between 1062 and 730 Ma and $^{206}Pb/^{238}U$ dates between 696 and 577 Ma. Analyses of spots in the cores of grains big_5 and big_12 also are included in this group because outer parts of these grains have $^{206}Pb/^{207}Pb$ dates of 827 and 922 Ma, respectively. Similarly, we include analyses big_9_15, big_11_21, and big_14_27 in this group because neighboring spots in the same cathodoluminescence domains in the interiors of these grains have $^{206}Pb/^{207}Pb$ dates between 1062 and 730 Ma. Based on U/Pb isotope analyses of zircon from this granitoid body, Owens and Tucker (2003) interpreted a discordia upper intercept of ca. 1000 Ma to result from inheritance of Mesoproterozoic zircon and the lower intercept of 600 +7/-9 Ma to be the time of granitoid intrusion. Guided by this previous dating, we interpret Group 1 zircon to be xenocrysts inherited from Late Mesoproterozoic Goochland Terrane rocks. Nine of the 21 analyses in Group 1 have U contents between 60 and 22 ppm. These low concentrations overlap those of zircon in the Montpelier Anorthosite but are lower than the concentrations in zircon from the State Farm Gneiss, Neoproterozoic granitoid sample 511004, and the other zircon grains in sample 511001. We conclude that these low U grains were inherited from the Montpelier Anorthosite or a similar source whereas the higher U xenocrysts were inherited from the State Farm Gneiss or a similar source. εHf values of the Group 1 analyses at 1035 Ma ranged between +11.7 and +2.5, consistent with derivation from the Montpelier Anorthosite. εHf values more positive than +2.7 do not overlap the εHf values of State Farm Gneiss zircon. The remaining analyses comprise Age Group 2. These analyses are concordant or slightly discordant and have $^{206}Pb/^{207}Pb$ dates between 694 and 556 Ma. Based on the previous dating, we interpret Group 2 analyses to be zircon that crystallized at ca. 600 Ma. The εHf values at 600 Ma were +0.7 to -1.4 (Fig. 12).

Only one analysis from sample 512001, spot 18 in grain 14, yielded concordant dates near the Sabot Amphibolite protolith eruption age of 552±11 Ma (Tables S2, S3; Figs. 11E, 13I; see Section 5.1 for discussion of eruption age). At 90 ppm, this spot has the lowest U concentration of any spot measured in sample 512001. We interpret this part of grain 14 to be magmatic zircon that crystallized near the time of eruption of the Sabot Amphibolite protolith. The εHf value of this spot at 550 Ma was +8.8. The other analyses from sample 512001 fall into two groups as follows: (1) Discordant analyses with $^{206}Pb/^{207}Pb$ dates between ca. 626 and 557 Ma; and (2) Concordant analyses with dates between about 500 and 450 Ma. All but one spot in Group 1 have U/Th ratios between 6.9 and 1.1, whereas U/Th ratios in Group 2 zircon range as high as 37.6. We interpret Group 1 to be zircon that crystallized near the time of protolith eruption and then lost lead during ca. 450 Ma metamorphism. We take Group 2 to be metamorphic zircon (see Section 5.1 for discussion of the age of metamorphic zircon growth). εHf values for Group 1 zircon were +12.1 to +9.0 at 550 Ma.

4.5 Oxygen isotopes in zircon and quartz

Tables S3 and S11 and Figure 14 present our oxygen isotope data. Figure 13 shows images of zircon crystals from each sample along with oxygen isotope values for the indicated spots. There is a trend of lower $\delta^{18}O$ values in zircon from the three progressively younger groups of rocks (State Farm Gneiss, Neoproterozoic granitoid, Sabot Amphibolite; Fig. 14).

$\delta^{18}O$ values from Montpelier Anorthosite sample Mont1 zircon occupy the range +8.4 to +7.6‰ (Tables S3, S11). This sample did not yield sufficient quartz for analysis.

$\delta^{18}O$ values from State Farm Gneiss sample 511005 zircon range from +9.7 to +6.4‰ (Tables S3, S11). Two U/Pb isotopic analyses from this sample were more than 20% discordant (analyses big_7_9 and big_21_31) and spot big_20_30 was located in a metamorphic grain (Table S3; Fig. 11B). Excluding the values from these three spots as well as values from spots without U/Pb isotope data, most $\delta^{18}O$ values from sample 511005 zircon fall in the range +8.3 to +7.2‰ (Fig. 14). There are also three isotopically heavier outliers at +9.7, +9.0, and +8.7‰. The $\delta^{18}O$ value for the multi-grain quartz separate from sample 511005 was +9.0‰ (Table S3).

Analyses of zircon from Neoproterozoic granitoid sample 511004 yielded $\delta^{18}O$ values between +6.7 and +1.8‰ (Tables S3, S11). Removing xenocrystic grain 22, analyses more than 20% discordant, and spots without U/Pb isotope data leaves a still-large span from +6.4 to +1.8‰. The multi-grain quartz separate yielded a $\delta^{18}O$ value of +5.4‰ (Table S3).

Analyses of zircon from Neoproterozoic granitoid sample 511001 yielded $\delta^{18}O$ values between +8.3 and +6.2‰ (Tables S3, S11). Removing xenocrysts, analyses more than 20% discordant, and analyses without U/Pb isotope data from the same spot leaves a range between +6.8 and +6.2‰ (Fig. 14). The $\delta^{18}O$ value for the multi-grain quartz separate from this sample was +10.0‰ (Table S3).

All except three spots in zircon from Sabot Amphibolite felsic sample 512001 yielded $\delta^{18}O$ values between +9.5 and +7.2‰ (Tables S3, S11). The three exceptions are spots 18, 18b, and 18e in the interior of grain 14, which gave values of +5.6, +5.3, and +5.1‰, respectively (Tables S3, S11; Fig. 13I). The multi-grain quartz separate from sample 512001 yielded a $\delta^{18}O$ value of +12.3‰ (Table S3).

5. DISCUSSION

5.1 Eruption age of the Sabot Amphibolite protolith

Before discussing the zircon U-Pb isotope data, we consider the following three endmember interpretations of the contacts between the felsic and mafic layers in the Sabot Amphibolite. (I) The two rock types belong to entirely separate units, and all contacts between the felsic and mafic layers are now and have always been high strain zones. None of the contacts were ever intrusive or depositional. (II) The felsic layers were originally intrusions into the mafic volcanic rocks. The contacts between the felsic and mafic layers are parallel to the tectonic foliation within the layers due to post-intrusion deformation. (III) The felsic layers are volcanic rocks erupted at broadly the same time as the mafic rocks; the contacts between the felsic and mafic layers were originally depositional. Elements of these three endmember options can be combined into other alternatives. For example, a high strain zone can overprint an original depositional or intrusive contact. Another alternative is that option II is correct for some felsic layers and option III for others.

All the Proterozoic rocks in the Goochland Terrane were metamorphosed and deformed pervasively and intensely, mostly obscuring original intrusive and depositional contacts. Consequently, we cannot rule out high strain zone or intrusive contacts between all the felsic and mafic layers in the Sabot Amphibolite. However, we discount option I for the following reasons. (A) The rocks near the contacts do not appear more highly strained than the rocks distal to the contacts. (B) The contacts are sharp in outcrop; at this scale the different compositions are not intermingled as often occurs in high strain zones. The interfingering of the two compositions at the millimeter scale, however, could have resulted from deformation focused on the contact. (C) There is no independent evidence for the extreme interpretation that the felsic and mafic layers formed entirely separately with no original relationship between them.

We prefer the interpretation that these were originally depositional, not intrusive, contacts between felsic and mafic volcanic rocks for the following reasons. (A) Some of the meter-scale felsic layers appear to have been built from successive centimeter- to decimeter-scale felsic layers, which is expected for deposition of volcanic rocks but may not be as common in dikes or sills. (B) The microscopic interfingering of felsic and mafic layers is consistent with deposition of pulses of mafic and felsic lavas. Accordingly, throughout the remainder of the article we use the interpretation that the protoliths of these rocks were interbedded felsic and mafic volcanic strata that erupted at broadly the same time. If our interpretation is incorrect and the dated felsic layer actually was an intrusion into the mafic rocks, then the crystallization age of the felsic layer is a minimum age for eruption of the mafic volcanic rocks.

There are two plausible interpretations of the age significance of the U-Th-Pb isotope data from sample Sabot1. (1) The old cores with low U/Th ratios crystallized from the magma that formed the volcanic protolith whereas both the rims and young grains with high U/Th ratios grew during metamorphism. (2) The old, low U/Th cores were inherited from older Proterozoic igneous rocks in the Goochland Terrane whereas the high U/Th rims and young grains crystallized from the magma that formed the volcanic protolith. We prefer the first option for the following four reasons. First, the U/Th ratio in igneous zircon typically is lower than in metamorphic zircon (Hoskin and Schaltegger, 2003). Using option one, the low U/Th analyses correspond to igneous zircon and the high U/Th analyses to metamorphic zircon, in accordance with the conclusions of Hoskin and Schaltegger (2003, and references therein). In contrast, following option two, the high U/Th analyses came from igneous zircon. Second, our measured U/Th ratios in igneous zircon from the Montpelier Anorthosite, State Farm Gneiss, and Neoproterozoic granitoid range from 1.2 to 7.6 (Table S2; see also Owens and Tucker, 2003). The U/Th ratios for the Sabot1 core analyses we use to date eruption range from 0.8 to 4.3; three analyses yielded U/Th ratios less than 1.2 (Table S9). It is difficult to explain the fact that three of these twelve Sabot Amphibolite zircon cores have U/Th ratios less than 1.2 but none of the 108 analyses of zircon from the older Proterozoic rocks yielded a U/Th ratio less than 1.2 if these Sabot Amphibolite grains were inherited from the older igneous rocks. Third, the Montpelier Anorthosite and State Farm Gneiss contain zircon that crystallized at ca. 1050-1010 Ma (Table S3; Owens and Tucker, 2003). Both studied Neoproterozoic granitoid bodies also bear Late Mesoproterozoic zircon xenocrysts in addition to ca. 650-600 Ma zircon (Table S3; Owens and Tucker, 2003). If the volcanic protolith of the Sabot Amphibolite inherited zircon from these sources, we would expect Mesoproterozoic and/or 650-600 Ma zircon in the Sabot Amphibolite as well, but we found no zircon of these ages in sample Sabot1. Nearly complete resetting of conjectural older Proterozoic xenocrystic zircon in the Sabot Amphibolite by loss of nearly all previously-incorporated lead is not a compelling argument because there is no obvious mechanism to reset older Proterozoic zircon in the Sabot Amphibolite but not in the underlying State Farm Gneiss or Neoproterozoic granitoid. Finally, fourth, option two implies little or no growth of zircon during metamorphism to amphibolite and possibly granulite facies. However, we might expect metamorphic zircon crystallization in the Sabot Amphibolite felsic unit because zircon grew during metamorphism at these conditions in felsic rocks in other locales (e.g., Ustaomer et al., 2012; He et al., 2016; Tollo et al., 2017).

Accepting interpretations III and 1, we take the eruption age of the volcanic protolith of the Sabot Amphibolite felsic unit to be the weighted mean of the twelve old, low U/Th core analyses that are at least 98% concordant (Fig. 8C). This age is 552±11 Ma (MSWD = 0.67). This study did not aim to date the metamorphism of the Sabot Amphibolite, and consequently the study's design produced interpretations of the age(s) of metamorphism that are less well determined than the protolith eruption age. Nonetheless, we tentatively interpret the cluster of seven high U/Th analyses that are at least 97%

concordant between ca. 451-437 Ma to date growth of metamorphic zircon (Table S9). We also suggest that the following analyses may date growth of zircon during metamorphism: (A) The two high U/Th rim analyses at ca. 425-423 Ma that are 96-97% concordant, and (B) The two high U/Th rim analyses at ca. 415-414 Ma that are 96-98% concordant. The discordant dates that fall between these age groups resulted from lead loss and/or mixing of age domains during laser ablation. The discordant dates at ca. 414 and 400 Ma resulted from lead loss.

5.2 Interpretation of zircon spot O isotope measurements

All U/Pb isotopic analyses from Montpelier Anorthosite sample Mont1 were very discordant (Table S3; Fig. 11A). Accordingly, we interpret this sample's zircon δ_{18}O values of +8.4 to +7.6‰ to result from alteration after intrusion.

We interpret the main span of values from +8.3 to +7.2‰ in State Farm Gneiss sample 511005 zircon to be the result of the original magmatic crystallization of zircon. The three more positive outliers at +9.7, +9.0, and +8.7‰ may have resulted from unrecognized alteration of the zircon.

For zircon from Neoproterozoic granitoid sample 511004, plotting the OH/O ratio versus the δ_{18}O value of the concordant, non-xenocrystic analyses reveals a linear trend, with higher OH/O ratios corresponding to less positive δ_{18}O values (Fig. S2). This trend indicates that alteration of zircon from this sample resulted in addition of water and a decrease of δ_{18}O values. We therefore take the eight most positive of these δ_{18}O values as the best indicator of values during zircon crystallization in the sample 511004 magma (Fig. S2). These eight values range between +6.4 and +5.9‰ (Fig. 14).

Analyses of zircon from Neoproterozoic granitoid sample 511001 yielded a narrow range of $\delta^{18}O$ values, from +6.8 to +6.2‰. We interpret these values to have been set during crystallization of zircon in the sample 511001 magma.

Spot 18 was the only analysis in any grain from sample 512001 of the Sabot Amphibolite that produced concordant U/Pb isotopic dates near the eruption age of the Sabot Amphibolite protolith; all other analyses were discordant or came from younger, metamorphic zircon (Table S3; Fig. 11E). Accordingly, we interpret the $\delta^{18}O$ values from spots 18, 18b, and 18e to be the result of zircon crystallization in the Sabot Amphibolite protolith magma (Fig. 14). These values overlap the range of $\delta^{18}O$ values from zircon equilibrated with a mantle composition (Valley et al., 1998). We interpret the $\delta^{18}O$ values from all other spots to result from alteration or growth of metamorphic zircon. Spot 18c in the core of grain 14 had a $\delta^{18}O$ value of +7.5‰ whereas neighboring spots 18, 18b, and 18e in the interior of the grain gave $\delta^{18}O$ values between +5.6 and +5.1‰ (Figs. 13I and 13J). Alteration of the O isotopic composition at spot 18c may have been more effective than at spots 18, 18b, and 18e because of higher U concentration at spot 18c, as indicated by the dark cathodoluminescence response at spot 18c compared to the generally bright response at spots 18, 18b, and 18e.

5.3 Evolution of Goochland Terrane continental crust

Our hafnium and uranium/lead isotope analyses in spots in zircon suggest the tectonic evolution illustrated in Figure 15. This interpretation is supported by our zircon oxygen isotope, whole rock neodymium isotope, and whole rock major and trace element abundance data.

Initial separation of Goochland Terrane crust from the depleted mantle occurred prior to intrusion of the Montpelier Anorthosite and State Farm Gneiss (Figs. 12, 15A). Although the age of this first crust formation is poorly known, in Figure 12 we show it near 1400 Ma because this is the Nd isotope model age for separation of State Farm Gneiss whole rocks from the depleted mantle (Owens and Samson, 2004). Note, however, that the depleted mantle model age is not necessarily the actual time of derivation of continental crust from the mantle; the model age can be compromised by many processes including derivation from mantle with an isotopic composition different than that of the model depleted mantle, as well as mixing preexisting continental crust with mantle melt. We do not ascribe tectonic significance to the model age because of this uncertainty. No one has identified pre-latest Mesoproterozoic rocks or xenocrysts in the Goochland Terrane, so the tectonic setting during this initial crust formation event is unknown.

All our chemical evidence is consistent with derivation of the magma that became the State Farm Gneiss from this initial Goochland Terrane crust with no additional sources required. Both the small spread of zircon spot initial εHf values (Fig. 12) and the small range of whole rock initial εNd values (Fig. 10) point to extraction from a single source of melt. These values are much less positive than latest Mesoproterozoic depleted mantle values, indicating that the melt source was preexisting crust (Fig. 12). Likewise, the zircon spot O isotope values between +8.3 and +7.2‰ are consistent with derivation from preexisting crust. In contrast, the magmas that became the four other Proterozoic units in the Goochland Terrane probably were produced by mixing melt derived from the depleted mantle with preexisting crust.

The discordancy of the U/Pb dates from all the Montpelier Anorthosite zircon complicates interpretation of both the U-Pb and Lu-Hf isotope data from this sample's zircon (Fig. 11A; Tables S2, S3). Two interpretations of these data are plausible. (A) The analyzed zircon crystallized during anorthosite intrusion at 1045±10 Ma and lost Pb during metamorphism at ca. 300 Ma. The array of initial εHf values in zircon spots that stretch from depleted mantle values to +1.4 resulted from mixing of a melt from the depleted mantle with preexisting Goochland Terrane crust (Fig. 12; Table S3). (B) The analyzed zircon crystallized during metamorphism at ca. 300 Ma.

Arguments in favor of an igneous origin include the following. (1) Option A is consistent with the interpretation by Aleinikoff et al. (1996) that the ca. 1045 Ma igneous zircon lost a small amount of Pb during metamorphism at ca. 300 Ma. These authors discussed mechanisms for Pb loss from Montpelier Anorthosite zircon despite low U contents. (2) An igneous origin also is consistent with the fact that these authors did not find metamorphic zircon with an age of ca. 300 Ma. (3) Interpretation A provides an explanation for the result that the $^{206}Pb/^{207}Pb$ dates are older than the $^{206}Pb/^{238}U$ dates in every grain. (4) The interpretation that mixing of melt from the depleted mantle with preexisting crust produced the large spread of initial εHf values is identical to one explanation for the abundance of quartz as well as the high K and Ba concentrations in the Montpelier Anorthosite (Owens and Dymek, 2016). (5) The ends of the range of the zircon spot εHf values at 1040 Ma match the known values of the possible mixing components, the depleted mantle and the initial Goochland Terrane crust. If the spread of εHf values at 1040 Ma actually resulted from assigning an incorrect crystallization age to the zircon, we might expect to calculate εHf values much more or less positive than these two components.

On the other hand, points that support a metamorphic origin include the following. (1) Metamorphic crystallization at ca. 300 Ma obviates the need to call for nearly complete

Pb loss from the zircon despite low U concentrations. (2) Interpretation B resolves the apparent conflict between the presence of a large range in zircon spot εHf values but little spread in whole rock εNd values at 1040 Ma.

We cannot rule out either possibility. However, we favor interpretation A because it is most consistent with the previously-published data and interpretations. If an igneous origin is correct, one speculative way to explain the large spread in zircon spot εHf values but not in whole rock εNd values at 1040 Ma is zircon crystallization both before and during assimilation of the crustal rocks into the magma. After complete assimilation, the crustal component dominated the Nd isotopic composition of the magma as a whole.

Neoproterozoic granitoid samples 511004 and 511001 both contain zircon xenocrysts derived from the State Farm Gneiss or crust of similar age. Sample 511001 additionally contains zircon xenocrysts inherited from the Montpelier Anorthosite or similar rocks. The Montpelier Anorthosite is geographically closer in map view to the granitoid body at location 511001 than it is to the body at location 511004 (Fig. 2). This proximity may explain the presence of zircon derived from the Montpelier Anorthosite in sample 511001 but not sample 511004. Zircon in the Neoproterozoic granitoid bodies had εHf values between +6.0 and -1.4 at the time of intrusion, whereas the State Farm Gneiss whole rock is estimated to have had an εHf value near -5 at 650-600 Ma (Fig. 12). Although inadvertent mixing of different isotopic domains in zircon during laser ablation may have produced part of the large spread of initial εHf values in zircon from sample 511004, none of the initial values of zircon from either Neoproterozoic granitoid body was near the estimated State Farm Gneiss whole rock εHf value at 650-600 Ma. The more positive initial εHf values of the Neoproterozoic granitoid zircon require mixing of the State Farm Gneiss with a source more enriched in ^{176}Hf to produce the Neoproterozoic granitoid magma. We infer that this more enriched source was melt from the depleted mantle (Figs. 12, 15D). Whole-rock initial εNd values near zero (Fig. 10) similarly suggest mixing of a source enriched in ^{143}Nd with the latest Mesoproterozoic rocks, as also inferred by Owens and Samson (2004). Because of the lower initial values, our zircon Hf isotope data suggest a greater contribution of latest Mesoproterozoic rocks to sample 511001 than to sample 511004. O isotope values in the zircon in the two Neoproterozoic granitoid bodies range from +6.8 to +5.9‰, consistent with at least partial derivation of the Neoproterozoic granitoid magmas from preexisting crust.

The range of initial εHf values of spots in zircon from Sabot Amphibolite felsic sample 512001 from near depleted mantle values to +8.8 indicates derivation of melt dominantly from the depleted mantle, with a contribution from the older Goochland Terrane rocks (Figs. 12, 15E). Whole rock initial εNd values show a similar spread from depleted mantle values to +1.5, likewise revealing mixing of these two sources (Fig. 10). O isotope values from the only analyzed magmatic zircon crystal unaffected by lead loss are +5.6 to +5.1‰, which similarly point to derivation from the mantle (Fig. 14). Finally, tectonic discrimination using trace elements from the mafic parts of the Sabot Amphibolite indicates a mid-ocean ridge affinity (Fig. 5C; Table S8), consistent with derivation mostly from the depleted mantle (Salters and Stracke, 2004).

The tectonic setting for all of this latest Mesoproterozoic and Neoproterozoic magmatism may have been extensional. The tectonic environment for the oldest magmatism is the most poorly known. However, like other latest Mesoproterozoic anorthosite and related granitoid in eastern North America, Bartholomew and Hatcher (2010) and McLelland et al. (2010) inferred that the Montpelier Anorthosite and State Farm Gneiss magmas formed during extension related to Grenvillian post-orogenic collapse.

Tectonic discrimination of State Farm Gneiss based on major and trace elements yields mixed results for the felsic samples, but all the intermediate samples lie in the within-plate field in discriminations that test for this option (Fig. 5; Tables S4, S5). A within-plate setting is consistent with extension at the end of orogeny. Based on major and trace element compositions, Owens and Tucker (2003) interpreted the Neoproterozoic granitoid to be the product of continental rifting. Our major and trace element discrimination supports this interpretation because nearly all the samples plot in the within-plate field in discriminations that test for this option (Fig. 5; Tables S6, S7). Finally, trace element discrimination of the mafic parts of the Sabot Amphibolite reveals a dominant mid-ocean ridge affinity, which in continental crust is most easily explained by production in a rift (Fig. 5C; Table S8). The bimodal composition of the Sabot magmatism, with few rocks of intermediate composition (Fig. 4; Table S1), is consistent with eruption in a rift setting (e.g., Corti, 2009). No Proterozoic faults are known from the Goochland Terrane, disallowing structural testing of the extensional interpretation. However, the decrease of $\delta^{18}O$ values in zircon from progressively younger groups of rocks indicates less crustal contamination of mantle melt through time, consistent with extensional thinning of the crust (Fig. 14).

Accepting the igneous interpretation for the origin of the Montpelier Anorthosite zircon, punctuated addition of juvenile continental crust to the Goochland Terrane spanned at least 500 M.y and perhaps 850 M.y. or longer. Production of the melts that became the Montpelier Anorthosite at ca. 1045 Ma, the Neoproterozoic granitoid between ca. 660 and 580 Ma, and the Sabot Amphibolite protolith at ca. 550 Ma all involved a component of melt from the depleted mantle. All this magmatism was caused by processes operating during the terminal stages of the Grenville orogeny followed by continental breakup.

Further back in time, initial Goochland Terrane crust was extracted from the depleted mantle prior to intrusion of the Montpelier Anorthosite and State Farm Gneiss magmas, possibly near 1400 Ma. Thus the Proterozoic magmas of the Goochland Terrane are evidence for extension-related, punctuated addition of juvenile crust to this continental sliver over at least 500 M.y.

Although the additions of juvenile crust spanned a long time, the cumulative new continental crust produced during latest Mesoproterozoic and Neoproterozoic time appears to have been volumetrically minor because the combined modern spatial extents of the Montpelier Anorthosite, Neoproterozoic granitoid, and Sabot Amphibolite are small compared to the map extents of the State Farm Gneiss (Fig. 2). Based on the relatively large area of exposed State Farm Gneiss, the volumetrically most important crust-forming event during Proterozoic time was the initial formation of Goochland Terrane continental crust prior to latest Mesoproterozoic time (Fig. 15A). This early event could have been even more volumetrically important than suggested by the geologic map in Figure 2 if rocks like the State Farm Gneiss underlie parts of the Maidens Gneiss. Unfortunately, the tectonic setting for the initial formation of Goochland Terrane continental crust is unknown (Fig. 15A). However, our data indicate that addition of juvenile crust during ca. 1050-550 Ma extension was volumetrically minor, consistent with the conclusions of Stern and Scholl (2010) for the modern Earth. Our data also highlight the episodic nature of such additions.

5.4 Alteration of the oxygen isotope compositions of quartz in Goochland Terrane rocks

To assess whether the O isotope compositions of quartz in the State Farm Gneiss, Neoproterozoic granitoid, and Sabot Amphibolite were altered after cooling following intrusion or eruption, we calculated a temperature for each sample using the quartz-zircon O isotope thermometer as formulated by Valley et al. (2003). The thermometer requires equilibrium of O isotopes in quartz and zircon to yield a valid temperature. If a geologist inputs values from quartz and zircon that are not in isotopic equilibrium, the user still can mathematically operate the equation that underlies the thermometer as long as the $\delta^{18}O$ value of the quartz is more positive than that of the zircon. In the case of isotopic disequilibrium, however, the output would have no physical meaning; it would not be a temperature at which equilibrium was attained between the two minerals. For each sample, we used the mean $\delta^{18}O$ value of the spots in igneous, unaltered zircon that we use for the interpretations in section 5.3. The results are given in Table S12.

Only the quartz and zircon from Neoproterozoic granitoid sample 511001 yielded a temperature consistent with little post-cooling alteration of the quartz O isotope composition (Lackey et al., 2008). This sample produced a narrow range of zircon $\delta^{18}O$ values, from +6.8 to +6.2‰, indicating little alteration of the O isotope composition of zircon as well as quartz in this unit.

In contrast, the calculated temperature for State Farm Gneiss sample 511005 is 1240 °C, hotter than granite intrusion temperatures (Lackey et al., 2008). The quartz in Neoproterozoic granitoid sample 511004 has a less positive $\delta^{18}O$ value than the zircon, which renders the thermometer inoperable. Finally, the calculated temperature for Sabot Amphibolite sample 512001 is 340 °C, colder than expected for quartz that equilibrated with zircon during post-eruptive cooling (Lackey et al., 2008). The too-hot and too-cold temperatures from the State Farm Gneiss and the Sabot Amphibolite, respectively, and especially the less positive $\delta_{18}O$ value in quartz than in zircon from Neoproterozoic granitoid sample 511004, indicate that the O isotope values of quartz were altered to be out of equilibrium with those of co-existing zircon. Because quartz and zircon O isotopes are not in equilibrium in each of the three samples, the thermometer equation can yield or fail to yield a result mathematically (Table S12), but the outputs have no physical meaning. They are not temperatures of equilibrium between quartz and zircon. Instead, the calculations demonstrate post-intrusion or post-eruption alteration of the O isotope compositions of quartz in these three units. These three samples span the range of Proterozoic magmatic ages in the Goochland Terrane, suggesting that alteration of the O isotope composition of quartz may be widespread in the Proterozoic rocks of the terrane. If correct, the O isotope compositions of many of the Proterozoic whole rocks likewise may have been modified by processes such as metamorphism that occurred after intrusion or eruption. The extent of alteration of the Proterozoic rocks after intrusion or eruption thus must be assessed prior to interpreting whole rock O isotope measurements.

5.5 Implications for the Proterozoic tectonic affinity of the Goochland Terrane

Interpretation that the Goochland Terrane was part of or near Laurentia during the Proterozoic Eon relies on geological links between these two pieces of continental crust. To ascribe a Laurentian affinity to the Goochland Terrane, geologists commonly point to similarities between the Proterozoic intrusive rocks of the Goochland Terrane and those of the nearby Blue Ridge Province (Farrar, 1984; Aleinikoff et al., 1996; Glover et al., 1997; Owens and Samson, 2004). This correlation mostly works well for the latest Mesoproterozoic rocks. The intrusion age as well as the unusual chemistry and mineralogy of the Montpelier Anorthosite match those of the Roseland Anorthosite in the Blue Ridge

Province (Owens and Dymek, 2016), and the intrusion age and chemistry of the State Farm Gneiss is similar to many granitic bodies in the Blue Ridge Province (Tollo et al., 2006; 2017). Whole rock initial εNd values also overlap for the Montpelier and Roseland anorthosite bodies (Fig. 10). However, the seven published analyses of ca. 1050-1010 Ma Blue Ridge meta-granitoid all have more negative initial εNd values than the State Farm Gneiss, suggesting sources with different Nd isotopic compositions (Fig. 10). Another similarity is that rocks in both the Goochland Terrane and the Blue Ridge Province were metamorphosed at ca. 1000 Ma (Aleinikoff et al., 1996; Southworth et al., 2010; Tollo et al., 2017; our analysis of State Farm Gneiss zircon grain big_20_30).

Likewise, the compositions of the Neoproterozoic igneous rocks in the Goochland Terrane are similar to those in the Blue Ridge Province. Neoproterozoic granitoid in both regions has alkaline to mildly peralkaline, A-type compositions (Owens and Tucker, 2003; Tollo et al., 2004). Sabot Amphibolite mafic and felsic rocks also have similar compositions to those in the Catoctin Formation in the Blue Ridge Province to the west (Figs. 1, 4). Initial εNd values of Sabot Amphibolite meta-basalt mostly overlap the initial εNd values of Catoctin Formation meta-basalt, although the Sabot Amphibolite samples reach more positive values (Fig. 10). If this difference remains after more analyses of Catoctin Formation meta-basalt, it suggests that some Sabot Amphibolite meta-basalt incorporated less preexisting crust than did any mafic rocks in the Catoctin Formation.

Despite these similarities, one point still requires clarification during future studies: Neoproterozoic magmatism in the Goochland Terrane appears to have occurred at least 10 M.y. after compositionally similar magmatism in the nearby Blue Ridge Province. This conclusion is clear for the older felsic magmatism, as pointed out by Bartholomew and Tollo (2004). In the Blue Ridge Province, dominantly felsic and minor mafic rift-related magmatism occurred between ca. 780 and 670 Ma (Tollo et al., 2004; 2012; Holm-Denoma et al., 2014; McClellan and Gazel, 2014), whereas in the Goochland Terrane, rift-related granitoid intruded between ca. 660 and 580 Ma (Owens and Tucker, 2003). The conclusion is less certain for the younger mafic magmatism because of uncertainties in the eruption age of the Sabot Amphibolite protolith. In the Blue Ridge Province, flood basalt of the Catoctin Formation mostly erupted at ca. 570 to 560 Ma; the Catoctin Formation also contains felsic dikes as young as 555±4 Ma (Southworth et al., 2009; Burton and Southworth, 2010). Our new dating places eruption of the Sabot Amphibolite protolith at 552±11 Ma (Fig. 8C). This new age overlaps the age of eruption of the Catoctin Formation considering analytical uncertainties, so we cannot rule out broadly contemporaneous eruption of the two units. However, the younger central age of the dated zircon from the Sabot Amphibolite protolith suggests eruption after the main pulse of Catoctin Formation eruption. Any reconstruction that locates the Goochland Terrane near Laurentia during Neoproterozoic time must explain the younger intrusive and possibly extrusive Neoproterozoic magmatism in the Goochland Terrane compared to the Blue Ridge Province. For example, magmatism could have occurred slightly later in a position outboard of and/or along strike with respect to the Blue Ridge Province, as proposed by Hatcher (1989) and Bartholomew and Tollo (2004). Several other authors likewise have inferred more than 100 km of translation of the Goochland Terrane along the Laurentian margin during Paleozoic time (e.g., Glover et al., 1997; Bailey et al., 2004).

6. CONCLUSIONS

Our element abundance and isotope data lead to the following conclusions.

1. Uranium/lead isotope dating of spots in zircon from a felsic layer intercalated with the dominant mafic rocks of the Sabot Amphibolite indicate that eruption of the protolith occurred at 552±11 Ma.
2. Goochland Terrane crust initially formed prior to latest Mesoproterozoic intrusion of the Montpelier Anorthosite and State Farm Gneiss. Extraction of the initial Goochland Terrane crust from the depleted mantle might have occurred near 1400 Ma, which is the Nd isotope model age for extraction of State Farm Gneiss whole rocks from the depleted mantle.
3. The magma that became the State Farm Gneiss protolith could have been sourced solely from partial melting of this initial Goochland Terrane crust.
4. In contrast, the magma that became the Montpelier Anorthosite may have been a mixture of the initial Goochland Terrane crust and melt extracted from the depleted mantle. This addition of juvenile continental crust may have occurred in an extensional setting during orogenic collapse at the end of the Grenville Orogeny.
5. The magmas that became the Neoproterozoic granitoid similarly were a mixture of melt from the depleted mantle and latest Mesoproterozoic rocks such as the Montpelier Anorthosite and the State Farm Gneiss. This addition of juvenile continental crust probably took place during early rifting of the Goochland Terrane.
6. The mafic Sabot Amphibolite protolith had trace element abundances similar to those of mid-ocean ridge basalt and was derived dominantly from partial melting of the depleted mantle during continental rifting.

7. In summary, the Proterozoic rocks of the Goochland Terrane represent punctuated addition of juvenile crust to this continental sliver between ca. 1050 and 550 Ma. This juvenile crust formed in extensional tectonic regimes.
8. After intrusion or eruption, the O isotopic compositions of quartz in the State Farm Gneiss, Neoproterozoic granitoid, and Sabot Amphibolite were altered.

ACKNOWLEDGEMENTS

Philip Piccoli enabled our use of the electron microprobe at the University of Maryland. We acknowledge the support of the Maryland NanoCenter and its NispLab (Nanoscale Imaging, Spectroscopy, and Properties Laboratory), which is supported in part by the National Science Foundation (NSF) as a MRSEC (Materials Research Science and Engineering Center) shared experimental facility. We thank John Valley for assistance with SIMS analysis and review of an early draft of this paper. Likewise, we thank Jeffrey Vervoort and Christopher Fisher for assistance with LASS analysis and review of an early version of this article. We are grateful to George Gehrels, Mark Pecha, and the staff of the Arizona LaserChron Center for facilitating our zircon analyses in their laboratory. The Arizona LaserChron Center is supported by NSF grant EAR 1338583. WiscSIMS is supported by NSF (EAR 1355590, 1658823) and the University of Wisconsin-Madison. SIMS analysis was supported by NSF grant EAR 0838058 to John Valley. We thank Robert Stern for efficient editorial handling as well as Arne Willner and four anonymous reviewers for helpful reviews.

DECLARATION OF INTEREST STATEMENT

No potential conflict of interest.

REFERENCES

Agrawal, S., Guevara, M., and Verma, S.P., 2008, Tectonic discrimination of basic and ultrabasic volcanic rocks through log-transformed ratios of immobile trace elements: International Geology Review, v. 50, p. 1057–1079, doi: 10.2747/0020-6814.50.12.1057.

Aleinikoff, J.N., Zartman, R.E., Walter, M., Rankin, D.W., Lyttle, P.T., and Burton, W.C., 1995, U-Pb ages of metarhyolites of the Catoctin and Mount Rogers formations, central and southern Appalachians; evidence for two pulses of Iapetan rifting: American Journal of Science, v. 295, p. 428–454, doi:10.2475/ajs.295.4.428.

Aleinikoff, J.N., Horton, J.W., and Walter, M., 1996, Middle Proterozoic age for the Montpelier Anorthosite, Goochland terrane, eastern Piedmont, Virginia: Geological Society of America Bulletin, v. 108, p. 1481–1491, doi: 10.1130/0016-7606(1996)108<1481:MPAFTM>2.3.CO;2.

Armstrong, R.L., 1968, A model for the evolution of strontium and lead isotopes in a dynamic Earth: Reviews of Geophysics, v. 6, p. 175–199, doi: 10.1029/RG006i002p00175.

Badger, R.L., Ashley, K.T., and Cousens, B.L., 2010, Stratigraphy and geochemistry of the Catoctin volcanics: Implications for mantle evolution during the breakup of Rodinia, *in* Tollo, R.P., Bartholomew, M.J., Hibbard, J.P., and Karabinos, P.M. eds., From Rodinia to Pangea: The lithotectonic record of the Appalachian region, Boulder, Geological Society of America, Memoir, v. 206, p. 397–415, doi:10.1130/2010.1206(17).

Badger, R.L., and Sinha, A.K., 2004, Geochemical stratigraphy and petrogenesis of the Catoctin volcanic province, central Appalachians, *in* Tollo, R.P., Corriveau, L., McLelland, J., and Bartholomew, M.J. eds., Proterozoic Tectonic Evolution of the Grenville Orogen in North America, Boulder, Geological Society of America, Memoir, v. 197, p. 435–458, doi:10.1130/0-8137-1197-5.435.

Bailey, C.M., Francis, B.E., and Fahrney, E.E., 2004, Strain and vorticity analysis of transpressional high-strain zones from the Virginia Piedmont, USA, in Alsop, G.I., Holdsworth, R.E., McCaffrey, K.J.W., and Hand, M. eds., Flow processes in faults and shear zones, London, Geological Society, Special Publication, v. 224, p. 249–

264, doi:10.1144/GSL.SP.2004.224.01.16.

Bartholomew, M.J., and Tollo, R.P., 2004, Northern ancestry for the Goochland terrane as a displaced fragment of Laurentia: Geology, v. 32, p. 669–672, doi:10.1130/G20520.1.

Bartholomew, M.J., and Hatcher, R.D., 2010, The Grenville orogenic cycle of southern Laurentia: Unraveling sutures, rifts, and shear zones as potential piercing points for Amazonia: Journal of South American Earth Sciences, v. 29, p. 4–20, doi: 10.1016/j.jsames.2009.08.007.

Black, L.P., Kamo, S.L., Allen, C.M., Davis, D.W., Aleinikoff, J.N., Valley, J.W., Mundil, R., Campbell, I.H., Korsch, R.J., Williams, I.S., and Foudoulis, C., 2004, Improved 206Pb/238U microprobe geochronology by the monitoring of a trace-element-related matrix effect; SHRIMP, ID–TIMS, ELA–ICP–MS and oxygen isotope documentation for a series of zircon standards: Chemical Geology, v. 205, p. 115–140, doi: 10.1016/j.chemgeo.2004.01.003.

Bouvier, A., Vervoort, J.D., and Patchett, P.J., 2008, The Lu–Hf and Sm–Nd isotopic composition of CHUR: Constraints from unequilibrated chondrites and implications for the bulk composition of terrestrial planets: Earth and Planetary Science Letters, v. 273, p. 48–57, doi: 10.1016/j.epsl.2008.06.010.

Burton, W.C., Froelich, A.J., Pomeroy, J.S., and Lee, K.Y., 1995, Geology of the Waterford Quadrangle, Virginia and Maryland, and the Virginia part of the Point of Rocks quadrangle: U.S. Geological Survey Bulletin 2095, 30 p., doi:10.3133/b2095.

Burton, W.C., and Southworth, S., 2010, A model for Iapetan rifting of Laurentia based on Neoproterozoic dikes and related rocks, *in* Tollo, R.P., Bartholomew, M.J., Hibbard, J.P., and Karabinos, P.M. eds., From Rodinia to Pangea: The lithotectonic record of the Appalachian region, Boulder, Geological Society of America, Memoir, v. 206, p. 455–476, doi: 10.1130/2010.1206(20).

Cawood, P.A., Hawkesworth, C.J., and Dhuime, B., 2013, The continental record and the generation of continental crust: Geological Society of America Bulletin, v. 125, p. 14–32, doi: 10.1130/B30722.1.

Chauvel, C., Garcon, M., Bureau, S., Besnault, A., Jahn, B., and Ding, Z., 2014, Constraints from loess on the Hf–Nd isotopic composition of the upper continental crust: Earth and Planetary Science Letters, v. 388, p. 48–58, doi: 10.1016/j.epsl.2013.11.045.

Condie, K.C., Bickford, M.E., Aster, R.C., Belousova, E., and Scholl, D.W., 2011, Episodic zircon ages, Hf isotopic composition, and the preservation rate of continental crust: Geological Society of America Bulletin, v. 123, p. 951–957, doi: 10.1130/B30344.1.

Corti, G., 2009, Continental rift evolution: From rift initiation to incipient break-up in the Main Ethiopian Rift, East Africa: Earth-Science Reviews, v. 96, p. 1–53, doi: 10.1016/j.earscirev.2009.06.005.

Couture, R.A., and Dymek, R.F., 1996, A reexamination of absorption and enhancement effects in X-ray fluorescence trace element analysis: American Mineralogist, v. 81, p. 639–650, doi: 10.2138/am-1996-5-611.

Couture, R.A., Smith, M.S., and Dymek, R.F., 1993, X-ray fluorescence analysis of silicate rocks using fused glass discs and a side-window Rh source tube: accuracy, precision and reproducibility: Chemical Geology, v. 110, p. 315–328, doi: 10.1016/0009-2541(93)90326-E.

DePaolo, D.J., 1981, Neodymium isotopes in the Colorado Front Range and crust–mantle evolution in the Proterozoic: Nature, v. 291, p. 193–196, doi: 10.1038/291193a0.

Espenshade, G.H., 1986, Geology of the Marshall Quadrangle, Fauquier County, Virginia: U.S. Geological Survey Bulletin 1560, 60 p., doi:10.3133/b1560.

Farrar, S.S., 1984, The Goochland granulite terrane: Remobilized Grenville basement in the eastern Virginia Piedmont, *in* Bartholomew, M.J. ed., The Grenville Event in the Appalachians and Related Topics, Boulder, Geological Society of America, Special Paper, v. 194, p. 215–228, doi: 10.1130/SPE194-p215.

Fisher, C.M., Loewy, S.L., Miller, C.F., Berquist, P., Van Schmus, W.R., Hatcher, R.D., Wooden, J.L., and Fullagar, P.D., 2010, Whole-rock Pb and Sm-Nd isotopic constraints on the growth of southeastern Laurentia during Grenvillian orogenesis: Geological Society of America Bulletin, v. 122, p. 1646–1659, doi:10.1130/B30116.1.

Fisher, C.M., Vervoort, J.D., and DuFrane, S.A., 2014, Accurate Hf isotope determinations of complex zircons using the “laser ablation split stream” method: Geochemistry, Geophysics, Geosystems, v. 15, p. 121–139, doi: 10.1002/2013GC004962.

Fullagar, P.D., Goldberg, S.A., and Butler, J.R., 1997, Nd and Sr isotopic characterization of crystalline rocks from the Southern Appalachian Piedmont and Blue Ridge, North and South Carolina, *in* Sinha, A.K., Whalen, J.B., and Hogan, J.P. eds., The Nature of Magmatism in the Appalachian Orogen, Boulder, Geological Society of America, Memoir, v. 191, p. 165–179, doi:10.1130/0-8137-1191-6.165.

Gehrels, G., and Pecha, M., 2014, Detrital zircon U-Pb geochronology and Hf isotope geochemistry of Paleozoic and Triassic passive margin strata of western North America: Geosphere, v. 10, p. 49–65, doi: 10.1130/GES00889.1.

Gehrels, G.E., Valencia, V.A., and Ruiz, J., 2008, Enhanced precision, accuracy, efficiency, and spatial resolution of U-Pb ages by laser ablation-multicollector-inductively coupled plasma-mass spectrometry: Geochemistry, Geophysics, Geosystems, v. 9, Q03017, doi: 10.1029/2007GC001805.

Glover, III, L., 1989, Tectonics of the Virginia Blue Ridge and Piedmont, *in* Glover, III, L., Evans, N.H., Patterson, J.G., and Brown, W.R. eds., 28th International Geological Congress, Field trip guidebook, Washington, DC, American Geophysical Union, v. T363, p. 1–59, doi:10.1029/FT363.

Glover, III, L., Sheridan, R.E., Holbrook, W.S., Ewing, J., Talwani, M., Hawman, R.B., and Wang, P., 1997, Paleozoic collisions, Mesozoic rifting, and structure of the Middle Atlantic states continental margin: An “EDGE” Project report, *in* Glover, III, L. and Gates, A.E. eds., Central and Southern Appalachian sutures: results of the EDGE Project and related studies, Boulder, Geological Society of America, Special Paper, v. 314, p. 107–135, doi: 10.1130/0-8137-2314-0.107.

Goodge, J.W., Fanning, C.M., Fisher, C.M., and Vervoort, J.D., 2017, Proterozoic crustal evolution of central East Antarctica: Age and isotopic evidence from glacial igneous clasts, and links with Australia and Laurentia: Precambrian Research, v. 299, p. 151–176, doi: 10.1016/j.precamres.2017.07.026.

Goodwin, B.K., 1970, Geology of the Hylas and Midlothian Quadrangles, Virginia: Charlottesville, Virginia Division of Mineral Resources, Report of Investigations, v. 23, 51 p.

Hatcher, R.D., Jr., 1989, Appalachians introduction, *in* Hatcher, R.D., Thomas, W.A., and

Viele, G.W. eds., The Appalachian-Ouachita Orogen in the United States, Boulder, Geological Society of America, Geology of North America, v. F-2, p. 1–6, doi: 10.1130/DNAG-GNA-F2.1.

He, X.-F., Santosh, M., Tsunogae, T., Malaviarachchi, S.P.K., and Dharmapriya, P.L., 2016, Neoproterozoic arc accretion along the “eastern suture” in Sri Lanka during Gondwana assembly: Precambrian Research, v. 279, p. 57–80, doi: 10.1016/j.precamres.2016.04.006.

Hibbard, J.P., and Samson, S.D., 1995, Orogenesis exotic to the Iapetan cycle in the southern Appalachians, in Hibbard, J.P., van Staal, C.R., and Cawood, P.A. eds., Current perspectives in the Appalachian-Caledonian Orogen, Geological Association of Canada, Special Paper, v. 41, p. 191–205.

Hibbard, J.P., van Staal, C.R., Rankin, D.W., and Williams, H., 2006, Lithotectonic map of the Appalachian Orogen, Canada-United States of America: Geological Survey of Canada, Map 2096A, 1:1,500,000.

Holm-Denoma, C.S., McClellan, E., and Southworth, S., 2014, Three episodes of volcanism and erosion during Neoproterozoic extension in eastern Laurentia revealed by U-Pb dating of zircon from clasts of rhyolite and detrital zircon from sedimentary rocks of the Mount Rogers Formation, southwest Virginia, *in* Geological Society of America Abstracts with Programs, v. 46, p. 90.

Horton, J.W., Jr., Drake, A.A., Jr., and Rankin, D.W., 1989, Tectonostratigraphic terranes and their Paleozoic boundaries in the central and southern Appalachians, *in* Dallmeyer, R.D. ed., Terranes in the Circum-Atlantic Paleozoic Orogens, Boulder, Geological Society of America, Special Paper, v. 230, p. 213–246, doi: 10.1130/SPE230-p213.

Hoskin, P.W.O., and Schaltegger, U., 2003, The composition of zircon and igneous and metamorphic petrogenesis: Reviews in Mineralogy and Geochemistry, v. 53, p. 27–62, doi: 10.2113/0530027.

Keppie, J.D., Dostal, J., Murphy, J.B., and Nance, R.D., 1996, Terrane transfer between eastern Laurentia and western Gondwana in the early Paleozoic: Constraints on global reconstructions, *in* Nance, R.D. and Thompson, M.D. eds., Avalonian and related peri-Gondwanan terranes of the circum-North Atlantic, Geological Society of America, Special Paper, v. 304, p. 369–380, doi: 10.1130/0-8137-2304-3.369.

Kita, N.T., Ushikubo, T., Fu, B., and Valley, J.W., 2009, High precision SIMS oxygen isotope analysis and the effect of sample topography: Chemical Geology, v. 264, p. 43–57, doi: 10.1016/j.chemgeo.2009.02.012.

Korotev, R.L., 1987, National Bureau of Standards coal flyash (SRM 1633a) as a multielement standard for instrumental neutron activation analysis: Journal of Radioanalytical and Nuclear Chemistry, Articles, v. 110, p. 159–177, doi: 10.1007/BF02055018.

Lackey, J.S., Valley, J.W., Chen, J.H., and Stockli, D.F., 2008, Dynamic magma systems, crustal recycling, and alteration in the central Sierra Nevada Batholith: the oxygen isotope record: Journal of Petrology, v. 49, p. 1397–1426, doi: 10.1093/petrology/egn030.

Le Maitre, R.W., and 14 others, 2002, Igneous rocks: a classification and glossary of terms: Cambridge, U.K., Cambridge University Press, 236 p., doi: 10.1017/CBO9780511535581.

Ludwig, K.R., 2008, User's manual for Isoplot 3.70: Berkeley Geochronology Center Special Publication 4, 76 p.

Marr, J.D., Jr, 2002, Geologic map of the western portion of the Richmond 30 X 60-minute quadrangle, Virginia: Virginia Division of Mineral Resources, scale 1:100,000, Publication 165.

Martin, A.J., Southworth, S., Collins, J.C., Fisher, S.W., and Kingman, E.R., III., 2015, Laurentian and Amazonian sediment sources to Neoproterozoic–lower Paleozoic Maryland Piedmont rocks: Geosphere, v. 11, p. 1042–1061, doi: 10.1130/GES01140.1.

McClellan, E., and Gazel, E., 2014, The Cryogenian intra-continental rifting of Rodinia: Evidence from the Laurentian margin in eastern North America: Lithos, v. 206–207, p. 321–337, doi: 10.1016/j.lithos.2014.08.006.

McLelland, J.M., Selleck, B.W., Hamilton, M.A., and Bickford, M.E., 2010, Late- to post-tectonic setting of some major Proterozoic anorthosite–mangerite–charnockite–granite (AMCG) suites: The Canadian Mineralogist, v. 48, p. 729–750, doi: 10.3749/canmin.48.4.729.

Moorbath, S., 1975, Evolution of Precambrian crust from strontium isotopic evidence: Nature, v. 254, p. 395–398, doi: 10.1038/254395a0.

Owens, B.E., Buchwaldt, R., and Shirvell, C.R., 2010, Geochemical and geochronological evidence for Devonian magmatism revealed in the Maidens gneiss, Goochland terrane, Virginia, *in* Tollo, R.P., Bartholomew, M.J., Hibbard, J.P., and Karabinos, P.M. eds., From Rodinia to Pangea: The Lithotectonic Record of the Appalachian Region, Boulder, Geological Society of America, Memoir, v. 206, p. 725–738, doi: 10.1130/2010.1206(28).

Owens, B.E., and Dymek, R.F., 2016, Comparative petrology of the Montpelier and Roseland potassic anorthosites, Virginia: The Canadian Mineralogist, v. 54, p. 1563–1593, doi: 10.3749/canmin.1600002.

Owens, B.E., and Samson, S.D., 2004, Nd isotopic constraints on the magmatic history of the Goochland terrane, easternmost Grenvillian crust in the southern Appalachians, *in* Tollo, R.P., McLelland, J., Corriveau, L., and Bartholomew, M.J. eds., Proterozoic tectonic evolution of the Grenville Orogen in North America, Geological Society of America, Memoir, v. 197, p. 601–608, doi: 10.1130/0-8137-1197-5.601.

Owens, B.E., and Tucker, R.D., 2003, Geochronology of the Mesoproterozoic State Farm gneiss and associated Neoproterozoic granitoids, Goochland terrane, Virginia: Geological Society of America Bulletin, v. 115, p. 972–982, doi: 10.1130/B25258.1.

Patchett, P.J., and Chase, C.G., 2002, Role of transform continental margins in major crustal growth episodes: Geology, v. 30, p. 39, doi: 10.1130/0091-7613(2002)030<0039:ROTCMI>2.0.CO;2.

Pettingill, H.S., Sinha, A.K., and Tatsumoto, M., 1984, Age and origin of anorthosites, charnockites, and granulites in the Central Virginia Blue Ridge: Nd and Sr isotopic evidence: Contributions to Mineralogy and Petrology, v. 85, p. 279–291, doi:10.1007/BF00378106.

Pollock, J.C., Hibbard, J.P., and van Staal, C.R., 2012, A paleogeographical review of the peri-Gondwanan realm of the Appalachian orogen: Canadian Journal of Earth Sciences, v. 49, p. 259–288, doi: 10.1139/e11-049.

Rankin, D.W., 1994, Continental margin of the eastern United States: Past and present, in Speed, R.C. ed., Phanerozoic evolution of North American continent-ocean transitions, Boulder, Geological Society of America, p. 129–218, doi:10.1130/DNAG-COT-PEN.129.

Reymer, A., and Schubert, G., 1986, Rapid growth of some major segments of continental crust: Geology, v. 14, p. 299, doi: 10.1130/0091-7613(1986)14<299:RGOSMS>2.0.CO;2.

Salters, V.J.M., and Stracke, A., 2004, Composition of the depleted mantle: Geochemistry, Geophysics, Geosystems, v. 5, Q05004, doi: 10.1029/2003GC000597.

Samson, S.D., Hibbard, J.P., and Wortman, G.L., 1995, Nd isotopic evidence for juvenile crust in the Carolina terrane, southern Appalachians: Contributions to Mineralogy and Petrology, v. 121, p. 171–184, doi: 10.1007/s004100050097.

Scherer, E., Munker, C., and Mezger, K., 2001, Calibration of the lutetium-hafnium clock: Science, v. 293, p. 683–687, doi: 10.1126/science.1061372.

Soderlund, U., Patchett, P.J., Vervoort, J.D., and Isachsen, C.E., 2004, The 176Lu decay constant determined by Lu–Hf and U–Pb isotope systematics of Precambrian mafic intrusions: Earth and Planetary Science Letters, v. 219, p. 311–324, doi: 10.1016/S0012-821X(04)00012-3.

Southworth, S., Aleinikoff, J.N., Tollo, R.P., Bailey, C.M., Burton, W.C., Hackley, P.C., and Fanning, C.M., 2010, Mesoproterozoic magmatism and deformation in the northern Blue Ridge, Virginia and Maryland: Application of SHRIMP U-Pb geochronology and integrated field studies in the definition of Grenvillian tectonic history, *in* Tollo, R.P., Bartholomew, M.J., Hibbard, J.P., and Karabinos, P.M. eds., From Rodinia to Pangea: The lithotectonic record of the Appalachian region, Geological Society of America, Geological Society of America Memoir, v. 206, p. 795–836, doi: 10.1130/2010.1206(31).

Southworth, S., Burton, W.C., Schindler, J.S., and Froelich, A.J., 2006, Geologic Map of Loudoun County, Virginia: United States Geological Survey Geologic Investigations Series Map I–2553, 1:50,000, 34 p.

Southworth, S., Tollo, R.P., Aleinikoff, J.N., Bailey, C., Burton, W.C., Crider, E., Hackley, P.C., Kunk, M.J., Mundil, R., Naeser, C.W., Naeser, N., and Smoot, J., 2009, New geologic map and geochronology of the Shenandoah National Park region, Virginia, *in* Geological Society of America Abstracts with Programs, v. 41, p. 365.

Spicuzza, M.J., Valley, J.W., Kohn, M.J., Girard, J.P., and Fouillac, A.M., 1998, The rapid heating, defocused beam technique: a CO2-laser-based method for highly precise and accurate determination of δ18O values of quartz: Chemical Geology, v. 144, p. 195–203, doi: 10.1016/S0009-2541(97)00131-9.

Stacey, J.S., and Kramers, J.D., 1975, Approximation of terrestrial lead isotope evolution by a two-stage model: Earth and Planetary Science Letters, v. 26, p. 207–221, doi: 10.1016/0012-821X(75)90088-6.

Stern, R.J., and Scholl, D.W., 2010, Yin and yang of continental crust creation and destruction by plate tectonic processes: International Geology Review, v. 52, p. 1–31, doi: 10.1080/00206810903332322.

Tollo, R.P., Aleinikoff, J.N., Bartholomew, M.J., and Rankin, D.W., 2004, Neoproterozoic A-type granitoids of the central and southern Appalachians: intraplate magmatism associated with episodic rifting of the Rodinian supercontinent: Precambrian Research, v. 128, p. 3–38, doi: 10.1016/j.precamres.2003.08.007.

Tollo, R.P., Aleinikoff, J.N., Borduas, E.A., Dickin, A.P., McNutt, R.H., and Fanning, C.M., 2006, Grenvillian magmatism in the northern Virginia Blue Ridge: Petrologic implications of episodic granitic magma production and the significance of postorogenic A-type charnockite: Precambrian Research, v. 151, p. 224–264, doi: 10.1016/j.precamres.2006.08.010.

Tollo, R.P., Aleinikoff, J.N., Dickin, A.P., Radwany, M.S., Southworth, C.S., and Fanning, C.M., 2017, Petrology and geochronology of Mesoproterozoic basement of the Mount Rogers area of southwestern Virginia and northwestern North Carolina: Implications for the Precambrian tectonic evolution of the southern Blue Ridge province: American Journal of Science, v. 317, p. 251–337, doi: 10.2475/03.2017.01.

Tollo, R.P., Aleinikoff, J.N., Mundil, R., Southworth, C.S., Cosca, M.A., Rankin, D.W., Rubin, A.E., Kentner, A.E., Parendo, C.A., and Ray, M.S., 2012, Igneous activity, metamorphism, and deformation in the Mount Rogers area of SW Virginia and NW North Carolina: A geologic record of Precambrian tectonic evolution of the southern Blue Ridge Province, *in* Eppes, M.C. and Bartholomew, M.J. eds., From the Blue Ridge to the Coastal Plain: Field Excursions in the Southeastern United States, Geological Society of America, Field Guide, v. 29, p. 1–66, doi: 10.1130/2012.0029(01).

Ustaomer, P.A., Ustaomer, T., Gerdes, A., Robertson, A.H.F., and Collins, A.S., 2012, Evidence of Precambrian sedimentation/magmatism and Cambrian metamorphism in the Bitlis Massif, SE Turkey utilising whole-rock geochemistry and U–Pb LA-ICP-MS zircon dating: Gondwana Research, v. 21, p. 1001–1018, doi: 10.1016/j.gr.2011.07.012.

Valley, J.W., 2003, Oxygen isotopes in zircon: Reviews in Mineralogy and Geochemistry, v. 53, p. 343–385, doi: 10.2113/0530343.

Valley, J.W., Bindeman, I.N., and Peck, W.H., 2003, Empirical calibration of oxygen isotope fractionation in zircon: Geochimica et Cosmochimica Acta, v. 67, p. 3257–3266, doi: 10.1016/S0016-7037(03)00090-5.

Valley, J.W., Kinny, P.D., Schulze, D.J., and Spicuzza, M.J., 1998, Zircon megacrysts from kimberlite: oxygen isotope variability among mantle melts: Contributions to Mineralogy and Petrology, v. 133, p. 1–11, doi: 10.1007/s004100050432.

Valley, J.W., and Kita, N.T., 2009, In situ oxygen isotope geochemistry by ion microprobe, *in* Fayek, M. ed., Secondary ion mass spectrometry in the earth sciences, MAC Short Course, v. 41, p. 19–63.

Valley, J.W., Kitchen, N., Kohn, M.J., Niendorf, C.R., and Spicuzza, M.J., 1995, UWG-2, a garnet standard for oxygen isotope ratios: Strategies for high precision and accuracy with laser heating: Geochimica et Cosmochimica Acta, v. 59, p. 5223–5231, doi: 10.1016/0016-7037(95)00386-X.

Verma, S.P., Pandarinath, K., Verma, S.K., and Agrawal, S., 2013, Fifteen new discriminant-function-based multi-dimensional robust diagrams for acid rocks and their application to Precambrian rocks: Lithos, v. 168–169, p. 113–123, doi: 10.1016/j.lithos.2013.01.014.

Verma, S.P., and Verma, S.K., 2013, First 15 probability-based multidimensional tectonic discrimination diagrams for intermediate magmas and their robustness against postemplacement compositional changes and petrogenetic processes: Turkish

Journal of Earth Sciences, v. 22, p. 931–995, doi: 10.3906/yer-1204-6.

Vervoort, J.D., Kemp, A., Fisher, C., and Bauer, A., 2016, Development of the depleted mantle reservoir and growth of the continental crust begins at ~ 3.8 Ga, Paper 5223, 35th International Geological Congress, Cape Town, South Africa.

Wang, X.-L., Coble, M.A., Valley, J.W., Shu, X.-J., Kitajima, K., Spicuzza, M.J., and Sun, T., 2014, Influence of radiation damage on Late Jurassic zircon from southern China: Evidence from in situ measurements of oxygen isotopes, laser Raman, U–Pb ages, and trace elements: Chemical Geology, v. 389, p. 122–136, doi: 10.1016/j.chemgeo.2014.09.013.

Woodhead, J.D., and Hergt, J.M., 2005, A preliminary appraisal of seven natural zircon reference materials for in situ Hf isotope determination: Geostandards and Geoanalytical Research, v. 29, p. 183–195, doi: 10.1111/j.1751-908X.2005.tb00891.x.

FIGURE CAPTIONS

1. (A) Generalized geologic map of the Appalachian Orogen. (B) Tectonic provinces of central Virginia and neighboring areas. Both maps modified from Hibbard et al. (2006).
2. Geologic map of the central part of the Goochland Terrane, central Virginia. Modified from Marr (2002) and Owens et al. (2010).
3. Photomicrographs of thin sections from each of the studied Goochland Terrane units. In (A), all minerals in the field of view are plagioclase feldspar. The grain at left is antiperthite. All photographs at the same scale. All images taken in cross-polarized light except (F). Mineral abbreviations: afs-alkali feldspar, amp-amphibole, bt-biotite, grt-garnet, ms-muscovite, pl-plagioclase feldspar, q-quartz.
4. Classification diagram for the Sabot Amphibolite samples. Each square represents one of the whole rock analyses in Table S1. Element abundances were normalized to a 100% total, volatile-free. The Catoctin Formation fields, shown here for comparison to the Sabot Amphibolite, include the compositions of most extrusive rocks and related dikes in Espenshade (1986), Burton et al. (1995), Badger and Sinha (2004), Southworth et al. (2006), and Badger et al. (2010). Classification scheme from Le Maitre et al. (2002).
5. Tectonic discrimination diagrams for analyses of whole rocks. (A) Discrimination of tectonic setting for the felsic samples from the State Farm Gneiss and Neoproterozoic granitoid using combined immobile major and trace elements (Verma et al., 2013). Six of the eleven State Farm Gneiss samples plot in the within-plate field (combined continental rift and ocean island field). Discriminant functions given in Table S4. (B) Discrimination for the intermediate samples from the State Farm Gneiss and

Neoproterozoic granitoid using only major elements (Verma and Verma, 2013). Discriminant functions given in Table S5. (C) Discrimination for the mafic samples from the Sabot Amphibolite using only trace elements (Agrawal et al., 2008). Discriminant functions given in Table S8. The discriminant function values are dimensionless.

6. Photographs of the contact between a felsic and mafic layer in the Sabot Amphibolite. A) The contact is sharp and planar at the outcrop scale. B) Centimeter- to decimeter-scale layers in the felsic unit are visible due to their different colors. C) The contact is not planar at the microscopic scale. Sample 512001, cross-polarized light. D) Microscopic interfingering of the two compositions. Sample 512001, cross-polarized light. The scale is the same for each photomicrograph. Mineral abbreviations: afs-alkali feldspar, amp-amphibole, bt-biotite, chl-chlorite, ms-muscovite, pl-plagioclase feldspar, q-quartz, rt-rutile, zrn-zircon.
7. Images of four zircon crystals from Sabot Amphibolite felsic sample Sabot1. Grain numbers correspond to those in Table S9. The left-hand column contains backscattered electron images and the right-hand column contains cathodoluminescence images. Circles represent 10 μm-diameter laser ablation spots that yielded the $^{206}Pb/^{238}U$ date shown.
8. (A) and (B) Concordia plots for 10 μm-diameter zircon U/Pb analyses from Sabot Amphibolite felsic sample Sabot1. Pb* refers to radiogenic lead. In (A), analyses colored black are interpreted to result from lead loss and/or mixture of igneous and metamorphic zircon during laser ablation. (C) Weighted mean $^{206}Pb/^{238}U$ date (horizontal green bar) for the twelve low U/Th, concordant analyses of zircon cores

(vertical red bars) that we use to determine the eruption age of the volcanic protolith of the Sabot Amphibolite.

9. U/Th ratio versus ^{206}Pb/^{238}U date for all spot analyses of zircon from Sabot Amphibolite sample Sabot1. All analyses older than ca. 500 Ma came from grain cores. Analyses younger than ca. 453 Ma produced a wider range in U/Th ratio as well as a higher mean U/Th ratio than older analyses. Grain rims mostly have higher U/Th ratios than cores. Uncertainties are not shown for clarity but are included in Table S9. Pb* refers to radiogenic lead.

10. Whole rock initial εNd values for the Goochland Terrane Proterozoic units. Only the Sabot Amphibolite protolith had initial εNd values near depleted mantle values at the time of intrusion or eruption. The Catoctin Formation meta-basalt field encompasses values calculated at 570 Ma in Badger et al. (2010). The Blue Ridge meta-anorthosite field is the analysis of Roseland Anorthosite sample H-22-81 calculated at 1040 Ma (Pettingill et al., 1984). The Blue Ridge meta-granitoid field includes five analyses of 1018 Ma granitoid in Fullagar et al. (1997) and two analyses of 1056 and 1019 Ma granitoid in Fisher et al. (2010), all calculated at 1030 Ma. The three fields for Blue Ridge Province rocks are shown for comparison to the values from the Goochland Terrane rocks.

11. Concordia diagrams for zircon from the Goochland samples (excluding sample Sabot1).

12. Plot of zircon εHf value at the time of zircon crystallization versus the age of zircon crystallization. All units except the State Farm Gneiss protolith received a melt component from the depleted mantle. The arrow showing the Hf isotopic evolution of the State Farm Gneiss whole rock was drawn using the average ^{176}Lu/^{177}Hf ratio of upper continental crust, 0.0125 (Chauvel et al., 2014). The numbered points and

vertical arrows refer to the processes illustrated in Figure 15; “mixing” means intermingling of material from the sources at the tails of the vertical arrows. Black circles indicate analyses of inherited zircon. “s.e.” is standard error. The error bar is an average for all the analyses; individual errors are given in Table S2.

13. Backscattered electron (left column) and cathodoluminescence (right column) images of some zircon grains from each of the Goochland Terrane samples excluding sample Sabot1. The circle indicates the analysis spot, which had a diameter of 15 μm for O and 30 or 40 μm for U/Pb and Hf isotopes. The date is the $^{206}Pb/^{207}Pb$ date.
14. Oxygen isotope values from spots in zircon interpreted to be values formed during initial zircon crystallization in the magma chamber for the indicated igneous unit. The plot does not include spots in xenocrystic, metamorphic, or altered zircon. Mantle zircon values from Valley et al. (1998).
15. Illustration of the interpreted magmatic evolution of the Goochland Terrane during Proterozoic time. Only the State Farm Gneiss protolith magma was derived entirely from melting of preexisting crust. All other units were the result of mixing melt from the depleted mantle with preexisting crust.

TABLES

1. Zircon sample summary.

ELECTRONIC SUPPLEMENT

Tables

S1. Sabot Amphibolite element abundances.

S2. Zircon spot LASS U/Pb and Hf isotope data.

S3. O, U/Pb, and Hf isotope data summary.

S4. Tectonic discrimination of State Farm Gneiss felsic whole rock samples.

S5. Tectonic discrimination of State Farm Gneiss intermediate whole rock samples.

S6. Tectonic discrimination of Neoproterozoic granitoid felsic whole rock samples.

S7. Tectonic discrimination of Neoproterozoic granitoid intermediate whole rock samples.

S8. Tectonic discrimination of Sabot Amphibolite mafic whole rock samples.

S9. Sample Sabot1 zircon U/Pb isotope data.

S10. Sabot Amphibolite whole-rock Sm and Nd isotope data.

S11. Zircon spot O isotope data.

S12. Results of quartz-zircon O isotope thermometry.

Figures

S1. Concordia diagrams for reference zircon R33 and Temora.

S2. Plot of corrected OH/O versus $\delta^{18}O$ value for spots in non-xenocrystic zircon that was at least 80% concordant from sample 511004. The OH/O ratio was corrected assuming that reference zircon KIM-5 was water-free. Two slightly negative OH/O ratios were set to zero in this plot.

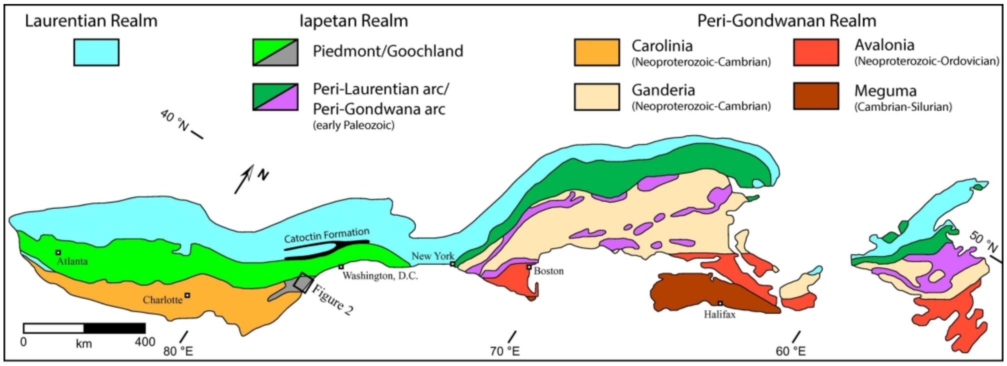

Figure 1 (Martin et al.)

Generalized geologic map of the Appalachian Orogen. Modified from Hibbard et al. (2006).

231x115mm (300 x 300 DPI)

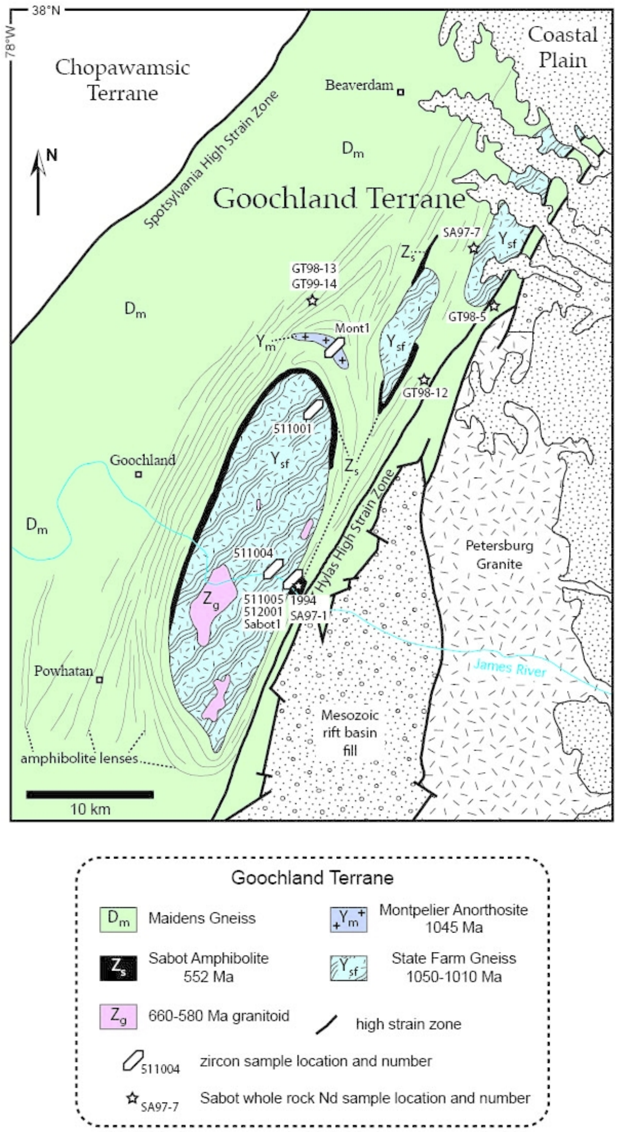

Figure 2 (Martin et al.)

Geologic map of the central part of the Goochland Terrane, central Virginia. Modified from Owens et al. (2010).

101x197mm (150 x 150 DPI)

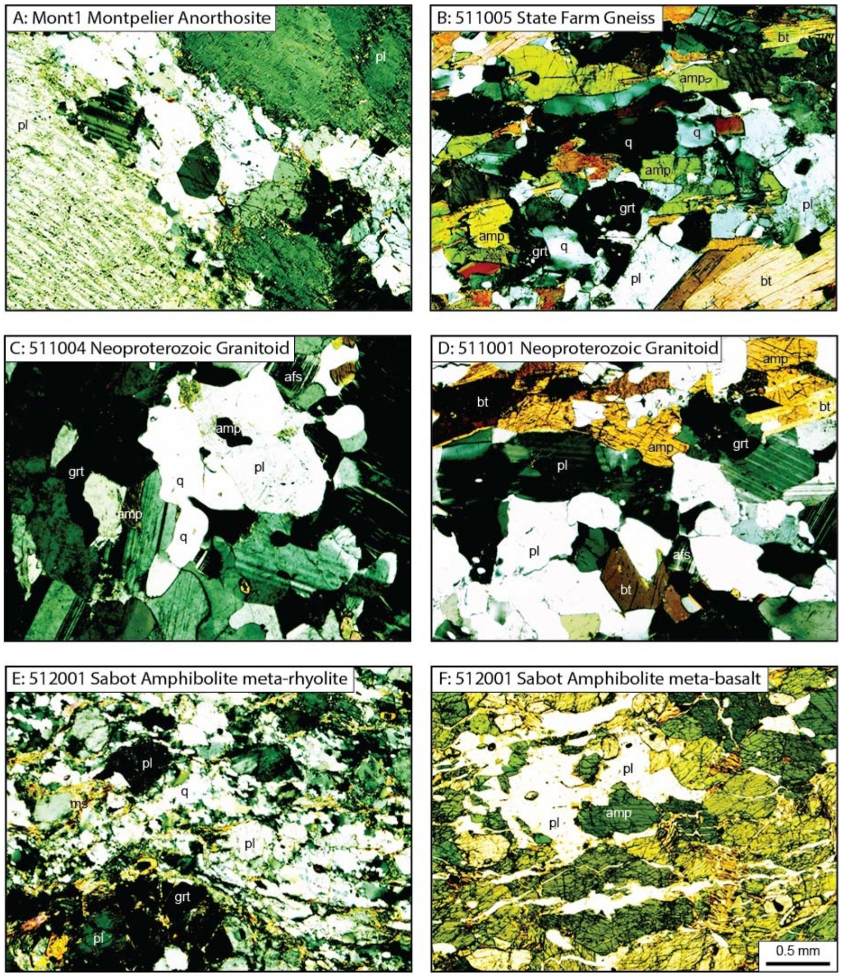

Figure 3 (Martin et al.)

Photomicrographs of thin sections from each of the studied Goochland Terrane units. In (A), all minerals in the field of view are plagioclase feldspar. All photographs at the same scale. All images taken in cross-polarized light except (F). Mineral abbreviations: afs-alkali feldspar, amp-amphibole, bt-biotite, grt-garnet, ms-muscovite, q-quartz.

156x225mm (150 x 150 DPI)

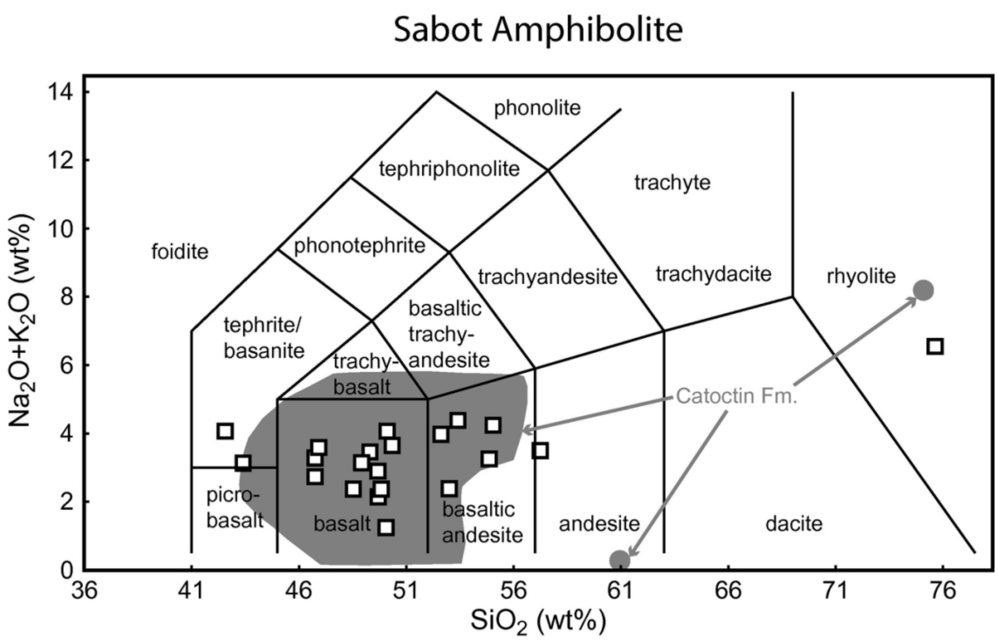

Figure 4 (Martin et al.)

Classification diagram for the Sabot Amphibolite samples. Each square represents one of the whole rock analyses in Table S1. Element abundances were normalized to a 100% total, volatile-free. The Catoctin Formation fields include the compositions of most extrusive rocks and related dikes in Espenshade (1986), Burton et al. (1995), Badger and Sinha (2004), Southworth et al. (2004), and Badger et al. (2010). Classification scheme from Le Maitre et al. (2002).

113x137mm (300 x 300 DPI)

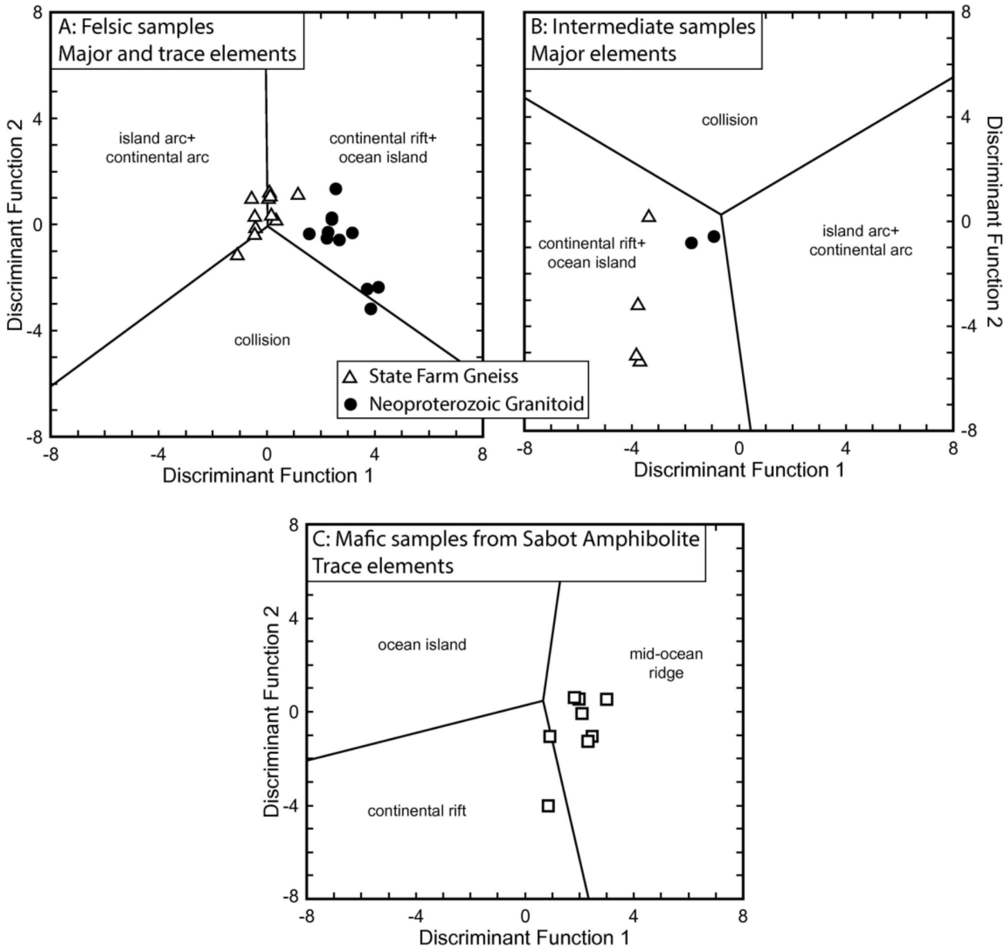

Tectonic discrimination diagrams for analyses of whole rocks. (A) Discrimination of tectonic setting for the felsic samples from the State Farm Gneiss and Neoproterozoic Granitoid using combined immobile major and trace elements (Verma et al., 2013). DF1 = $(-0.091 \times \ln(MgO/TiO_2)_{adj}) + (-0.228 \times \ln(P_2O_5/TiO_2)_{adj}) + (0.729 \times \ln(Nb/TiO_2)_{adj}) + (-0.237 \times \ln(Y/TiO_2)_{adj}) + (0.577 \times \ln(Zr/TiO_2)_{adj}) + 4.704$. DF2 = $(-0.268 \times \ln(MgO/TiO_2)_{adj}) + (-1.253 \times \ln(P_2O_5/TiO_2)_{adj}) + (-0.476 \times \ln(Nb/TiO_2)_{adj}) + (0.209 \times \ln(Y/TiO_2)_{adj}) + (-0.082 \times \ln(Zr/TiO_2)_{adj}) - 3.709$. (B) Discrimination for the intermediate samples from the State Farm Gneiss and Neoproterozoic Granitoid using only major elements (Verma and Verma, 2013). DF1 = $(-2.45605 \times \ln(TiO_2/SiO_2)_{adj}) + (1.11985 \times \ln(Al_2O_3/SiO_2)_{adj}) + (-2.22475 \times \ln(Fe_2O_3/SiO_2)_{adj}) + (2.48861 \times \ln(FeO/SiO_2)_{adj}) + (-0.212024 \times \ln(MnO/SiO_2)_{adj}) + (-0.06661 \times \ln(MgO/SiO_2)_{adj}) + (1.29066 \times \ln(CaO/SiO_2)_{adj}) + (-0.28377 \times \ln(Na_2O/SiO_2)_{adj}) + (-0.40211 \times \ln(K_2O/SiO_2)_{adj}) + (0.030635 \times \ln(P_2O_5/SiO_2)_{adj}) - 11.43097347$. DF2 = $(-0.57759 \times \ln(TiO_2/SiO_2)_{adj}) + (-0.01121 \times \ln(Al_2O_3/SiO_2)_{adj}) + (0.69125 \times \ln(Fe_2O_3/SiO_2)_{adj}) + (-1.99798 \times \ln(FeO/SiO_2)_{adj}) + (-1.72014 \times \ln(MnO/SiO_2)_{adj}) + (0.305275 \times \ln(MgO/SiO_2)_{adj}) + (0.816018 \times \ln(CaO/SiO_2)_{adj}) + (-1.791727 \times \ln(Na_2O/SiO_2)_{adj}) + (0.871298 \times \ln(K_2O/SiO_2)_{adj}) + (0.335479 \times \ln(P_2O_5/SiO_2)_{adj}) - 12.20158596$. (C) Discrimination for the mafic samples from the Sabot Amphibolite using only trace elements (Agrawal et al., 2008). DF1 = $-0.5558 \times \ln(La/Th) - 1.4260 \times \ln(Sm/Th) + 2.2935 \times \ln(Yb/Th) - 0.6890 \times \ln(Nb/Th) + 4.1422$. DF2 = $-0.9207 \times \ln(La/Th) + 3.6520 \times \ln(Sm/Th) - 1.9866 \times \ln(Yb/Th) + 1.0574 \times \ln(Nb/Th) - 4.4283$. The discriminant function values are dimensionless.

156x148mm (300 x 300 DPI)

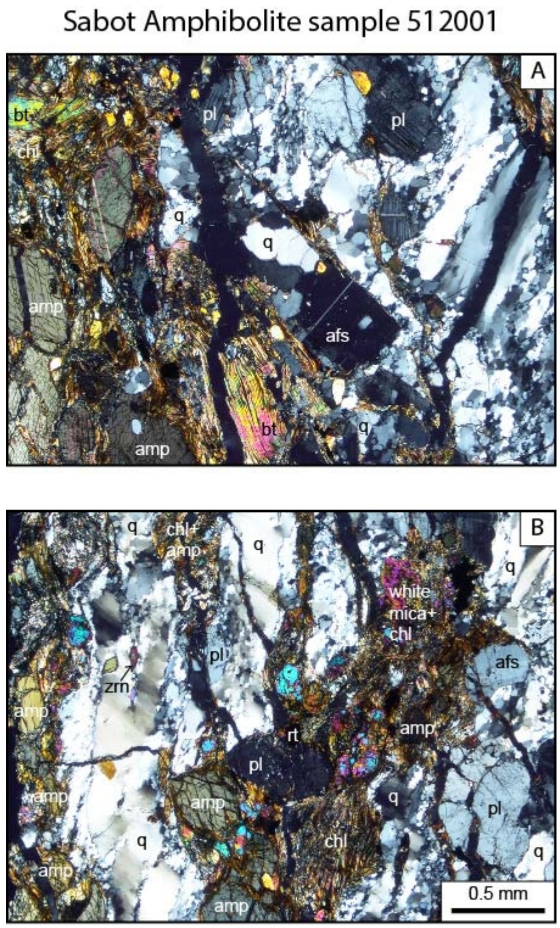

Figure 6 (Martin et al.)

Photomicrographs of the contact between a felsic and mafic layer in the Sabot Amphibolite. Part A shows that the contact is not planar at the microscopic scale. Part B shows microscopic interfingering of the two compositions. The scale is the same for each photograph and both were taken in cross-polarized light. Mineral abbreviations: afs-alkali feldspar, amp-amphibole, bt-biotite, chl-chlorite, ms-muscovite, q-quartz, rt-rutile, zrn-zircon.

76x166mm (150 x 150 DPI)

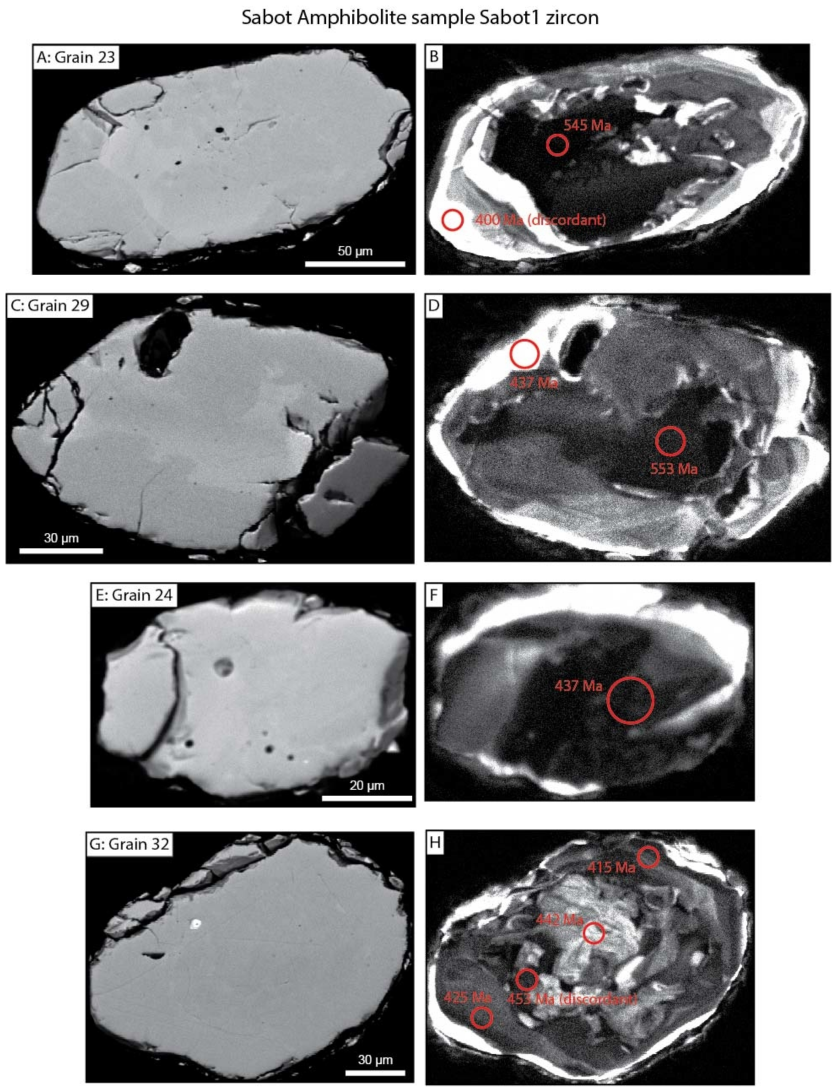

Figure 7 (Martin et al.)

Images of four zircon crystals from Sabot Amphibolite meta-rhyolite sample Sabot1. Grain numbers correspond to those in Table S9. The left-hand column contains backscattered electron images and the right-hand column contains cathodoluminescence images. Circles represent 10 µm-diameter laser ablation spots that yielded the 206Pb/238U date shown.

165x240mm (150 x 150 DPI)

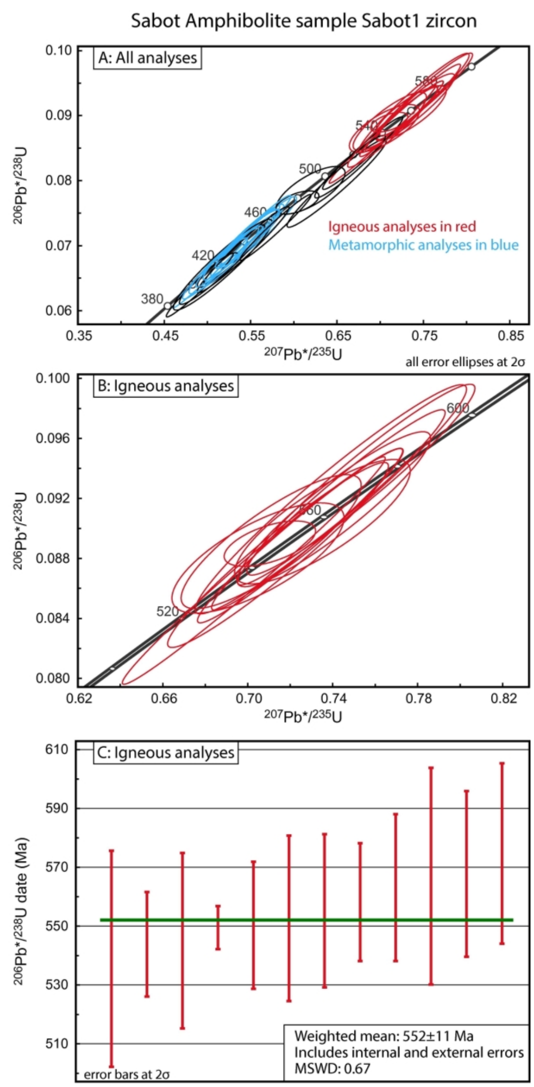

Figure 8 (Martin et al.)

(A) and (B) Concordia plots for 10 µm-diameter zircon U/Pb analyses from Sabot Amphibolite sample Sabot1. Pb* refers to radiogenic lead. In (A), analyses colored black are interpreted to result from lead loss and/or mixture of igneous and metamorphic zircon during laser ablation. (C) Weighted mean 206Pb/238U date (horizontal green bar) for the twelve low U/Th, concordant analyses of zircon cores (vertical red bars) that we use to determine the eruption age of the volcanic protolith of the Sabot Amphibolite.

108x248mm (300 x 300 DPI)

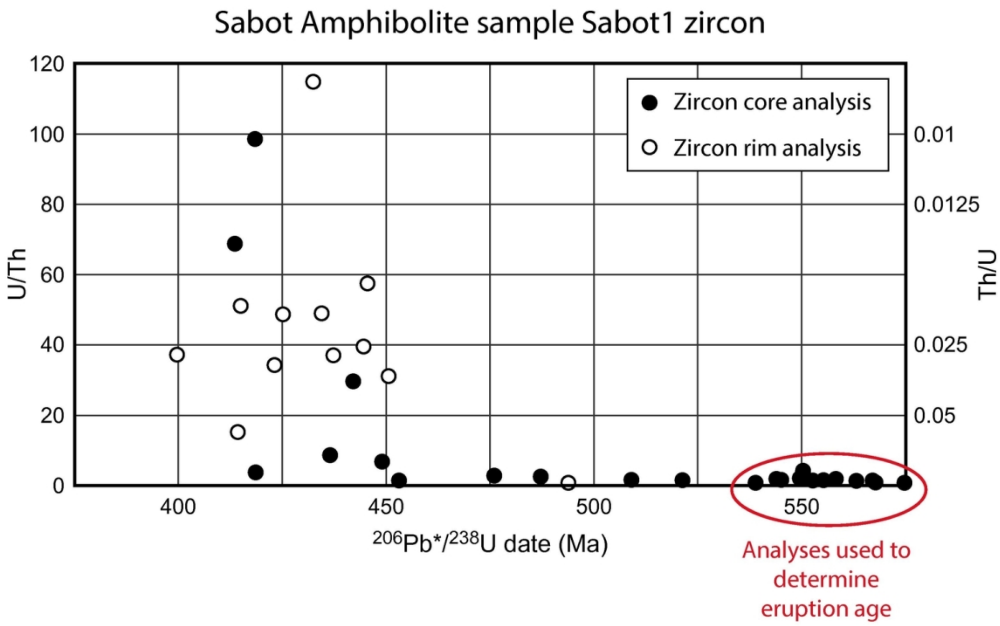

Figure 9 (Martin et al.)

U/Th ratio versus 206Pb/238U date for all spot analyses of zircon from Sabot Amphibolite sample Sabot1. All analyses older than ca. 500 Ma came from grain cores. Analyses younger than ca. 453 Ma produced a wider range in U/Th ratio as well as a higher mean U/Th ratio than older analyses. Grain rims mostly have higher U/Th ratios than cores. Uncertainties are not shown for clarity but are included in Table S9. Pb* refers to radiogenic lead.

130x125mm (300 x 300 DPI)

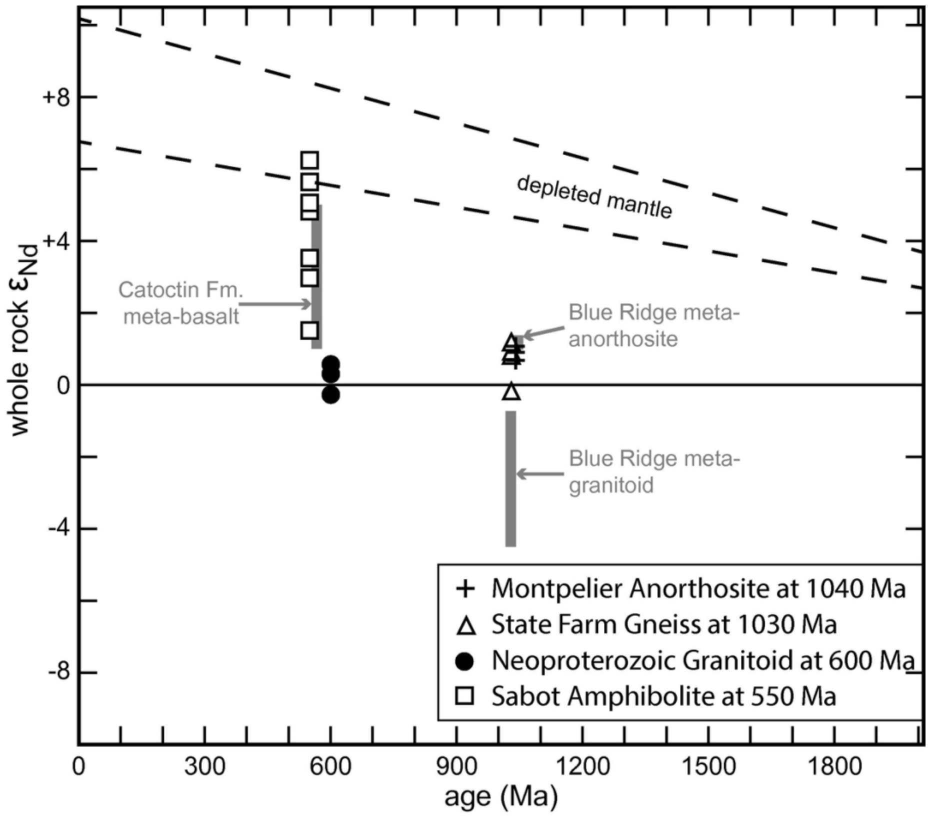

Figure 10 (Martin et al.)

Whole rock initial εNd values for the Goochland Terrane Proterozoic units. Only the Sabot Amphibolite protolith had initial εNd values near depleted mantle values at the time of intrusion or eruption. The Catoctin Formation meta-basalt field encompasses values calculated at 570 Ma in Badger et al. (2010). The Blue Ridge meta-anorthosite field is the analysis of Roseland Anorthosite sample H-22-81 calculated at 1040 Ma (Pettingill et al., 1984). The Blue Ridge meta-granitoid field includes five analyses of 1018 Ma granitoid in Fullagar et al. (1997) and two analyses of 1056 and 1019 Ma granitoid in Fisher et al. (2010), all calculated at 1030 Ma.

103x133mm (300 x 300 DPI)

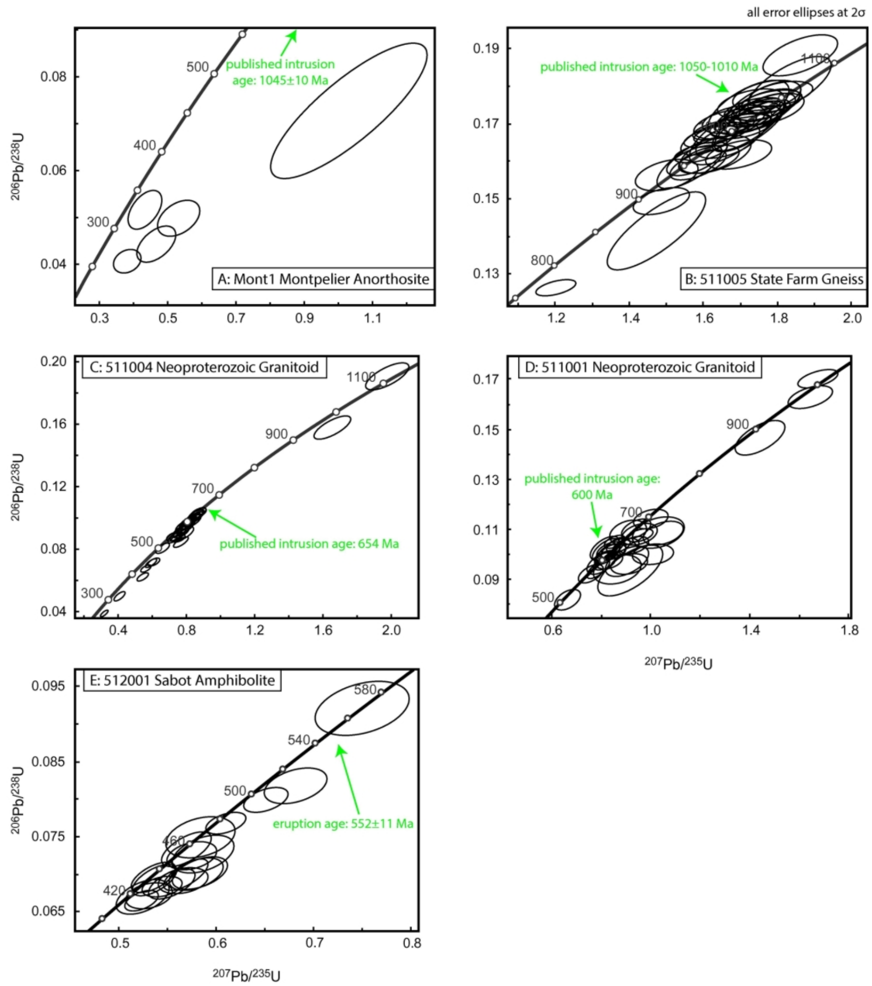

Figure 11 (Martin et al.)

Concordia diagrams for zircon from the Goochland samples (excluding sample Sabot1).

158x219mm (300 x 300 DPI)

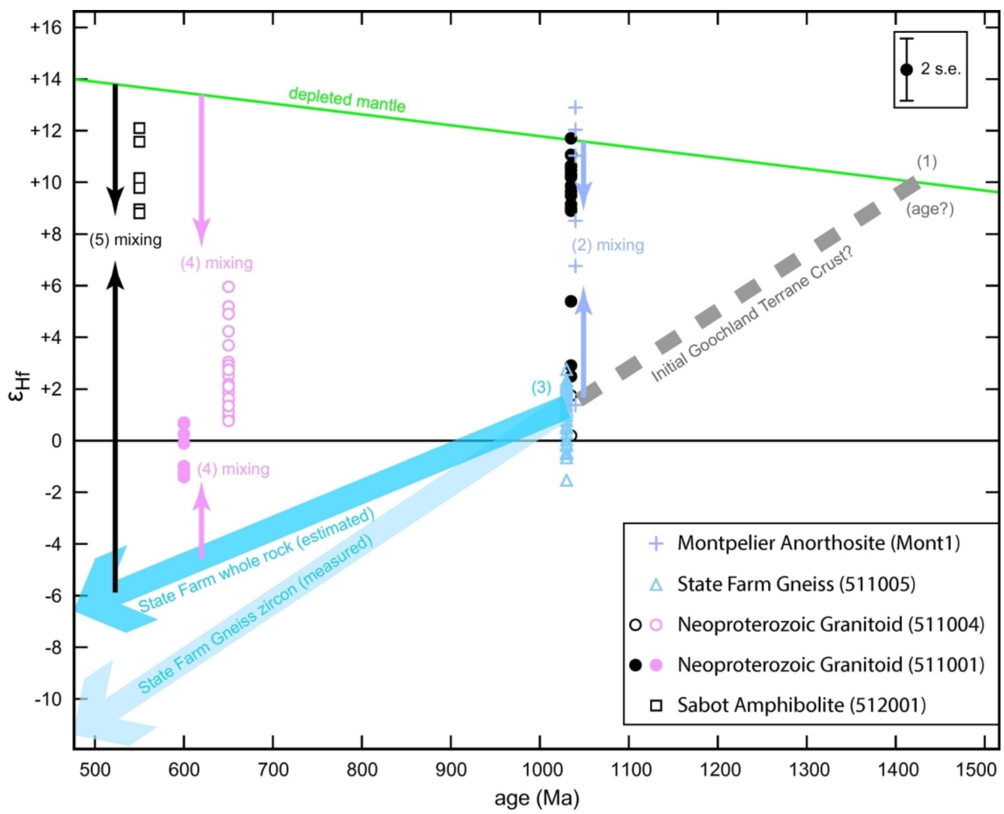

Figure 12 (Martin et al.)

Plot of zircon εHf value at the time of zircon crystallization versus the age of zircon crystallization. The arrow showing the Hf isotopic evolution of the State Farm Gneiss whole rock was drawn using the average 176Lu/177Hf ratio of upper continental crust, 0.0125 (Chauvel et al., 2014). All units except the State Farm Gneiss protolith received a melt component from the depleted mantle. "s.e." is standard error. The error bar is an average for all the analyses; individual errors are given in Table S2.

149x135mm (300 x 300 DPI)

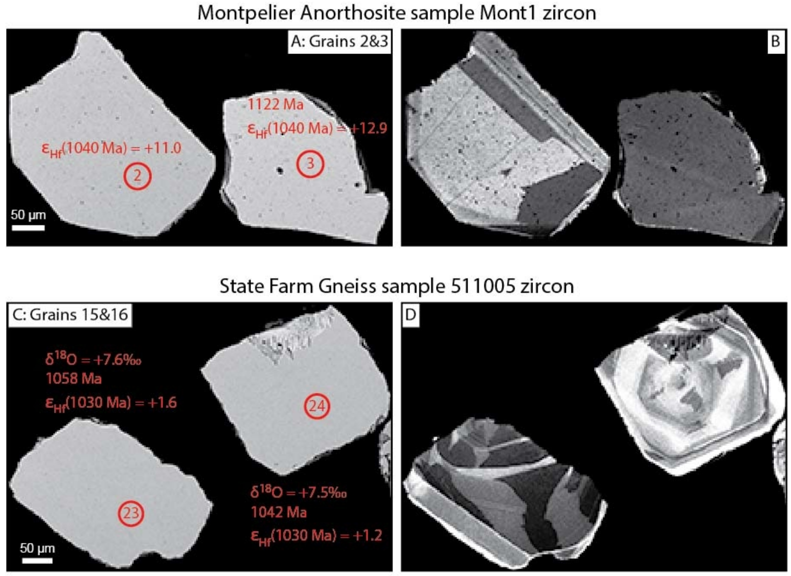

Figure 13 Page 1 (Martin et al.)

Backscattered electron (left column) and cathodoluminescence (right column) images of some zircon grains from each of the Goochland Terrane samples excluding sample Sabot1. The circle indicates the analysis spot, which had a diameter of 15 µm for O and 30 or 40 µm for U/Pb and Hf isotopes. The age is the 206Pb/207Pb age.

154x237mm (150 x 150 DPI)

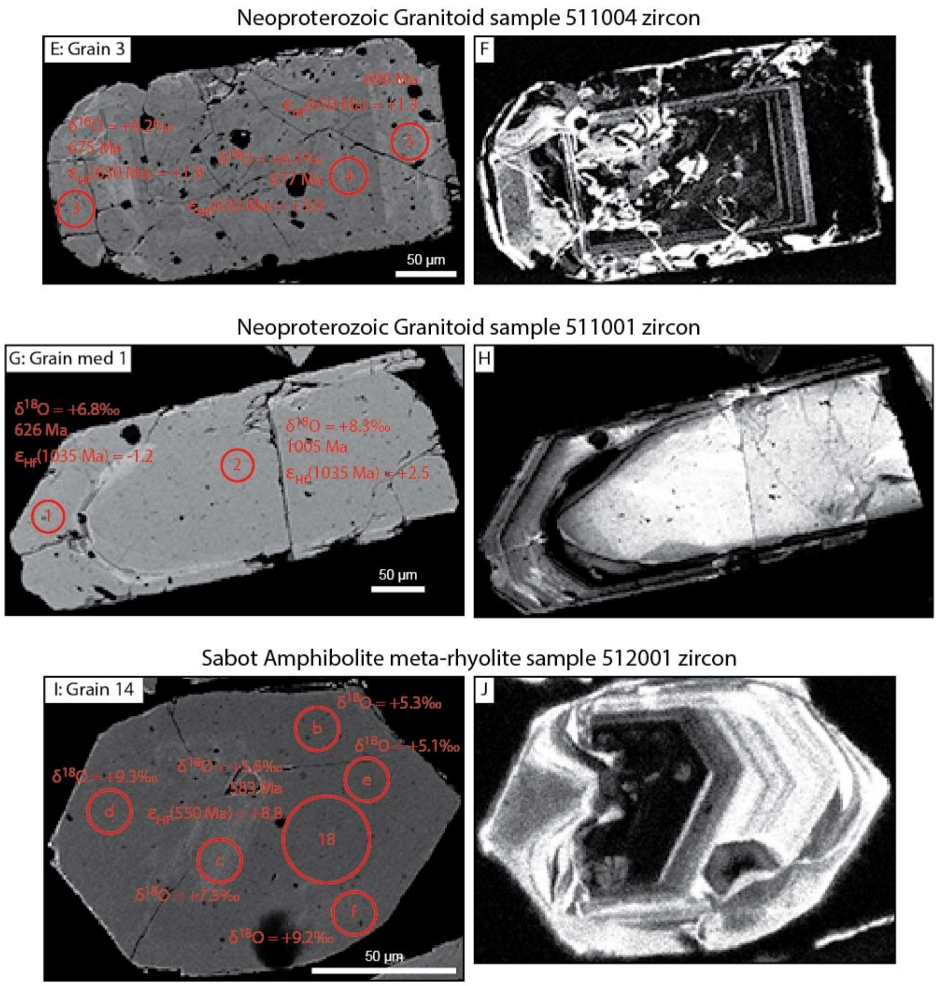

Figure 13 Page 2 (Martin et al.)

168x217mm (150 x 150 DPI)

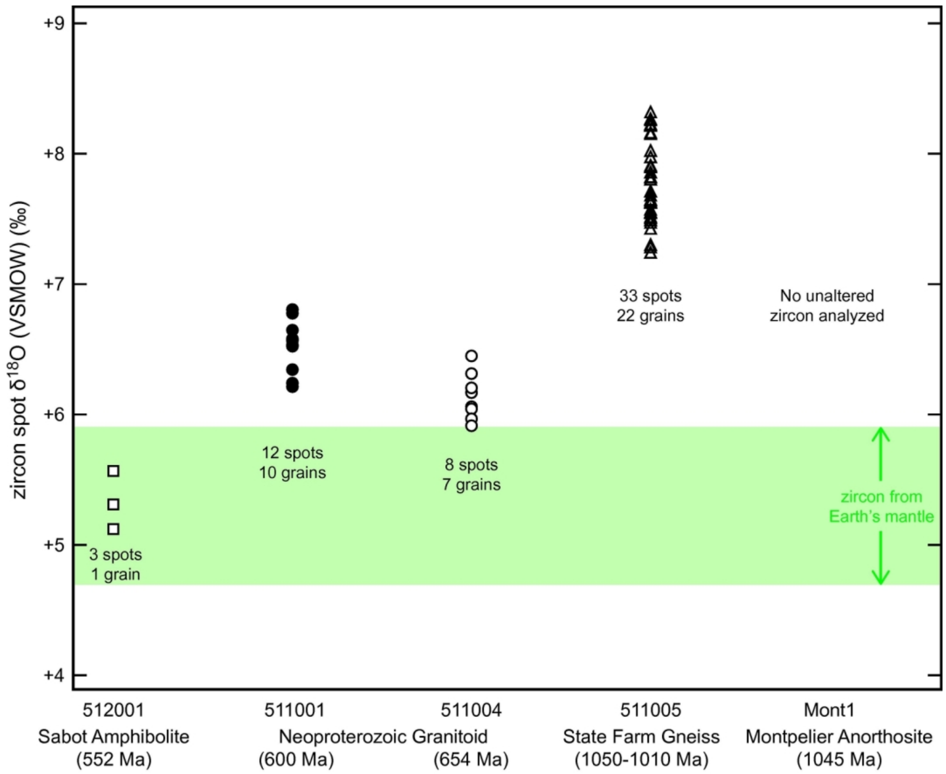

Figure 14 (Martin et al.)

Oxygen isotope values from spots in zircon interpreted to be values formed during initial zircon crystallization in the magma chamber for the indicated igneous unit. The plot does not include spots in xenocrystic, metamorphic, or altered zircon. Mantle zircon values from Valley et al. (1998).

141x179mm (300 x 300 DPI)

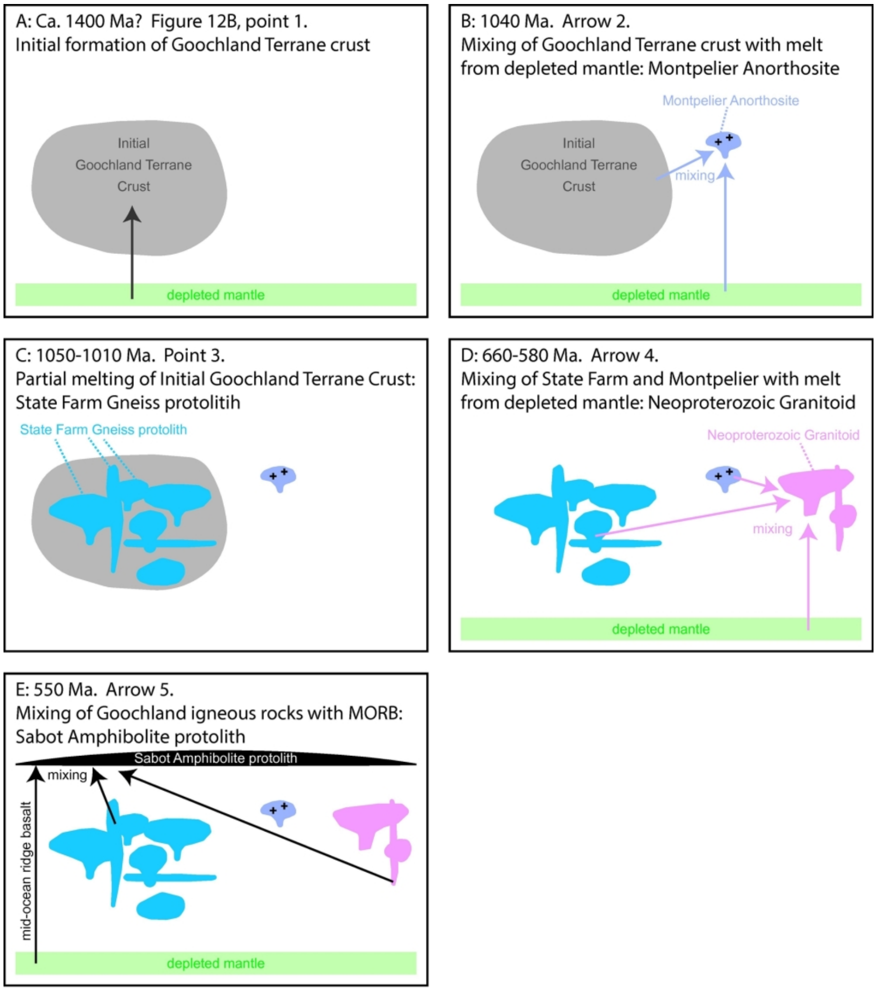

Figure 15 (Martin et al.)

Illustration of the interpreted magmatic evolution of the Goochland Terrane during Proterozoic time. Only the State Farm Gneiss protolith magma was derived entirely from melting of preexisting crust. All other units were the result of mixing melt from the depleted mantle with preexisting crust.

156x215mm (300 x 300 DPI)

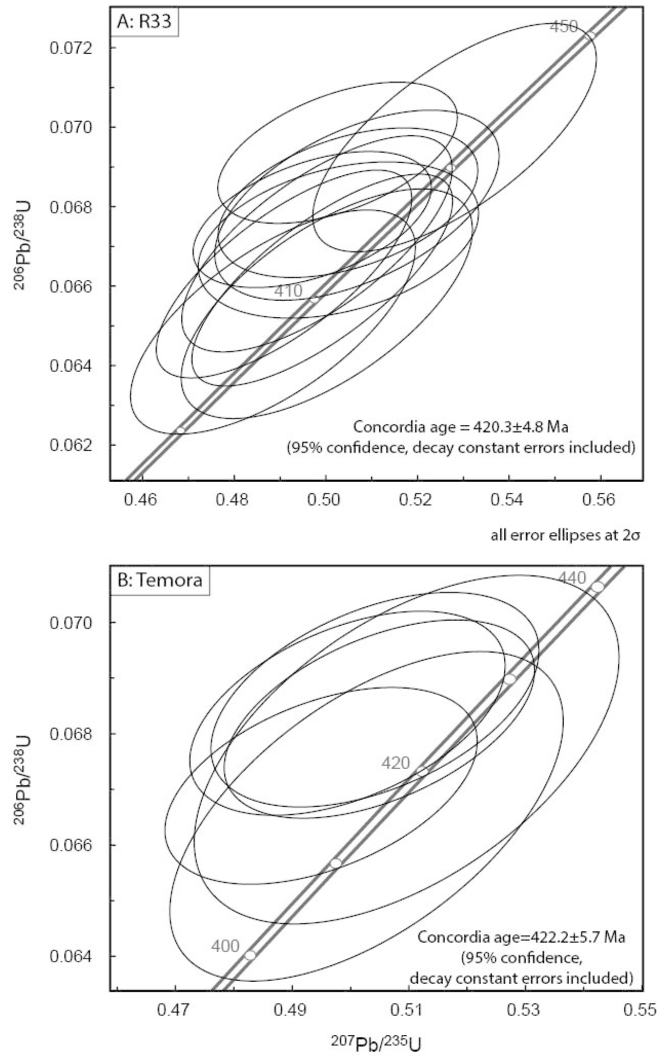

Figure S1 (Martin et al.)

107x197mm (150 x 150 DPI)

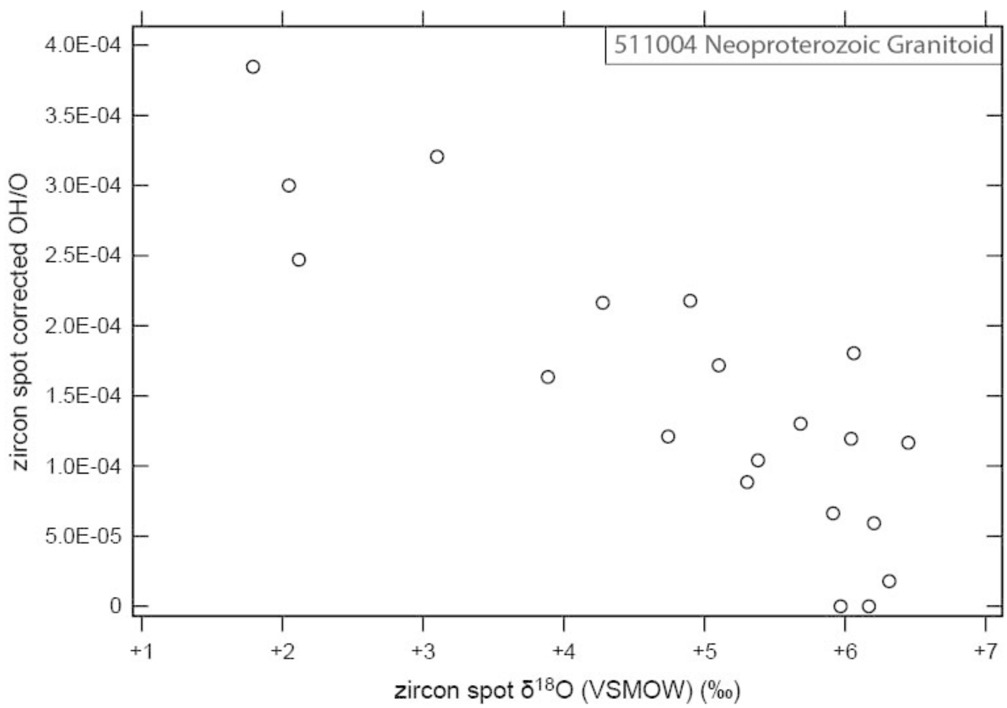

Figure S2 (Martin et al.)

128x141mm (150 x 150 DPI)

TABLE 1. ZIRCON SAMPLE SUMMARY

Sample number	Unit name	Protolith	Latitude °N	Longitude °W	Number of zircon in situ O analyses	Number of zircon in situ Hf analyses
Mont1	Montpelier Anorthosite	Anorthosite	37.77308	77.70949	17	6
511005	State Farm Gneiss	Granite	37.60992	77.74598	48	38
511004	Neoproterozoic granitoid	Syenite	37.61991	77.76598	46	23
511001	Neoproterozoic granitoid	Syenite	37.73087	77.73773	41	28
512001	Sabot Amphibolite[a]	Felsic layer	37.60992	77.74598	39	14
Sabot1	Sabot Amphibolite[a]	Felsic layer	37.60992	77.74598	not analyzed	not analyzed
				Totals:	**191**	**109**

Oxygen isotopes were analyzed at the University of Wisconsin Madison.
Hf and U/Pb isotopes from all samples except "Sabot1" were analyzed at Washington State University.
U/Pb isotopes in zircon from sample "Sabot1" were analyzed at the Arizona LaserChron Center.
[a]Zircon was extracted from a felsic layer within the Sabot Amphibolite.

Intrusion or eruption age (Ma)	Intrusion or eruption age reference
1045 ± 10	Aleinikoff et al., 1996
ca. 1050-1010	Owens and Tucker, 2003
ca. 654	Owens and Tucker, 2003
600 +7/-9	Owens and Tucker, 2003
552 ± 11	this study
552 ± 11	this study
analyses from 5 samples	

	SA-001	SA-002	SA-003	SA-004	SA-005	SA-006	SA-007	SA-008
XRF data (major and minor elements in weight percent, trace elements in parts per million)								
SiO2	49.69	46.21	49.38	42.73	42.21	53.08	46.22	46.58
TiO2	1.96	3.44	1.07	1.78	1.08	0.29	1.77	2.22
Al2O3	13.70	13.33	15.48	15.36	18.47	16.10	14.76	14.51
Fe2O3	13.44	18.58	15.64	18.01	16.54	8.20	13.43	14.66
MnO	0.21	0.27	0.27	0.35	0.23	0.17	0.23	0.19
MgO	5.90	4.48	4.94	5.96	5.60	6.53	8.27	7.09
CaO	10.02	8.82	9.66	11.08	10.94	10.65	11.24	10.18
Na2O	3.02	2.48	2.27	2.07	2.38	3.27	2.35	3.21
K2O	1.01	0.76	0.61	1.01	1.65	1.08	0.35	0.35
P2O5	0.21	0.46	0.08	0.09	0.06	0.01	0.24	0.28
LOI	0.41	0.81	0.52	1.46	0.62	0.33	0.60	0.39
Total	**99.57**	**99.64**	**99.92**	**99.90**	**99.78**	**99.71**	**99.46**	**99.66**
Sn	<2	3.1	<2.2	<2.3	<2.2	2.2	<2.1	2.4
Nb	13.7	14.2	<1	3.6	<1	<0.7	5.9	5.9
Zr	142.4	217.2	16.9	12.8	17.7	17.3	106.0	120.4
Y	26.8	64.0	14.0	12.7	13.7	10.1	30.4	31.6
Sr	252.0	133.8	116.4	74.3	122.9	114.1	256.4	223.3
Rb	14.9	10.0	11.5	28.3	15.9	13.2	7.6	3.4
Pb	8.3	<3.2	6.2	5.7	12.2	6.1	4.0	<3
Ga	20.7	21.4	19.0	22.0	22.6	11.7	17.0	18.1
Zn	113.4	178.3	123.0	133.0	146.0	60.6	105.9	116.1
Ni	70.3	53.2	11.4	12.2	6.9	17.7	131.9	75.3
V	329.6	446.1	387.6	505.4	525.0	199.5	297.4	330.6
Cr	74.0	48.2	13.2	<9	8.9	12.9	287.2	194.7
Ba	111.1	169.2	175.8	95.8	135.2	146.7	123.4	171.3
Co	43.2	49.2	38.6	43.6	41.4	35.7	49.1	46.4
INAA data (major elements in weight percent, trace elements in parts per million)								
Na2O	2.75	2.23	2.16	1.85	2.18	3.22	2.44	3.03
K2O	0.90	1.00	0.60	0.00	1.60	0.90	0.50	0.30
CaO	9.70	9.70	10.60	12.50	11.50	11.00	12.10	10.80
Sc	39.00	53.40	47.80	61.80	57.30	43.80	39.40	39.90
Cr	94.30		30.00	7.70	2.10	36.10	292.00	199.60
FeO	12.07	16.78	14.02	16.47	14.93	7.36	12.11	13.14
Co	45.70	51.50	40.10	41.60	42.00	36.30	51.00	46.60
Ni	80.00	100.00	0.00	10.00	10.00	20.00	110.00	72.00
As	0.00	0.00	0.60	0.40	0.00	0.00	1.10	0.20
Se	0.00	0.00	0.00	0.00	0.00	0.00	1.20	0.00
Br	0.50	0.00	0.00	0.40	0.10	0.30	0.30	0.30
Rb	17.00	19.00	13.00	29.00	20.00	14.00	10.00	9.00
Sr	220.00	90.00	95.00	0.00	140.00	120.00	290.00	240.00
Zr	180.00	230.00	0.00	20.00	30.00	0.00	120.00	100.00
Sb	0.04	0.00	0.12	0.04	0.03	0.00	0.00	0.01
Cs	0.10	0.13	0.08	0.34	0.08	0.00	0.01	0.05
Ba	125.00	203.00	173.00	100.00	150.00	128.00	134.00	173.00
La	17.27	14.84	2.61	2.64	4.19	7.30	7.33	8.64

Ce	37.40	36.80	6.20	5.90	11.10	8.50	17.40	21.80
Nd	24.00	32.00	2.00	7.00	16.00	6.00	13.00	14.00
Sm	5.60	8.42	1.59	1.55	2.23	1.53	4.06	4.95
Eu	1.69	2.75	0.83	0.96	0.84	0.47	1.45	1.87
Tb	0.97	1.82	0.39	0.39	0.45	0.29	0.83	0.99
Yb	2.86	6.60	1.53	1.41	1.64	1.13	3.08	3.29
Lu	0.42	0.95	0.25	0.23	0.25	0.18	0.46	0.48
Hf	4.00	6.05	0.60	0.52	0.72	0.72	2.92	3.39
Ta	0.86	0.96	0.09	0.32	0.02	0.21	0.42	0.44
W	0.00	0.00	0.00	0.00	0.00	0.00	0.00	0.00
Au	0.00	0.00	0.00	0.00	0.00	0.10	5.00	1.00
Th	1.72	0.99	0.54	0.33	0.41	2.81	0.32	0.39
U	0.38	0.42	0.28	0.84	0.34	0.49	0.14	0.03
Pr								
Gd								
Dy								
Ho								
Er								
Tm								

All rare earth elements as well as Sn, Nb, Pb, Ga, and Zn in samples GT00-20 and GT03-23 were analyzed by ICPMS.

TABLE S1. SABOT AMPHIBOLITE ELEMENT ABUNDANCES

SA-009	SA-010	SA-011	SA-012	GT98-004	GT98-005	GT98-010	GT98-012	GT98-013
48.91	52.21	49.94	48.30	54.83	56.50	54.68	49.16	49.53
1.76	1.35	0.73	1.30	1.27	0.76	1.47	0.54	0.17
14.76	15.70	14.93	14.06	15.27	15.89	14.65	15.66	15.68
11.97	9.78	11.11	13.03	14.18	11.05	12.78	7.12	4.10
0.20	0.19	0.18	0.24	0.31	0.21	0.18	0.12	0.08
7.24	5.13	8.44	8.18	2.94	3.40	4.01	9.48	11.32
10.74	10.57	10.19	10.45	7.76	7.37	7.25	14.68	16.83
2.72	3.31	2.92	2.50	2.92	3.07	3.24	1.97	1.04
0.71	0.63	0.70	0.60	0.33	0.38	0.97	0.15	0.19
0.18	0.35	0.05	0.06	0.13	0.07	0.11	0.04	0.00
0.46	0.44	0.60	0.82	0.35	0.79	0.59	0.32	0.41
99.65	**99.66**	**99.79**	**99.54**	**100.29**	**99.49**	**99.93**	**99.24**	**99.35**
<2.1	4.0	<2	<2.1	<4.2	<4.0	<4.0	5.3	<4.8
4.8	12.2	<2	<1	<3.1	<1.4	2.3	<1.4	<1.4
116.2	188.3	31.1	38.9	30.6	45.5	58.5	23.9	2.0
31.9	48.1	17.4	16.6	17.5	22.4	25.3	11.9	4.8
265.1	410.2	204.1	126.4	118.3	109.0	240.4	113.4	70.2
6.8	4.7	7.1	11.3	5.0	4.0	16.4	<3.2	4.9
9.5	10.2	6.8	<3	<8.8	<5.7	<7.3	<6.0	<5.1
18.9	20.2	13.4	15.8	15.8	16.0	17.1	10.2	7.1
112.8	93.9	47.1	94.3	108.4	82.8	39.6	28.3	16.5
124.7	89.0	95.1	91.7	<5.8	<8.8	9.1	118.8	256.5
275.8	170.3	202.9	350.3	179.6	181.5	404.5	183.4	136.8
267.0	184.5	199.3	179.7	<16	<16.4	<17	421.9	1121.7
94.2	89.3	66.8	33.7	34.6	50.4	159.4	180.6	122.7
46.9	35.4	43.9	52.3	18.9	25.8	29.7	39.7	33.4
2.58	3.32	2.95	2.67	2.87	3.24	3.20	1.91	0.79
0.60	0.50	0.90	0.60	0.80	0.21	0.70	0.10	0.26
11.50	10.90	10.90	11.10	8.40	7.80	7.60	15.10	16.80
38.50	27.70	42.80	46.80	40.30	34.80	36.30	43.10	48.90
276.00	185.40	212.00	173.00	3.30	8.50	10.80	412.00	1047.00
10.83	8.64	9.95	11.87	12.74	9.70	11.39	6.40	3.63
43.20	32.90	46.20	52.70	21.20	27.80	32.40	38.40	34.00
110.00	90.00	130.00	90.00	0.00	30.00	20.00	110.00	243.00
0.20	1.00	0.00	0.50	0.00	0.00	0.00	0.30	0.40
0.00	0.40	0.00	0.00	0.40	0.00	0.00	0.00	0.00
0.00	0.20	0.20	0.20	0.10	0.25	0.20	0.09	0.00
11.00	8.00	12.00	16.00	10.00	6.00	18.00	4.00	6.30
300.00	400.00	240.00	150.00	122.00	110.00	260.00	140.00	87.00
120.00	220.00	40.00	90.00	40.00	60.00	100.00	0.00	0.00
0.03	0.00	0.05	0.02	0.01	0.02	0.01	0.00	0.01
0.06	0.00	0.10	0.00	0.07	0.05	0.05	0.01	0.12
93.00	97.00	51.00	70.00	46.00	39.00	162.00	162.00	95.00
10.70	48.00	2.75	2.63	3.54	3.85	15.69	1.34	0.71

23.00	98.30	6.90	7.00	8.81	9.00	20.30	3.60	1.19
16.00	46.00	7.00	5.00	3.00	9.00	14.00	4.00	1.00
5.01	10.86	2.03	1.99	2.46	2.75	3.78	1.27	0.58
1.54	2.03	0.86	0.85	1.16	0.99	1.26	0.51	0.29
1.03	1.67	0.49	0.53	0.61	0.63	0.77	0.35	0.17
3.61	4.95	1.89	2.02	2.43	2.96	2.92	1.39	0.70
0.53	0.72	0.28	0.29	0.35	0.44	0.44	0.21	0.10
3.32	6.08	1.12	1.31	1.07	1.82	1.92	0.75	0.24
0.29	0.74	0.12	0.08	0.05	0.09	0.23	0.03	0.02
0.10	0.00	0.40	0.00	0.30	0.00	0.10	0.10	0.10
0.00	0.00	0.00	0.00	0.00	0.10	0.00	0.20	0.90
0.82	9.57	0.21	0.18	0.43	0.77	1.38	0.09	0.03
0.22	2.56	0.03	0.04	0.19	0.24	0.52	0.05	0.03

GT99-014	GT99-015	GT00-20	GT03-23	Approximate Detection Limit	Analysis of basalt standard WS-E
49.43	52.54	48.09	75.01		51.40
1.27	1.19	1.13	0.18		2.49
13.44	15.04	16.32	12.43		13.74
13.33	10.37	11.93	3.44		13.28
0.22	0.18	0.16	0.03		0.16
7.32	6.91	7.79	0.19		5.66
11.72	10.36	11.18	1.38		8.94
1.92	2.10	1.63	2.68		2.56
0.43	0.26	0.72	3.81		1.01
0.10	0.18	0.13	0.03		0.32
0.34	0.37	0.63	0.68		not reported
99.52	**99.50**	**99.71**	**99.85**		
<7.6	<4.8	<4.4	8	4.8	17
3.3	6.8	3.6	50.2	1.8	17
58.4	53.9	57.9	384	2.0	197
25.1	25.2	11.7	137	2.4	29
157.7	195.7	585.3	71	2.6	418
4.3	3.1	15.4		2.2	25
<8.9	<8.0	<7.4	<5	6.4	11
13.7	14.7	18.4	29	2.6	23
88.0	80.1	81.9	70	3.2	112
71.8	69.7	82.4		6.8	58
362.5	260.7	307.4	7	6.2	325
94.1	249.6	105.2		18.6	80
279.4	62.0	259.1	874	18	330
50.7	39.0	50.0		6.4	44
1.95	2.14	1.63			
0.00	0.00	0.75			
12.90	10.90	11.19			
53.80	39.60	35.00			
106.60	257.00	117.00	<20		
12.72	9.24				
53.10	36.80	48.00	<1		
80.00	70.00	73.00	<20		
0.00	0.10	<5	<5		
0.00	0.00				
0.10	0.30				
6.00	8.00	21.00	62.00		
130.00	210.00	612.00	76.00		
80.00	70.00	65.00	376.00		
0.00	0.04	-0.20	8.00		
0.04	0.02	0.30	0.20		
240.00	51.00	287.00	936.00		
3.60	8.47	18.60	54.21		

9.40	23.20	38.90	127.46
10.00	17.00	18.00	66.11
2.95	4.54	3.37	17.93
1.15	1.49	1.10	2.97
0.75	0.83	0.47	3.88
3.10	2.62	1.23	16.49
0.50	0.40	0.173	2.62
2.01	1.77	1.90	14.50
0.17	0.36	0.30	2.91
1.00	0.00	-0.50	<0.5
0.30	0.00		
0.17	0.89	3.50	9.71
0.12	0.36	0.80	1.77
		4.50	15.13
		3.12	20.04
		2.64	23.33
		0.52	4.80
		1.42	16.40
		0.206	2.62

TABLE S2. ZIRCON LASS URANIUM-LEAD AND LUTETIUM-HAFNIUM ISOTOPIC DATA

Analysis number	beam diam. (μm)	Isotope ratios							Apparent ages (Ma)				
		207Pb/235U	± 1σ	206Pb/238U	± 1σ	error corr.	207Pb/206Pb	± 1σ	207Pb/235U	± 1σ	206Pb/238U	± 1σ	207Pb/206Pb
Sample Mont1, Montpelier Anorthosite													
mont1_flu_1_1	-	-											
mont1_flu_2_2	-	-											
mont1_flu_3_3	40	0.5323	0.0253	0.0498	0.0016	0.411	0.0770	0.0035	433	17	313	10	1122
mont1_flu_4_4	40	0.4335	0.0202	0.0516	0.0017	0.497	0.0605	0.0025	366	14	324	10	623
mont1_flu_4_5	-	-											
mont1_flu_4_6	-	-											
mont1_flu_4_7	40	0.4668	0.0233	0.0443	0.0016	0.511	0.0760	0.0033	389	16	279	10	1094
mont1_flu_5_8	40	1.0307	0.0936	0.0727	0.0059	0.824	0.1022	0.0053	719	46	453	35	1664
mont1_flu_6_9	-	-											
mont1_flu_7_10	-	-											
mont1_flu_8_11	-	-											
mont1_flu_8_13	-	-											
mont1_flu_9_14	-	-											
mont1_flu_10_15	-	-											
mont1_flu_10_16	40	0.3816	0.0164	0.0407	0.0010	0.252	0.0677	0.0030	328	12	257	6	858
mont1_flu_10_17	-	-											
mont1_flu_11_18	-	-											
Sample 511005, State Farm Gneiss													
511005_big_2_1	40	1.5014	0.0349	0.1564	0.0017	0.410	0.0721	0.0015	931	14	937	9	990
511005_big_3_2	40	1.7272	0.0366	0.1754	0.0016	0.454	0.0740	0.0014	1019	14	1042	9	1040
511005_big_3_3	40	1.7282	0.0343	0.1712	0.0014	0.508	0.0758	0.0013	1019	13	1019	8	1090
511005_big_4_4	40	1.6458	0.0299	0.1684	0.0011	0.569	0.0734	0.0011	988	11	1003	6	1025
511005_big_5_5	40	1.6223	0.0298	0.1665	0.0012	0.582	0.0732	0.0011	979	11	993	7	1019
511005_big_5_6	40	1.7202	0.0358	0.1716	0.0017	0.558	0.0753	0.0013	1016	13	1021	9	1077
511005_big_6_7	40	1.5945	0.0292	0.1623	0.0011	0.579	0.0738	0.0011	968	11	970	6	1036
511005_big_6_8	40	1.7711	0.0366	0.1751	0.0017	0.544	0.0760	0.0013	1035	13	1040	9	1095
511005_big_7_9	40	1.2023	0.0223	0.1262	0.0009	0.552	0.0716	0.0011	802	10	766	5	974
511005_big_7_10	40	1.6589	0.0348	0.1700	0.0016	0.488	0.0733	0.0013	993	13	1012	9	1022
511005_big_7_11	40	1.6327	0.0390	0.1618	0.0021	0.534	0.0758	0.0015	983	15	967	12	1090
511005_big_8_12	40	1.6490	0.0301	0.1676	0.0011	0.578	0.0739	0.0011	989	11	999	6	1039
511005_big_8_13	40	1.8609	0.0414	0.1881	0.0022	0.577	0.0743	0.0014	1067	15	1111	12	1050
511005_big_9_14	40	1.6142	0.0336	0.1604	0.0015	0.514	0.0756	0.0014	976	13	959	8	1084
511005_big_9_15	40	1.4862	0.0308	0.1494	0.0014	0.474	0.0735	0.0013	925	12	898	8	1028
511005_big_10_16	40	1.6957	0.0366	0.1619	0.0016	0.435	0.0774	0.0015	1007	14	967	9	1131
511005_big_10_17	40	1.7013	0.0336	0.1693	0.0014	0.426	0.0743	0.0013	1009	13	1008	7	1048
511005_big_11_18	-	-											
511005_big_12_19	40	1.7059	0.0311	0.1701	0.0011	0.494	0.0741	0.0012	1011	12	1013	6	1043
511005_big_12_20	40	1.8087	0.0349	0.1781	0.0014	0.439	0.0750	0.0013	1049	13	1057	7	1069
511005_big_13_21	40	1.6819	0.0342	0.1712	0.0015	0.456	0.0726	0.0013	1002	13	1019	9	1002
511005_big_14_22	-	-											
511005_big_15_23	40	1.7557	0.0319	0.1738	0.0012	0.498	0.0746	0.0012	1029	12	1033	6	1058
511005_big_16_24	40	1.7401	0.0339	0.1736	0.0014	0.451	0.0740	0.0013	1024	12	1032	8	1042
511005_big_17_25	40	1.7842	0.0336	0.1761	0.0012	0.442	0.0748	0.0013	1040	12	1046	7	1064
511005_big_18_26	40	1.7709	0.0373	0.1776	0.0017	0.423	0.0737	0.0014	1035	14	1054	9	1033
511005_big_18_27	40	1.7823	0.0366	0.1741	0.0017	0.506	0.0756	0.0013	1039	13	1035	9	1086
511005_big_19_28	40	1.7420	0.0342	0.1726	0.0014	0.444	0.0746	0.0013	1024	13	1026	8	1057
511005_big_19_29	-	-											
511005_big_20_30	40	1.6165	0.0320	0.1660	0.0018	0.629	0.0716	0.0011	977	12	990	10	975
511005_big_21_31	40	1.4733	0.0543	0.1414	0.0043	0.792	0.0766	0.0017	919	22	853	24	1110
511005_big_22_32	40	1.6654	0.0353	0.1656	0.0019	0.546	0.0740	0.0013	995	13	988	10	1040
511005_big_23_33	40	1.7643	0.0341	0.1739	0.0018	0.625	0.0746	0.0011	1032	12	1033	10	1058
511005_big_23_34	40	1.7582	0.0428	0.1745	0.0028	0.661	0.0741	0.0014	1030	16	1037	15	1044
511005_big_24_35	40	1.5753	0.0307	0.1603	0.0017	0.620	0.0723	0.0011	961	12	958	9	993
511005_big_24_36	-	-											
511005_big_25_37	40	1.5863	0.0310	0.1590	0.0017	0.625	0.0733	0.0011	965	12	951	9	1024
511005_med_1_1	30	1.5703	0.0384	0.1596	0.0028	0.736	0.0726	0.0012	959	15	955	15	1001
511005_med_5_2	30	1.7214	0.0450	0.1741	0.0031	0.648	0.0729	0.0015	1017	17	1034	17	1012
511005_med_5_3	30	1.7232	0.0381	0.1695	0.0027	0.779	0.0749	0.0010	1017	14	1010	15	1067
511005_med_6_4	30	1.6738	0.0451	0.1668	0.0032	0.701	0.0740	0.0014	999	17	994	18	1041
511005_med_6_5	30	1.8315	0.0458	0.1804	0.0031	0.697	0.0748	0.0013	1057	16	1069	17	1064

511005_med_8_6	30	1.7209	0.0398	0.1693	0.0027	0.742	0.0750	0.0012	1016	15	1008	15	1068
511005_med_8_7	-	-											
511005_med_10_8	-	-											
511005_med_10_9	-	-											
511005_med_11_10	-	-											
511005_med_11_11	-	-											
Sample 511004, Neoproterozoic granitoid													
511004_1_1	30	0.8544	0.0205	0.1012	0.0017	0.684	0.0609	0.0011	627	11	621	10	636
511004_1_2	-	-											
511004_3_3	30	0.8715	0.0187	0.1032	0.0013	0.578	0.0620	0.0011	636	10	633	8	675
511004_3_4	30	0.7795	0.0158	0.0922	0.0011	0.617	0.0621	0.0010	585	9	569	7	677
511004_3_5	30	0.6101	0.0141	0.0717	0.0010	0.591	0.0625	0.0012	484	9	447	6	690
511004_4_6	-	-											
511004_4_7	30	0.8569	0.0164	0.1010	0.0012	0.657	0.0623	0.0009	628	9	620	7	683
511004_5_8	30	0.5632	0.0123	0.0676	0.0009	0.637	0.0612	0.0010	454	8	421	6	646
511004_6_9	30	0.8501	0.0162	0.0999	0.0011	0.645	0.0625	0.0009	625	9	614	7	691
511004_6_10	30	0.7247	0.0163	0.0880	0.0012	0.534	0.0605	0.0012	553	10	544	7	620
511004_7_11	30	0.7528	0.0163	0.0870	0.0010	0.482	0.0636	0.0012	570	9	538	6	727
511004_7_12	30	0.8565	0.0168	0.1021	0.0012	0.624	0.0616	0.0009	628	9	627	7	660
511004_8_13	-	-											
511004_8_14	-	-											
511004_9_15	30	0.7924	0.0207	0.0899	0.0017	0.735	0.0650	0.0012	593	12	555	10	773
511004_9_16	30	0.4091	0.0132	0.0498	0.0012	0.725	0.0605	0.0014	348	9	313	7	623
511004_10_17	30	0.8041	0.0178	0.0961	0.0015	0.784	0.0617	0.0009	599	10	591	9	664
511004_10_18	-	-											
511004_11_19	-	-											
511004_12_20	-	-											
511004_12_21	30	0.7710	0.0191	0.0909	0.0015	0.676	0.0625	0.0011	580	11	561	9	693
511004_13_22	30	0.8632	0.0210	0.1024	0.0017	0.720	0.0622	0.0011	632	11	628	10	680
511004_14_23	-	-											
511004_14_24	30	0.7646	0.0177	0.0917	0.0015	0.743	0.0615	0.0010	577	10	565	9	657
511004_15_25	30	-											
511004_15_26	30	0.8116	0.0204	0.0971	0.0017	0.682	0.0616	0.0011	603	11	598	10	661
511004_16_27	30	0.8056	0.0199	0.0959	0.0016	0.678	0.0619	0.0011	600	11	591	9	671
511004_16_28	30	0.7829	0.0187	0.0948	0.0016	0.716	0.0609	0.0010	587	11	584	9	636
511004_17_29	30	0.8374	0.0191	0.0991	0.0016	0.752	0.0623	0.0009	618	11	609	9	685
511004_18_30	30	0.7503	0.0181	0.0890	0.0015	0.696	0.0622	0.0011	568	10	549	9	681
511004_18_31	30	0.6616	0.0163	0.0805	0.0013	0.677	0.0606	0.0011	516	10	499	8	624
511004_18_32	-	-											
511004_19_33	30	0.7685	0.0177	0.0845	0.0014	0.758	0.0670	0.0010	579	10	523	8	839
511004_20_34	30	0.7982	0.0207	0.0944	0.0017	0.709	0.0623	0.0011	596	12	582	10	686
511004_20_35	30	0.5934	0.0135	0.0711	0.0011	0.759	0.0616	0.0009	473	9	443	7	659
511004_21_36	30	0.3196	0.0091	0.0389	0.0009	0.784	0.0607	0.0011	282	7	246	5	627
511004_22_37	-	-											
511004_22_38	30	1.6555	0.0440	0.1578	0.0030	0.728	0.0774	0.0014	992	17	945	17	1130
511004_22_39	30	1.9770	0.0517	0.1906	0.0035	0.704	0.0765	0.0014	1108	17	1124	19	1108
511004_22_40	-	-											
511004_23_41	-	-											
511004_24_42	30	0.8175	0.0180	0.0968	0.0015	0.781	0.0623	0.0009	607	10	595	9	684
511004_24_43	30	0.8378	0.0198	0.0979	0.0016	0.728	0.0631	0.0010	618	11	602	10	711
511004_25_44	30	0.7344	0.0171	0.0875	0.0015	0.756	0.0619	0.0009	559	10	541	9	669
511004_25_45	-	-											
511004_26_46	-	-											
511004_26_47	-	-											
511004_27_48	30	0.5449	0.0136	0.0622	0.0011	0.686	0.0646	0.0012	442	9	389	6	760
Sample 511001, Neoproterozoic granitoid													
511001_big_1_1	40	0.8126	0.0175	0.0965	0.0011	0.510	0.0626	0.0012	604	10	594	6	694
511001_big_1_2	-	-											
511001_big_1_3	-	-											
511001_big_2_4	40	-											
511001_big_4_5	40	0.9540	0.0287	0.1082	0.0018	0.366	0.0655	0.0019	680	15	662	10	791
511001_big_5_6	40	0.9318	0.0241	0.1038	0.0014	0.398	0.0667	0.0016	669	13	637	8	827
511001_big_5_7	40	0.8702	0.0194	0.1033	0.0011	0.450	0.0626	0.0012	636	10	634	7	693
511001_big_6_8	-	-											
511001_big_6_9	40	1.0325	0.0430	0.1088	0.0026	0.328	0.0705	0.0029	720	21	666	15	943
511001_big_7_10	40	0.8646	0.0396	0.0938	0.0024	0.290	0.0684	0.0031	633	21	578	14	882

511001_big_7_11	-	-											
511001_big_8_12	40	0.8479	0.0207	0.1012	0.0012	0.371	0.0622	0.0014	624	11	622	7	682
511001_big_8_13	40	0.8323	0.0177	0.1013	0.0011	0.539	0.0610	0.0011	615	10	622	7	640
511001_big_9_14	-	-											
511001_big_9_15	40	0.9079	0.0309	0.1088	0.0020	0.309	0.0620	0.0021	656	16	666	12	674
511001_big_9_16	40	1.0497	0.0336	0.1084	0.0020	0.380	0.0719	0.0022	729	17	664	11	984
511001_big_9_17	40	0.8983	0.0218	0.1031	0.0013	0.406	0.0647	0.0014	651	12	632	7	766
511001_big_10_18	40	0.9121	0.0311	0.0961	0.0017	0.285	0.0705	0.0024	658	16	591	10	944
511001_big_11_19	-	-											
511001_big_11_20	40	1.0081	0.0345	0.1002	0.0017	0.184	0.0748	0.0026	708	17	616	10	1062
511001_big_11_21	40	0.9425	0.0243	0.1102	0.0016	0.507	0.0641	0.0014	674	13	674	9	746
511001_big_11_22	40	0.9573	0.0210	0.1076	0.0011	0.452	0.0667	0.0013	682	11	659	6	829
511001_big_12_23	40	0.8199	0.0166	0.0995	0.0009	0.513	0.0618	0.0011	608	9	611	5	669
511001_big_12_24	40	0.9054	0.0356	0.0973	0.0025	0.522	0.0698	0.0024	655	19	599	15	922
511001_big_13_25	40	0.7566	0.0203	0.0923	0.0015	0.540	0.0615	0.0014	572	12	569	9	656
511001_big_14_26	40	0.8291	0.0240	0.0977	0.0014	0.310	0.0636	0.0018	613	13	601	8	730
511001_big_14_27	40	0.8407	0.0236	0.1012	0.0015	0.410	0.0623	0.0016	620	13	622	9	684
511001_big_15_28	40	0.8539	0.0177	0.1050	0.0010	0.524	0.0610	0.0011	627	10	644	6	638
511001_big_16_29	40	1.6755	0.0333	0.1702	0.0015	0.558	0.0739	0.0012	999	13	1013	8	1038
511001_big_16_30	40	1.0003	0.0289	0.1141	0.0016	0.329	0.0658	0.0018	704	15	696	9	799
511001_big_17_31	40	1.6458	0.0372	0.1628	0.0018	0.492	0.0758	0.0015	988	14	972	10	1091
511001_med_1_1	30	0.8215	0.0203	0.0999	0.0017	0.667	0.0606	0.0011	609	11	614	10	626
511001_med_1_2	30	1.4432	0.0415	0.1464	0.0028	0.615	0.0727	0.0017	907	17	881	16	1005
511001_med_3_3	30	0.6635	0.0215	0.0818	0.0016	0.482	0.0598	0.0017	517	13	507	10	597
511001_med_3_4	30	0.9162	0.0538	0.0937	0.0041	0.649	0.0721	0.0033	660	28	577	24	989
511001_med_5_5	30	0.7874	0.0189	0.0943	0.0016	0.715	0.0615	0.0010	590	11	581	9	658
511001_med_5_6	30	0.7973	0.0234	0.0964	0.0018	0.538	0.0610	0.0015	551	12	525	10	659
511001_med_6_7	30	0.8184	0.0222	0.1016	0.0018	0.621	0.0594	0.0013	607	12	624	11	581
511001_med_10_8	30	0.8478	0.0196	0.1027	0.0017	0.733	0.0609	0.0010	623	11	630	10	634
511001_med_13_9	30	0.8150	0.0236	0.1024	0.0019	0.573	0.0587	0.0014	605	13	628	11	556
511001_med_17_10	-	-											
Sample 512001, Sabot Amphibolite felsic layer													
512001_Hf_1_1	-	-											
512001_Hf_2_2	30	0.5835	0.0145	0.0749	0.0011	0.315	0.0569	0.0014	467	9	466	7	486
512001_Hf_3_3	30	0.5831	0.0115	0.0702	0.0009	0.476	0.0606	0.0011	466	7	437	5	626
512001_Hf_4_4	30	0.5540	0.0099	0.0687	0.0008	0.580	0.0589	0.0009	448	6	428	5	563
512001_Hf_4_5	-	-											
512001_Hf_5_6	-	-											
512001_Hf_6_7	30	0.5362	0.0094	0.0692	0.0009	0.626	0.0565	0.0008	436	6	432	5	473
512001_Hf_7_8	30	0.5690	0.0094	0.0700	0.0008	0.679	0.0594	0.0007	457	6	436	5	580
512001_Hf_7_9	30	0.5860	0.0129	0.0727	0.0010	0.428	0.0589	0.0012	468	8	452	6	562
512001_Hf_8_10	-	-											
512001_Hf_9_11	-	-											
512001_Hf_9_12	-	-											
512001_Hf_10_13	-	-											
512001_Hf_11_14	-	-											
512001_Hf_11_15	-	-											
512001_Hf_12_16	-	-											
512001_Hf_13_17	30	0.5691	0.0103	0.0734	0.0010	0.633	0.0566	0.0008	457	7	456	6	477
512001_Hf_14_18	30	0.7496	0.0197	0.0921	0.0015	0.355	0.0594	0.0015	568	11	568	9	583
512001_Hf_15_19	30	0.5243	0.0110	0.0670	0.0009	0.478	0.0571	0.0011	428	7	418	6	497
512001_Hf_16_20	30	0.5352	0.0092	0.0696	0.0008	0.596	0.0561	0.0008	435	6	434	5	457
512001_Hf_17_21	30	0.5438	0.0083	0.0684	0.0006	0.323	0.0573	0.0009	441	5	427	3	504
512001_Hf_17_22	30	0.5311	0.0098	0.0671	0.0007	0.309	0.0570	0.0010	433	6	419	4	493
512001_Hf_18_23	30	0.5663	0.0105	0.0691	0.0007	0.290	0.0591	0.0011	456	7	431	4	570
512001_Hf_19_24	30	0.6811	0.0131	0.0818	0.0010	0.390	0.0600	0.0011	527	8	507	6	605
512001_Hf_20_25	-	-											
512001_Hf_20_26	-	-											
512001_Hf_20_27	-	-											
512001_Hf_21_28	30	0.6103	0.0084	0.0768	0.0006	0.472	0.0573	0.0007	484	5	477	4	503
512001_Hf_21_29	30	0.5229	0.0072	0.0665	0.0005	0.510	0.0567	0.0007	427	5	415	3	480
512001_Hf_22_30	-	-											
512001_Hf_23_31	30	0.6513	0.0094	0.0800	0.0007	0.465	0.0587	0.0008	509	6	496	4	557
512001_Hf_18b	-	-											
512001_Hf_18c	-	-											
512001_Hf_18d	-	-											
512001_Hf_18e	-	-											

512001_Hf_18f	-	-											
512001_Hf_23_32	30	0.5792	0.0112	0.0700	0.0009	0.450	0.0597	0.0011	464	7	436	5	592
512001_Hf_24_33	30	0.5746	0.0106	0.0725	0.0008	0.326	0.0572	0.0010	461	7	451	5	498
512001_Hf_24_34	-	-											
FC1 standard													
12_18_1_1	40												
12_18_3	40												
12_18_4	40												
12_18_5_2	40												
12_18_6_1	40												
12_18_7_1	40												
12_18_8_1	40												
12_18_9_1	40												
12_18_10_1	40												
12_18_11_1	40												
12_18_12_1	40												
12_18_13_1	40												
12_18_14	40												
12_18_15	40												
12_18_1_2	30												
12_18_2	30												
12_18_3_1	30												
12_18_4_1	30												
12_18_5_1	30												
12_18_6_2	30												
12_18_7_2	30												
12_18_8_2	30												
12_19_1	30												
12_19_2	30												
12_19_3	30												
12_19_4	30												
12_19_5	30												
12_19_6	30												
12_19_7	30												
12_19_8	30												
12_19_9	30												
12_19_10	30												
12_19_11	30												
12_19_12	30												
12_19_13	30												
12_19_14	30												
12_19_15	30												
12_19_16	30												
12_19_17	30												
12_19_18	40												
12_19_19	40												
12_19_21	40												
12_19_22	40												
R33 standard													
12_18_1	40	0.5027	0.0125	0.0672	0.0008	0.346	0.0556	0.0013	414	8	419	5	437
12_18_2	40	0.5048	0.0116	0.0681	0.0008	0.430	0.0551	0.0011	415	8	425	5	415
12_18_3	40	0.4970	0.0106	0.0677	0.0007	0.478	0.0546	0.0010	410	7	422	4	394
12_18_4	40	0.5026	0.0107	0.0694	0.0007	0.499	0.0538	0.0010	413	7	432	4	364
12_18_5	40	0.5068	0.0127	0.0680	0.0010	0.519	0.0553	0.0012	416	9	424	6	426
12_19_1	30	0.5281	0.0126	0.0697	0.0012	0.690	0.0546	0.0009	431	8	435	7	397
12_19_2	30	0.5002	0.0130	0.0656	0.0012	0.645	0.0550	0.0011	412	9	409	7	414
12_19_3	30	0.4885	0.0127	0.0651	0.0012	0.662	0.0553	0.0011	404	9	407	7	425
12_19_4	30	0.4981	0.0121	0.0671	0.0011	0.695	0.0548	0.0010	410	8	418	7	402
12_19_5	30	0.4909	0.0114	0.0663	0.0011	0.728	0.0546	0.0009	406	8	414	6	395
12_19_6	30	0.4992	0.0116	0.0662	0.0011	0.746	0.0556	0.0009	411	8	413	7	438

Temora standard														
12_18_1	40	-												
12_18_2	40	0.5050	0.0109	0.0683	0.0007	0.491	0.0550	0.0010	415	7	426	4	411	
12_18_3	40	0.4950	0.0109	0.0671	0.0007	0.453	0.0548	0.0011	408	7	418	4	405	
12_18_4	40	0.4995	0.0111	0.0684	0.0007	0.467	0.0543	0.0011	411	7	426	5	383	
12_18_5	40	0.5042	0.0115	0.0686	0.0008	0.457	0.0546	0.0011	415	8	428	5	396	
12_19_1	30	0.5027	0.0138	0.0665	0.0012	0.577	0.0545	0.0012	414	9	415	7	378	
12_19_2	30	0.5096	0.0149	0.0677	0.0013	0.529	0.0543	0.0014	418	10	422	8	370	

± 1σ	U conc (ppm)	U / Th	Duration (s)	corrected 176Hf / 177Hf	± 2SE	176Lu / 177Hf	± 2SE	176Yb / 177Hf
			Sample Mont1, Montpelier Anorthosite					
			59.5	0.282480	0.000035	0.000728	0.000013	0.012950
			59.5	0.282465	0.000034	0.001401	0.000053	0.024900
87	21	4.7	52.2	0.282491	0.000024	0.000042	0.000001	0.001053
87	53	6.6	31.6	0.282320	0.000055	0.000150	0.000003	0.003655
			55.9	0.282369	0.000021	0.000127	0.000002	0.003310
			-					
86	28	4.7	-					
93	10	1.8	46.1	0.282166	0.000022	0.000035	0.000000	0.001105
			-					
			-					
			-					
			-					
			-					
			-					
89	34	7.6	-					
			-					
			-					
			Sample 511005, State Farm Gneiss					
43	156	3.4	61.8	0.282189	0.000018	0.000372	0.000012	0.009640
38	115	5.2	57.5	0.282173	0.000023	0.000480	0.000000	0.012639
34	134	4.9	60.4	0.282198	0.000020	0.000374	0.000002	0.009697
31	666	5.9	61.8	0.282153	0.000019	0.000337	0.000004	0.008900
31	680	4.6	46.0	0.282098	0.000026	0.000444	0.000010	0.011630
34	167	2.7	60.4	0.282215	0.000022	0.000245	0.000002	0.006673
31	612	4.6	59.0	0.282128	0.000019	0.000444	0.000004	0.011608
34	192	2.6	60.4	0.282160	0.000022	0.000289	0.000003	0.007950
32	746	7.3	56.1	0.282189	0.000031	0.000386	0.000011	0.010060
37	143	3.7	60.4	0.282188	0.000022	0.000305	0.000001	0.008121
40	94	4.2	-					
31	669	4.4	54.6	0.282138	0.000019	0.000556	0.000012	0.015120
36	189	2.9	41.7	0.282177	0.000032	0.000258	0.000005	0.007480
35	202	2.4	59.0	0.282208	0.000023	0.000483	0.000002	0.013272
36	399	3.9	59.0	0.282185	0.000015	0.000439	0.000017	0.011990
38	198	2.8	48.9	0.282177	0.000030	0.000317	0.000062	0.008600
36	262	1.8	41.7	0.282131	0.000031	0.000657	0.000081	0.017400
			-					
32	499	3.9	60.4	0.282178	0.000018	0.000600	0.000015	0.015090
35	169	6.8	40.3	0.282156	0.000035	0.000473	0.000008	0.012190
36	132	2.5	60.4	0.282201	0.000023	0.000310	0.000004	0.008423
			-					
32	389	4.0	59.0	0.282195	0.000015	0.000895	0.000012	0.024320
35	157	6.6	60.4	0.282175	0.000017	0.000428	0.000007	0.011010
34	243	5.2	61.8	0.282172	0.000017	0.000606	0.000003	0.015793
38	111	2.7	60.4	0.282197	0.000022	0.000208	0.000010	0.005840
35	132	3.5	61.8	0.282191	0.000024	0.000290	0.000006	0.007910
35	150	2.1	59.0	0.282204	0.000018	0.000316	0.000005	0.008860
			-					
31	5055	15.6	50.1	0.282182	0.000033	0.001530	0.000190	0.035300
44	268	3.8	51.5	0.282173	0.000017	0.000349	0.000003	0.009800
35	175	3.2	43.3	0.282172	0.000029	0.000365	0.000003	0.009740
30	1043	3.9	61.0	0.282156	0.000020	0.000357	0.000005	0.009590
36	220	3.7	61.0	0.282194	0.000023	0.000325	0.000004	0.008910
31	764	6.9	52.8	0.282128	0.000022	0.000411	0.000002	0.010838
			-					
31	740	5.7	59.6	0.282124	0.000024	0.000517	0.000016	0.013770
33	299	1.2	55.9	0.282141	0.000032	0.000368	0.000002	0.009602
40	116	2.7	58.3	0.282187	0.000035	0.000218	0.000010	0.005780
28	800	6.5	59.5	0.282137	0.000030	0.000414	0.000005	0.010810
38	157	2.7	59.5	0.282193	0.000031	0.000252	0.000011	0.006740
36	174	2.6	59.5	0.282197	0.000032	0.000289	0.000008	0.007640

31	307	3.7	42.5	0.282148	0.000028	0.000387	0.000006	0.009840
			-					
			-					
			-					
			-					
			-					
Sample 511004, Neoproterozoic granitoid								
37	1121	1.4	-					
			-					
37	559	5.9	49.8	0.282441	0.000023	0.001070	0.000140	0.028600
34	1186	1.2	59.5	0.282494	0.000036	0.002751	0.000053	0.079900
39	1751	2.3	59.5	0.282440	0.000039	0.002340	0.000100	0.067600
			-					
31	1077	1.6	58.3	0.282502	0.000032	0.003380	0.000120	0.100500
36	1209	4.1	-					
31	1125	2.5	53.4	0.282435	0.000035	0.001271	0.000038	0.033200
41	673	3.4	58.3	0.282510	0.000036	0.001280	0.000120	0.037100
40	1152	4.3	-					
33	1393	2.2	-					
			-					
			-					
37	765	1.6	38.9	0.282537	0.000043	0.001273	0.000070	0.036700
47	641	2.2	48.6	0.282483	0.000041	0.003020	0.000130	0.088000
29	1912	2.8	41.3	0.282423	0.000037	0.001890	0.000100	0.051500
			-					
			-					
			-					
38	556	7.5	26.7	0.282429	0.000029	0.000666	0.000058	0.016700
36	1224	3.0	-					
			-					
33	680	3.7	54.6	0.282431	0.000026	0.002030	0.000098	0.052500
			24.3	0.282466	0.000039	0.000738	0.000057	0.017300
39	997	3.8	-					
38	772	3.3	35.3	0.282470	0.000028	0.001420	0.000120	0.037500
35	876	1.8	39.1	0.282501	0.000033	0.001800	0.000180	0.049800
32	989	4.3	48.3	0.282428	0.000030	0.001243	0.000043	0.031000
37	488	3.7	34.0	0.282568	0.000040	0.002060	0.000240	0.052100
39	778	2.1	-					
			-					
31	1885	2.2	-					
39	903	2.3	-					
32	1997	2.2	48.6	0.282432	0.000027	0.002920	0.000120	0.082000
38	1828	3.6	38.9	0.282545	0.000045	0.002596	0.000027	0.062170
			-					
36	368	2.9	57.1	0.282145	0.000036	0.000512	0.000021	0.013840
37	190	3.0	60.7	0.282190	0.000031	0.000573	0.000002	0.015420
			-					
			-					
29	2180	1.7	53.4	0.282495	0.000034	0.003500	0.000150	0.102800
34	1904	2.6	-					
32	2303	2.7	49.8	0.282473	0.000042	0.002981	0.000063	0.085900
			-					
			-					
			-					
38	1882	2.8	27.9	0.282471	0.000038	0.003020	0.000150	0.087700
Sample 511001, Neoproterozoic granitoid								
39	364	2.7	61.7	0.282437	0.000027	0.000957	0.000014	0.026460
			-					
			-					
			60.6	0.282436	0.000022	0.002010	0.000130	0.047300
59	110	2.8	50.9	0.282428	0.000031	0.000540	0.000016	0.014260
49	78	2.4	52.0	0.282440	0.000032	0.000778	0.000074	0.020300
42	193	1.4	60.6	0.282454	0.000026	0.001310	0.000170	0.035900
			-					
81	22	2.1	58.5	0.282456	0.000024	0.000738	0.000002	0.019500
91	22	2.9	-					

			-					
48	438	3.1	-					
38	414	2.5	-					
			-					
70	29	2.2	58.5	0.282416	0.000022	0.000425	0.000007	0.010930
60	31	2.0	58.5	0.282441	0.000031	0.000580	0.000035	0.016900
46	99	1.7	58.5	0.282436	0.000021	0.000807	0.000028	0.022250
68	57	1.7	60.6	0.282423	0.000029	0.001105	0.000005	0.030610
			-					
69	220	1.3	52.0	0.282446	0.000028	0.000888	0.000025	0.024870
46	99	2.3	60.6	0.282433	0.000022	0.000752	0.000039	0.020900
40	182	1.8	59.5	0.282444	0.000028	0.001267	0.000025	0.035940
37	451	2.1	59.5	0.282430	0.000026	0.001680	0.000150	0.050500
68	32	2.6	52.0	0.282469	0.000034	0.000477	0.000007	0.013380
48	276	5.8	-					
58	53	2.0	60.6	0.282400	0.000025	0.000991	0.000007	0.027400
54	60	2.6	59.5	0.282401	0.000022	0.000691	0.000025	0.019110
38	597	2.8	-					
33	483	4.1	24.4	0.282292	0.000041	0.000527	0.000045	0.014400
57	98	2.4	30.2	0.282399	0.000043	0.000812	0.000051	0.022300
39	352	3.8	31.6	0.282226	0.000018	0.000740	0.000110	0.019700
39	275	3.1	57.1	0.282379	0.000030	0.000676	0.000001	0.017923
45	87	3.1	51.0	0.282206	0.000037	0.000319	0.000026	0.008160
61	167	5.0	-					
89	23	2.0	59.5	0.282407	0.000041	0.000489	0.000009	0.012340
36	802	5.2	48.6	0.282380	0.000034	0.001176	0.000030	0.029480
48	160	2.3	43.7	0.282412	0.000034	0.000753	0.000053	0.019600
46	179	1.5	44.9	0.282401	0.000037	0.001986	0.000099	0.054200
34	742	2.0	25.5	0.282443	0.000042	0.001621	0.000052	0.045500
51	135	2.5	59.5	0.282388	0.000038	0.000896	0.000069	0.023900
			-					
			Sample 512001, Sabot Amphibolite felsic layer					
			-					
53	871	2.3	31.1	0.282812	0.000035	0.001186	0.000087	0.029500
38	793	2.4	-					
32	960	2.9	28.9	0.282792	0.000039	0.002610	0.000360	0.058000
			-					
			-					
30	630	2.7	47.4	0.282830	0.000028	0.002150	0.000200	0.054000
26	939	1.3	39.3	0.282772	0.000049	0.004530	0.000300	0.109000
44	227	6.9	38.3	0.282713	0.000042	0.002127	0.000094	0.046100
			-					
			-					
			-					
			-					
			-					
			-					
			-					
31	657	6.8	22.1	0.282761	0.000047	0.001585	0.000035	0.035920
54	90	2.2	35.2	0.282698	0.000040	0.001088	0.000014	0.028850
41	521	15.2	-					
30	715	19.8	51.9	0.282687	0.000032	0.000827	0.000024	0.021730
32	824	37.6	-					
40	529	35.5	17.1	0.282783	0.000038	0.000825	0.000022	0.020680
39	638	16.1	-					
39	394	1.1	27.1	0.282831	0.000077	0.004960	0.000440	0.131000
			-					
			-					
			-					
27	950	2.2	29.8	0.282796	0.000037	0.003203	0.000041	0.078900
26	1128	35.7	21.7	0.282757	0.000037	0.002101	0.000022	0.050230
			-					
28	881	1.8	22.6	0.282744	0.000038	0.002857	0.000093	0.080800
			-					
			-					
			-					
			-					

			-					
38	395	2.4	-					
39	547	3.2	32.9	0.282806	0.000037	0.001990	0.000100	0.043300
			-					
			FC1 standard					
			58.2	0.282180	0.000026	0.000509	0.000010	0.013760
			58.2	0.282176	0.000030	0.000717	0.000023	0.020230
			56.9	0.282170	0.000025	0.000780	0.000003	0.022460
			61.0	0.282173	0.000023	0.000556	0.000002	0.015370
			58.2	0.282160	0.000030	0.000689	0.000020	0.019950
			58.2	0.282171	0.000027	0.000869	0.000003	0.024479
			44.7	0.282162	0.000030	0.000985	0.000010	0.028230
			58.2	0.282193	0.000024	0.000943	0.000011	0.027380
			59.6	0.282171	0.000024	0.000972	0.000002	0.028280
			58.2	0.282183	0.000024	0.001030	0.000004	0.030348
			59.6	0.282193	0.000026	0.001130	0.000013	0.033090
			59.6	0.282184	0.000022	0.000947	0.000025	0.028200
			58.2	0.282133	0.000028	0.000573	0.000038	0.016200
			58.2	0.282163	0.000026	0.000710	0.000010	0.020720
			34.7	0.282158	0.000043	0.001087	0.000001	0.030790
			-					
			-					
			-					
			40.6	0.282153	0.000033	0.001083	0.000001	0.031110
			-					
			28.9	0.282183	0.000044	0.000986	0.000017	0.028400
			27.5	0.282173	0.000038	0.001066	0.000002	0.030700
			59.5	0.282143	0.000044	0.000796	0.000025	0.021640
			53.4	0.282103	0.000038	0.001017	0.000025	0.027950
			57.1	0.282115	0.000043	0.000963	0.000084	0.026500
			57.1	0.282174	0.000035	0.001085	0.000008	0.030170
			44.9	0.282120	0.000052	0.001034	0.000044	0.029800
			49.8	0.282198	0.000036	0.000933	0.000046	0.027000
			51.0	0.282140	0.000049	0.000970	0.000012	0.027780
			59.5	0.282178	0.000037	0.001018	0.000008	0.029430
			52.2	0.282176	0.000038	0.000915	0.000059	0.026500
			60.7	0.282185	0.000035	0.000968	0.000008	0.028420
			59.5	0.282189	0.000031	0.000850	0.000012	0.024810
			36.4	0.282096	0.000050	0.000303	0.000016	0.009030
			29.1	0.282112	0.000044	0.000504	0.000006	0.013850
			-					
			-					
			59.5	0.282197	0.000031	0.000928	0.000012	0.025680
			61.9	0.282129	0.000031	0.000520	0.000020	0.013960
			60.7	0.282167	0.000025	0.000653	0.000020	0.018280
			31.6	0.282173	0.000025	0.000353	0.000011	0.009940
			58.3	0.282179	0.000028	0.000742	0.000007	0.020800
			58.3	0.282164	0.000021	0.000929	0.000004	0.027270
			mean	**0.282163**				
			2 s.d.	**0.000053**				
			R33 standard					
52	138	1.3	54.9	0.282744	0.000028	0.002099	0.000020	0.057140
46	216	1.2	57.9	0.282719	0.000027	0.003193	0.000051	0.088600
42	367	1.0	61.0	0.282751	0.000032	0.004813	0.000068	0.135000
41	354	1.0	61.0	0.282760	0.000031	0.005390	0.000280	0.153500
47	230	1.3	61.0	0.282737	0.000029	0.002598	0.000083	0.076000
38	879	1.1	57.1	0.282791	0.000034	0.003760	0.000130	0.094600
44	739	1.3	53.4	0.282744	0.000046	0.001520	0.000036	0.037250
43	659	1.4	55.9	0.282770	0.000029	0.002225	0.000060	0.056900
38	579	1.4	59.5	0.282774	0.000029	0.002615	0.000038	0.068410
35	937	1.2	59.5	0.282750	0.000034	0.001973	0.000043	0.050400
34	930	1.5	59.5	0.282755	0.000035	0.002090	0.000110	0.053800
			mean	**0.282754**				
			2 s.d.	**0.000037**				

			Temora standard					
			58.2	0.282679	0.000024	0.002259	0.000041	0.060100
41	325	1.6	61.0	0.282656	0.000032	0.001854	0.000006	0.049450
44	277	3.4	61.0	0.282691	0.000027	0.000915	0.000044	0.022230
43	292	3.6	61.0	0.282634	0.000024	0.000713	0.000005	0.017430
45	278	2.7	63.7	0.282644	0.000024	0.001401	0.000027	0.035590
66	222	2.3	58.3	0.282652	0.000041	0.001221	0.000003	0.029520
70	173	3.8	58.3	0.282686	0.000041	0.000874	0.000006	0.020060
			mean	**0.282663**				
			2 s.d.	**0.000041**				

± 2SE	178Hf/177Hf	± 2SE	180Hf/177Hf	± 2SE	total Hf beam (volts)	ε_{Hf} today	± 2SE	Age to calc εHf (Ma)	176Hf/177Hf at age	ε_{Hf} at unit age
0.000240	1.467132	0.000047	1.886957	0.000084	7.5	-10.8	1.2	1040	0.282466	+12.0
0.000910	1.467190	0.000055	1.887000	0.000110	6.2	-11.3	1.2	1040	0.282438	+11.0
0.000027	1.467167	0.000029	1.886842	0.000083	24.8	-10.4	0.8	1040	0.282490	+12.9
0.000048	1.467137	0.000036	1.887110	0.000180	20.8	-16.4	1.9	1040	0.282317	+6.8
0.000059	1.467197	0.000019	1.886998	0.000069	22.3	-14.7	0.7	1040	0.282366	+8.5
0.000013	1.467190	0.000029	1.887035	0.000095	17.8	-21.9	0.8	1040	0.282165	+1.4
0.000290	1.467184	0.000036	1.886936	0.000064	13.6	-21.1	0.6	1030	0.282182	+1.7
0.000019	1.467195	0.000038	1.886895	0.000061	13.5	-21.6	0.8	1030	0.282164	+1.1
0.000066	1.467174	0.000028	1.886982	0.000078	14.2	-20.8	0.7	1030	0.282191	+2.1
0.000120	1.467189	0.000032	1.886940	0.000079	13.3	-22.4	0.7	1030	0.282146	+0.5
0.000300	1.467158	0.000036	1.886972	0.000095	14.0	-24.3	0.9	1030	0.282089	-1.5
0.000066	1.467183	0.000035	1.886903	0.000086	13.0	-20.2	0.8	1030	0.282210	+2.7
0.000093	1.467161	0.000040	1.886947	0.000071	13.3	-23.2	0.7	1030	0.282119	-0.5
0.000097	1.467157	0.000032	1.886898	0.000054	13.0	-22.1	0.8	1030	0.282154	+0.8
0.000330	1.467170	0.000033	1.886960	0.000100	13.9	-21.1	1.1	1030	0.282181	+1.7
0.000032	1.467197	0.000038	1.886948	0.000067	13.3	-21.1	0.8	1030	0.282182	+1.8
0.000320	1.467195	0.000033	1.886892	0.000081	13.0	-22.9	0.7	1030	0.282127	-0.2
0.000150	1.467165	0.000034	1.887069	0.000091	12.5	-21.5	1.1	1030	0.282172	+1.4
0.000022	1.467221	0.000034	1.886922	0.000091	12.9	-20.4	0.8	1030	0.282199	+2.3
0.000460	1.467187	0.000035	1.886970	0.000078	13.2	-21.2	0.5	1030	0.282176	+1.6
0.001700	1.467185	0.000036	1.887010	0.000083	13.8	-21.5	1.1	1030	0.282171	+1.4
0.002200	1.467132	0.000029	1.887040	0.000100	15.9	-23.1	1.1	1030	0.282118	-0.5
0.000330	1.467192	0.000035	1.886920	0.000066	13.8	-21.5	0.6	1030	0.282166	+1.2
0.000140	1.467175	0.000045	1.887060	0.000140	13.0	-22.2	1.2	1030	0.282147	+0.5
0.000098	1.467168	0.000036	1.886831	0.000073	12.2	-20.7	0.8	1030	0.282195	+2.2
0.000380	1.467172	0.000026	1.886968	0.000071	13.4	-20.9	0.5	1030	0.282178	+1.6
0.000230	1.467185	0.000029	1.886949	0.000065	14.2	-21.6	0.6	1030	0.282167	+1.2
0.000044	1.467155	0.000032	1.886911	0.000072	14.4	-21.7	0.6	1030	0.282160	+1.0
0.000300	1.467199	0.000027	1.886900	0.000077	13.0	-20.8	0.8	1030	0.282193	+2.1
0.000110	1.467156	0.000032	1.886923	0.000081	13.5	-21.0	0.9	1030	0.282185	+1.9
0.000110	1.467187	0.000032	1.886871	0.000085	12.7	-20.5	0.6	1030	0.282198	+2.3
0.003900	1.467173	0.000034	1.886981	0.000086	16.6	-21.3	1.2		not calculated	
0.000200	1.467180	0.000035	1.886931	0.000079	13.4	-21.6	0.6	1030	0.282166	+1.2
0.000110	1.467171	0.000041	1.887020	0.000110	14.1	-21.7	1.0	1030	0.282165	+1.1
0.000140	1.467177	0.000030	1.886912	0.000066	15.3	-22.2	0.7	1030	0.282149	+0.6
0.000140	1.467186	0.000033	1.886975	0.000071	13.2	-20.9	0.8	1030	0.282188	+1.9
0.000097	1.467185	0.000033	1.886882	0.000086	13.8	-23.2	0.8	1030	0.282120	-0.4
0.000360	1.467184	0.000031	1.886928	0.000085	13.0	-23.4	0.9	1030	0.282114	-0.7
0.000046	1.467158	0.000050	1.886960	0.000120	7.9	-22.8	1.1	1030	0.282134	+0.0
0.000250	1.467166	0.000040	1.886935	0.000099	7.0	-21.1	1.2	1030	0.282183	+1.8
0.000130	1.467201	0.000046	1.887070	0.000110	7.6	-22.9	1.1	1030	0.282129	-0.1
0.000260	1.467192	0.000048	1.886860	0.000110	7.1	-20.9	1.1	1030	0.282188	+2.0
0.000170	1.467194	0.000040	1.886880	0.000100	7.5	-20.8	1.1	1030	0.282191	+2.1

0.000130	1.467172	0.000056	1.886990	0.000150	9.2	-22.5	1.0	1030	0.282140	+0.3
0.004000	1.467170	0.000035	1.887057	0.000086	16.4	-12.2	0.8	650	0.282428	+1.9
0.001900	1.467177	0.000036	1.887025	0.000087	7.1	-10.3	1.3	650	0.282460	+3.0
0.002900	1.467144	0.000050	1.887019	0.000089	7.2	-12.2	1.4	650	0.282411	+1.3
0.003300	1.467160	0.000039	1.886950	0.000120	7.9	-10.0	1.1	650	0.282461	+3.0
0.001000	1.467129	0.000032	1.886970	0.000110	15.0	-12.4	1.2	650	0.282419	+1.6
0.003800	1.467157	0.000044	1.886969	0.000098	9.6	-9.7	1.3	650	0.282494	+4.2
0.002300	1.467134	0.000048	1.887000	0.000110	8.5	-8.8	1.5	650	0.282521	+5.2
0.003600	1.467219	0.000039	1.886820	0.000130	7.0	-10.7	1.5	650	0.282446	+2.5
0.002900	1.467122	0.000051	1.887093	0.000094	18.9	-12.8	1.3	650	0.282400	+0.9
0.001600	1.467184	0.000038	1.887030	0.000140	12.2	-12.6	1.0	650	0.282421	+1.6
0.002800	1.467185	0.000043	1.887060	0.000100	7.2	-12.5	0.9	650	0.282406	+1.1
0.001800	1.467131	0.000047	1.886890	0.000140	12.8	-11.3	1.4	650	0.282457	+2.9
0.002900	1.467242	0.000046	1.886931	0.000074	13.3	-11.1	1.0	650	0.282453	+2.8
0.005300	1.467277	0.000056	1.887050	0.000140	8.3	-10.0	1.2	650	0.282479	+3.7
0.001400	1.467159	0.000030	1.887100	0.000100	13.1	-12.6	1.1	650	0.282413	+1.3
0.005900	1.467191	0.000052	1.886910	0.000160	8.1	-7.7	1.4	650	0.282543	+6.0
0.003600	1.467175	0.000039	1.886939	0.000095	8.5	-12.5	1.0	650	0.282396	+0.8
0.000940	1.467183	0.000050	1.886880	0.000130	8.0	-8.5	1.6	650	0.282513	+4.9
0.000610	1.467242	0.000044	1.887000	0.000140	6.6	-22.6	1.3	1035	0.282135	+0.2
0.000110	1.467153	0.000041	1.886920	0.000100	6.9	-21.0	1.1	1035	0.282179	+1.7
0.004900	1.467188	0.000042	1.886840	0.000110	9.1	-10.3	1.2	650	0.282452	+2.7
0.002300	1.467113	0.000045	1.886930	0.000120	9.3	-11.0	1.5	650	0.282437	+2.2
0.004300	1.467179	0.000035	1.886910	0.000110	10.1	-11.1	1.3	650	0.282434	+2.1
0.000400	1.467192	0.000034	1.886880	0.000075	15.5	-12.3	1.0	600	0.282426	+0.7
0.003100	1.467185	0.000034	1.886973	0.000064	13.4	-12.3	0.8	600	0.282413	+0.2
0.000490	1.467189	0.000041	1.886958	0.000086	13.5	-12.6	1.1	1035	0.282417	+10.2
0.002000	1.467202	0.000037	1.886914	0.000087	10.7	-12.2	1.1	1035	0.282425	+10.5
0.004900	1.467202	0.000029	1.886968	0.000072	11.0	-11.7	0.9	1035	0.282428	+10.6
0.000120	1.467185	0.000036	1.886860	0.000110	9.9	-11.6	0.8	1035	0.282442	+11.1

0.000220	1.467151	0.000042	1.886980	0.000091	10.2	-13.0	0.8	1035	0.282411	+9.9
0.001400	1.467186	0.000042	1.886970	0.000130	9.2	-12.2	1.1	1035	0.282430	+10.6
0.000890	1.467165	0.000030	1.887002	0.000091	11.0	-12.3	0.7	1035	0.282420	+10.3
0.000350	1.467141	0.000038	1.887023	0.000091	9.4	-12.8	1.0	1035	0.282401	+9.6
0.000790	1.467175	0.000041	1.886836	0.000079	12.6	-12.0	1.0	1035	0.282429	+10.6
0.001200	1.467184	0.000030	1.886817	0.000076	11.9	-12.4	0.8	1035	0.282418	+10.2
0.000730	1.467205	0.000028	1.886906	0.000086	11.0	-12.1	1.0	1035	0.282419	+10.3
0.005000	1.467210	0.000033	1.887067	0.000092	11.4	-12.6	0.9	1035	0.282397	+9.5
0.000370	1.467175	0.000039	1.886830	0.000120	9.6	-11.2	1.2	1035	0.282460	+11.7
0.000240	1.467191	0.000036	1.886956	0.000092	9.8	-13.6	0.9	1035	0.282389	+8.9
0.000690	1.467165	0.000034	1.886932	0.000086	10.2	-13.6	0.8	1035	0.282393	+9.1
0.001300	1.467163	0.000063	1.886880	0.000110	14.2	-17.4	1.5	1035	0.282282	+5.4
0.001400	1.467194	0.000066	1.887180	0.000240	9.4	-13.7	1.5	1035	0.282383	+9.0
0.003000	1.467179	0.000036	1.886893	0.000079	14.2	-19.8	0.6	1035	0.282212	+2.9
0.000058	1.467176	0.000050	1.886900	0.000110	8.9	-14.4	1.1	600	0.282371	-1.2
0.000700	1.467116	0.000043	1.886830	0.000110	6.9	-20.5	1.3	1035	0.282200	+2.5
0.000190	1.467195	0.000052	1.887130	0.000120	5.2	-13.4	1.5	1035	0.282397	+9.5
0.000830	1.467159	0.000053	1.886890	0.000120	7.5	-14.3	1.2	600	0.282367	-1.4
0.001400	1.467112	0.000052	1.886920	0.000110	7.2	-13.2	1.2	600	0.282404	-0.1
0.002800	1.467164	0.000043	1.887040	0.000130	6.3	-13.6	1.3	600	0.282379	-1.0
0.001400	1.467160	0.000049	1.886970	0.000150	9.2	-12.1	1.5	600	0.282425	+0.6
0.001900	1.467134	0.000053	1.886890	0.000110	6.6	-14.0	1.3	600	0.282378	-1.0
0.002600	1.467176	0.000050	1.886840	0.000110	13.1	+1.0	1.2		not calculated	
0.007800	1.467200	0.000037	1.886910	0.000130	11.8	+0.2	1.4	550	0.282765	+11.6
0.005500	1.467172	0.000038	1.886826	0.000090	10.7	+1.6	1.0		not calculated	
0.007000	1.467172	0.000048	1.886960	0.000130	9.3	-0.5	1.7	550	0.282725	+10.2
0.001900	1.467114	0.000057	1.887280	0.000150	11.1	-2.5	1.5	550	0.282691	+9.0
0.000890	1.467203	0.000053	1.886730	0.000140	11.0	-0.8	1.7		not calculated	
0.000210	1.467182	0.000061	1.886760	0.000140	7.9	-3.1	1.4	550	0.282687	+8.8
0.000540	1.467127	0.000047	1.887110	0.000093	10.3	-3.5	1.1		not calculated	
0.000850	1.467196	0.000048	1.887020	0.000140	14.0	-0.1	1.3		not calculated	
0.015000	1.467246	0.000058	1.886760	0.000190	8.1	+1.6	2.7	550	0.282780	+12.1
0.001500	1.467212	0.000045	1.886880	0.000110	11.5	+0.4	1.3		not calculated	
0.000650	1.467232	0.000037	1.887120	0.000110	13.0	-1.0	1.3		not calculated	
0.002900	1.467148	0.000049	1.886810	0.000120	13.4	-1.4	1.3	550	0.282715	+9.8

0.004600	1.467163	0.000036	1.886880	0.000170	10.4	+0.7	1.3	not calculated
0.000280	1.467151	0.000043	1.886880	0.000110	9.6	-21.4	0.9	
0.000670	1.467202	0.000038	1.886968	0.000093	9.8	-21.5	1.1	
0.000150	1.467217	0.000035	1.886953	0.000090	9.8	-21.8	0.9	
0.000032	1.467216	0.000029	1.886980	0.000098	12.5	-21.6	0.8	
0.000550	1.467193	0.000039	1.886967	0.000086	11.9	-22.1	1.1	
0.000038	1.467175	0.000037	1.886979	0.000085	11.7	-21.7	1.0	
0.000300	1.467144	0.000038	1.886970	0.000140	11.2	-22.0	1.1	
0.000210	1.467229	0.000033	1.886874	0.000087	11.4	-20.9	0.9	
0.000150	1.467182	0.000033	1.886891	0.000079	11.3	-21.7	0.9	
0.000058	1.467168	0.000040	1.886919	0.000097	11.1	-21.3	0.9	
0.000180	1.467175	0.000035	1.886958	0.000087	10.6	-20.9	0.9	
0.000580	1.467154	0.000035	1.886938	0.000079	11.7	-21.3	0.8	
0.001300	1.467150	0.000031	1.887040	0.000110	11.2	-23.1	1.0	
0.000270	1.467184	0.000037	1.886953	0.000099	10.0	-22.0	0.9	
0.000130	1.467176	0.000044	1.886990	0.000130	7.4	-22.2	1.5	
0.000110	1.467188	0.000054	1.886910	0.000140	7.7	-22.4	1.2	
0.000520	1.467209	0.000067	1.886790	0.000150	7.0	-21.3	1.6	
0.000140	1.467147	0.000071	1.887000	0.000130	7.8	-21.6	1.3	
0.000760	1.467122	0.000062	1.887180	0.000140	5.7	-22.7	1.6	
0.000710	1.467167	0.000053	1.887150	0.000150	6.6	-24.1	1.3	
0.002400	1.467168	0.000059	1.887200	0.000130	6.5	-23.7	1.5	
0.000190	1.467180	0.000041	1.886830	0.000100	6.7	-21.6	1.2	
0.001300	1.467080	0.000051	1.887080	0.000150	6.3	-23.5	1.8	
0.001400	1.467178	0.000061	1.886980	0.000120	6.4	-20.8	1.3	
0.000420	1.467214	0.000052	1.887090	0.000150	6.4	-22.8	1.7	
0.000240	1.467193	0.000053	1.886930	0.000110	6.0	-21.5	1.3	
0.001900	1.467194	0.000056	1.886990	0.000160	6.0	-21.5	1.3	
0.000390	1.467191	0.000048	1.886910	0.000110	6.3	-21.2	1.2	
0.000350	1.467235	0.000046	1.886820	0.000094	6.9	-21.1	1.1	
0.000430	1.467179	0.000057	1.887200	0.000170	7.4	-24.4	1.8	
0.000250	1.467166	0.000061	1.886960	0.000150	8.6	-23.8	1.6	
0.000310	1.467183	0.000042	1.886880	0.000110	7.0	-20.8	1.1	
0.000590	1.467157	0.000039	1.886914	0.000095	6.8	-23.2	1.1	
0.000680	1.467235	0.000044	1.887040	0.000100	11.8	-21.9	0.9	
0.000380	1.467201	0.000039	1.887000	0.000110	13.3	-21.6	0.9	
0.000130	1.467173	0.000027	1.886827	0.000084	11.7	-21.4	1.0	
0.000260	1.467170	0.000037	1.886881	0.000079	11.5	-22.0	0.7	
						-22.0		
						1.9		
0.000600	1.467177	0.000044	1.886849	0.000095	9.5	-1.4	1.0	
0.001500	1.467196	0.000039	1.886923	0.000090	9.6	-2.3	1.0	
0.001900	1.467221	0.000039	1.886922	0.000072	9.7	-1.2	1.1	
0.007900	1.467179	0.000029	1.886882	0.000087	9.8	-0.9	1.1	
0.002900	1.467188	0.000035	1.886893	0.000096	9.9	-1.7	1.0	
0.003200	1.467183	0.000044	1.886970	0.000120	7.2	+0.2	1.2	
0.000960	1.467164	0.000045	1.887080	0.000110	6.7	-1.4	1.6	
0.001700	1.467178	0.000054	1.886780	0.000110	7.3	-0.5	1.0	
0.000960	1.467160	0.000049	1.886840	0.000110	7.5	-0.4	1.0	
0.001400	1.467245	0.000044	1.887042	0.000087	7.3	-1.2	1.2	
0.003100	1.467164	0.000041	1.886917	0.000090	7.4	-1.1	1.2	
						-1.1		
						1.3		

0.001000	1.467211	0.000041	1.886940	0.000094	8.6	-3.7	0.8
0.000220	1.467231	0.000035	1.886950	0.000100	9.1	-4.6	1.1
0.000900	1.467187	0.000031	1.886867	0.000087	9.8	-3.3	1.0
0.000170	1.467162	0.000034	1.886984	0.000085	10.1	-5.3	0.8
0.000810	1.467191	0.000034	1.886942	0.000080	9.7	-5.0	0.8
0.000130	1.467193	0.000051	1.886899	0.000098	5.9	-4.7	1.5
0.000200	1.467215	0.000048	1.886880	0.000096	5.9	-3.5	1.5
						-4.3	
						1.4	

TABLE S3. SUMMARY OF RESULTS OF O, U-Pb, AND Lu-Hf ISOTOPE ANALYSES

Analysis number	Grain	Spot	Location in grain	$\delta^{18}O$ VSMOW (‰)	±2σ (‰)	$^{206}Pb/^{238}U$ age (Ma)	$^{206}Pb/^{207}Pb$ age (Ma)	Concordance (%)	ε_{Hf} at intrusion or eruption age
Sample Mont1, Montpelier Anorthosite (1040 Ma), zircon, in situ									
mont1_flu_1_1	1	1	core	8.0	0.3	-	-		+12.0
mont1_flu_2_2	2	2	core	7.6	0.3	-	-		+11.0
mont1_flu_3_3	3	3	core	7.7	0.3	313	1122	28	+12.9
mont1_flu_4_4	4	4	core	8.3	0.3	324	623	52	+6.8
mont1_flu_4_5	4	5	core	8.2	0.3	-	-		+8.5
mont1_flu_4_6	4	6	rim	8.0	0.3	-	-		-
mont1_flu_4_7	4	7	rim	8.4	0.3	279	1094	26	-
mont1_flu_5_8	5	8	core	8.2	0.3	453	1664	27	+1.4
mont1_flu_6_9	6	9	core	8.0	0.3	-	-		-
mont1_flu_7_10	7	10	core	8.3	0.3	-	-		-
mont1_flu_8_11	8	11	core	8.3	0.3	-	-		-
mont1_flu_8_13	8	13	core	8.3	0.3	-	-		-
mont1_flu_9_14	9	14	core	8.3	0.3	-	-		-
mont1_flu_10_15	10	15	core	7.8	0.3	-	-		-
mont1_flu_10_16	10	16	core	7.9	0.3	257	858	30	-
mont1_flu_10_17	10	17	rim	7.6	0.3	-	-		-
mont1_flu_11_18	11	18	core	8.3	0.3	-	-		-
Sample 511005, State Farm Gneiss (1030 Ma), zircon, in situ									
511005_big_2_1	2	1	core	7.7	0.2	937	990	95	+1.7
511005_big_3_2	3	2	core	7.6	0.2	1042	1040	100	+1.1
511005_big_3_3	3	3	core	7.8	0.2	1019	1090	93	+2.1
511005_big_4_4	4	4	core	9.7	0.2	1003	1025	98	+0.5
511005_big_5_5	5	5	core	8.3	0.2	993	1019	97	-1.5
511005_big_5_6	5	6	rim	8.2	0.2	1021	1077	95	+2.7
511005_big_6_7	6	7	core	9.0	0.2	970	1036	94	-0.5
511005_big_6_8	6	8	rim	7.9	0.2	1040	1095	95	+0.8
511005_big_7_9	7	9	core	7.7	0.2	766	974	79	+1.7
511005_big_7_10	7	10	mantle	8.2	0.2	1012	1022	99	+1.8
511005_big_7_11	7	11	rim	8.3	0.2	967	1090	89	-
511005_big_8_12	8	12	core	8.3	0.2	999	1039	96	-0.2
511005_big_8_13	8	13	rim	8.2	0.2	1111	1050	106	+1.4
511005_big_9_14	9	14	rim	7.5	0.3	959	1084	88	+2.3
511005_big_9_15	9	15	core	7.6	0.3	898	1028	87	+1.6
511005_big_10_16	10	16	rim?	7.5	0.3	967	1131	85	+1.4
511005_big_10_17	10	17	core	7.2	0.3	1008	1048	96	-0.5
511005_big_11_18	11	18	core	7.7	0.3	-	-		-
511005_big_12_19	12	19	core	7.6	0.3	1013	1043	97	+1.2
511005_big_12_20	12	20	rim	7.6	0.3	1057	1069	99	+0.5
511005_big_13_21	13	21	rim	7.4	0.3	1019	1002	102	+2.2
511005_big_14_22	14	22	core	6.8	0.3	-	-		-
511005_big_15_23	15	23	core	7.6	0.3	1033	1058	98	+1.6
511005_big_16_24	16	24	core	7.5	0.3	1032	1042	99	+1.2
511005_big_17_25	17	25	core	7.7	0.3	1046	1064	98	+1.0
511005_big_18_26	18	26	core	7.7	0.3	1054	1033	102	+2.1
511005_big_18_27	18	27	core	7.8	0.3	1035	1086	95	+1.9
511005_big_19_28	19	28	core	7.9	0.3	1026	1057	97	+2.3
511005_big_19_29	19	29	rim	6.6	0.3	-	-		-
511005_big_20_30	20	30	core	6.9	0.2	990	975	102	not calculated
511005_big_21_31	21	31	core	7.9	0.2	853	1110	77	+1.2
511005_big_22_32	22	32	core	7.5	0.2	988	1040	95	+1.1
511005_big_23_33	23	33	core	8.0	0.2	1033	1058	98	+0.6
511005_big_23_34	23	34	rim	8.0	0.2	1037	1044	99	+1.9
511005_big_24_35	24	35	core	7.5	0.2	958	993	96	-0.4
511005_big_24_36	24	36	rim	7.5	0.2	-	-		-
511005_big_25_37	25	37	core	8.7	0.2	951	1024	93	-0.7
511005_med_1_1	1	1	core	7.3	0.1	955	1001	95	+0.0

511005_med_5_2	5	2	rim	8.2	0.1	1034	1012	102	+1.8
511005_med_5_3	5	3	core	8.2	0.1	1010	1067	95	-0.1
511005_med_6_4	6	4	core	7.9	0.1	994	1041	96	+2.0
511005_med_6_5	6	5	mantle	7.8	0.1	1069	1064	100	+2.1
511005_med_8_6	8	6	mantle	7.3	0.1	1008	1068	94	+0.3
511005_med_8_7	8	7	core	7.2	0.1	-	-		-
511005_med_10_8	10	8	mantle	7.9	0.1	-	-		-
511005_med_10_9	10	9	core	8.8	0.1	-	-		-
511005_med_11_10	11	10	rim	6.4	0.1	-	-		-
511005_med_11_11	11	11	core	7.6	0.1	-	-		-
Sample 511005, State Farm Gneiss, quartz, multi-grain separate									
511005qtz	-	-	-	9.0	0.17				
Sample 511004, Neoproterozoic granitoid (650 Ma), zircon, in situ									
511004_1_1	1	1	rim	-	-	621	636	98	-
511004_1_2	1	2	core	5.2	0.3	-	-		-
511004_3_3	3	3	rim	6.2	0.3	633	675	94	+1.9
511004_3_4	3	4	core	6.1	0.3	569	677	84	+3.0
511004_3_5	3	5	mantle	3.7	0.3	447	690	65	+1.3
511004_4_6	4	6	rim	4.7	0.3	-	-		-
511004_4_7	4	7	mantle	2.0	0.3	620	683	91	+3.0
511004_5_8	5	8	core	1.8	0.3	421	646	65	-
511004_6_9	6	9	rim	6.0	0.3	614	691	89	+1.6
511004_6_10	6	10	core	5.1	0.3	544	620	88	+4.2
511004_7_11	7	11	rim	3.9	0.3	538	727	74	-
511004_7_12	7	12	core	3.1	0.3	627	660	95	-
511004_8_13	8	13	core	3.6	0.3	-	-		-
511004_8_14	8	14	core	1.9	0.3	-	-		-
511004_9_15	9	15	rim	4.3	0.3	555	773	72	+5.2
511004_9_16	9	16	core	2.2	0.3	313	623	50	+2.5
511004_10_17	10	17	rim	3.9	0.3	591	664	89	+0.9
511004_10_18	10	18	core	2.2	0.3	-	-		-
511004_11_19	11	19	core	4.9	0.3	-	-		-
511004_12_20	12	20	rim	-	-	-	-		-
511004_12_21	12	21	core	6.3	0.3	561	693	81	+1.6
511004_13_22	13	22	core	6.4	0.3	628	680	92	-
511004_14_23	14	23	rim	2.2	0.3	-	-		-
511004_14_24	14	24	core	4.7	0.3	565	657	86	+1.1
511004_15_25	15	25	core	5.0	0.3	-	-		+2.9
511004_15_26	15	26	rim	5.3	0.3	598	661	90	-
511004_16_27	16	27	rim	6.2	0.3	591	671	88	+2.8
511004_16_28	16	28	core	4.9	0.3	584	636	92	+3.7
511004_17_29	17	29	core	5.7	0.3	609	685	89	+1.3
511004_18_30	18	30	core	6.0	0.3	549	681	81	+6.0
511004_18_31	18	31	mantle	5.4	0.3	499	624	80	-
511004_18_32	18	32	rim	2.2	0.3	-	-		-
511004_19_33	19	33	core	2.1	0.3	523	839	62	-
511004_20_34	20	34	mantle	4.3	0.3	582	686	85	-
511004_20_35	20	35	core	1.9	0.3	443	659	67	+0.8
511004_21_36	21	36	mantle	3.6	0.3	246	627	39	+4.9
511004_22_37	22	37	rim	3.8	0.3	-	-		-
511004_22_38[a]	22	38	core	4.5	0.3	945	1130	84	+0.2
511004_22_39[a]	22	39	core	4.8	0.3	1124	1108	101	+1.7
511004_22_40	22	40	mantle	2.9	0.3	-	-		-
511004_23_41	23	41	core	6.6	0.3	-	-		-
511004_24_42	24	42	core	2.1	0.3	595	684	87	+2.7
511004_24_43	24	43	mantle	5.9	0.3	602	711	85	-
511004_25_44	25	44	core	1.8	0.3	541	669	81	+2.2
511004_25_45	25	45	mantle	1.8	0.3	-	-		-
511004_26_46	26	46	core	6.7	0.2	-	-		-

511004_26_47	26	47	core	6.7	0.2	-	-		-
511004_27_48	27	48	core	2.7	0.2	389	760	51	+2.1
Sample 511004, Neoproterozoic granitoid, quartz, multi-grain separate									
511004qtz	-	-	-	5.4	0.17				
Sample 511001, Neoproterozoic granitoid (600 Ma), zircon, in situ									
511001_big_1_1	1	1	rim	6.6	0.3	594	694	86	+0.7
511001_big_1_2	1	2	core	6.7	0.3	-	-		-
511001_big_1_3	1	3	rim	6.6	0.3	-	-		-
511001_big_2_4	2	4	core	6.3	0.3	-	-		+0.2
511001_big_4_5[a]	4	5	rim	7.1	0.3	662	791	84	+10.2
511001_big_5_6[a]	5	6	rim	6.9	0.3	637	827	77	+10.5
511001_big_5_7[a]	5	7	core	6.7	0.3	634	693	91	+10.6
511001_big_6_8	6	8	rim	7.0	0.3	-	-		-
511001_big_6_9[a]	6	9	core	6.9	0.3	666	943	71	+11.1
511001_big_7_10	7	10	core	7.0	0.3	578	882	66	-
511001_big_7_11	7	11	rim	7.0	0.3	-	-		-
511001_big_8_12	8	12	rim	6.5	0.3	622	682	91	-
511001_big_8_13	8	13	core	6.2	0.3	622	640	97	-
511001_big_9_14	9	14	rim	6.7	0.3	-	-		-
511001_big_9_15[a]	9	15	mantle	6.7	0.3	666	674	99	+9.9
511001_big_9_16[a]	9	16	mantle	6.7	0.3	664	984	67	+10.6
511001_big_9_17[a]	9	17	core	6.4	0.3	632	766	83	+10.3
511001_big_10_18[a]	10	18	core	6.8	0.3	591	944	63	+9.6
511001_big_11_19	11	19	rim	6.7	0.3	-	-		-
511001_big_11_20[a]	11	20	core	6.6	0.3	616	1062	58	+10.6
511001_big_11_21[a]	11	21	core	6.9	0.3	674	746	90	+10.2
511001_big_11_22[a]	11	22	core	6.6	0.3	659	829	79	+10.3
511001_big_12_23[a]	12	23	core	6.5	0.3	611	669	91	+9.5
511001_big_12_24[a]	12	24	rim	6.7	0.3	599	922	65	+11.7
511001_big_13_25	13	25	core	6.3	0.3	569	656	87	-
511001_big_14_26[a]	14	26	core	6.8	0.3	601	730	82	+8.9
511001_big_14_27[a]	14	27	core	6.8	0.3	622	684	91	+9.1
511001_big_15_28	15	28	rim	6.6	0.2	644	638	101	-
511001_big_16_29[a]	16	29	core	8.2	0.2	1013	1038	98	+5.4
511001_big_16_30[a]	16	30	rim	6.9	0.2	696	799	87	+9.0
511001_big_17_31[a]	17	31	core	7.8	0.2	972	1091	89	+2.9
511001_med_1_1	1	1	rim	6.8	0.2	614	626	98	-1.2
511001_med_1_2[a]	1	2	core	8.3	0.2	881	1005	88	+2.5
511001_med_3_3	3	3	rim	6.2	0.2	507	597	85	-
511001_med_3_4[a]	3	4	core	6.5	0.2	577	989	58	+9.5
511001_med_5_5	5	5	core	6.2	0.2	581	658	88	-1.4
511001_med_5_6	5	6	rim	6.5	0.2	525	659	80	-0.1
511001_med_6_7	6	7	core	6.8	0.2	624	581	107	-1.0
511001_med_10_8	10	8	rim	6.6	0.2	630	634	99	+0.6
511001_med_13_9	13	9	core	6.6	0.2	628	556	113	-1.0
511001_med_17_10	17	10	rim	6.5	0.2	-	-		-
Sample 511001, Neoproterozoic granitoid, quartz, multi-grain separate									
511001qtz	-	-	-	10.0	0.17				
Sample 512001, Sabot Amphibolite felsic layer (550 Ma), zircon, in situ									
512001_Hf_1_1	1	1	core	7.2	0.2	-	-		-
512001_Hf_2_2	2	2	core	8.4	0.2	466	486	96	not calculated
512001_Hf_3_3	3	3	core	8.5	0.2	437	626	70	-
512001_Hf_4_4	4	4	core	8.3	0.2	428	563	76	+11.6
512001_Hf_4_5	4	5	rim	9.2	0.2	-	-		-
512001_Hf_5_6	5	6	core	8.3	0.2	-	-		-
512001_Hf_6_7	6	7	core	8.7	0.2	432	473	91	not calculated

512001_Hf_7_8	7	8	rim	8.9	0.2	436	580	75	+10.2
512001_Hf_7_9	7	9	core	8.2	0.2	452	562	80	+9.0
512001_Hf_8_10	8	10	core	8.3	0.2	-	-		-
512001_Hf_9_11	9	11	core	7.8	0.2	-	-		-
512001_Hf_9_12	9	12	rim	8.6	0.2	-	-		-
512001_Hf_10_13	10	13	core	8.5	0.2	-	-		-
512001_Hf_11_14	11	14	core	9.1	0.2	-	-		-
512001_Hf_11_15	11	15	rim	9.5	0.2	-	-		-
512001_Hf_12_16	12	16	core	8.8	0.2	-	-		-
512001_Hf_13_17	13	17	core	8.2	0.2	456	477	96	not calculated
512001_Hf_14_18	14	18	mantle	5.6	0.2	568	583	97	+8.8
512001_Hf_15_19	15	19	mantle	9.4	0.2	418	497	84	-
512001_Hf_16_20	16	20	mantle	9.3	0.2	434	457	95	not calculated
512001_Hf_17_21	17	21	mantle	9.3	0.2	427	504	85	-
512001_Hf_17_22	17	22	rim	9.3	0.2	419	493	85	not calculated
512001_Hf_18_23	18	23	core	9.3	0.2	431	570	76	-
512001_Hf_19_24	19	24	core	8.7	0.2	507	605	84	+12.1
512001_Hf_20_25	20	25	core	7.9	0.2	-	-		-
512001_Hf_20_26	20	26	rim	9.1	0.2	-	-		-
512001_Hf_20_27	20	27	rim	8.8	0.2	-	-		-
512001_Hf_21_28	21	28	core	8.6	0.2	477	503	95	not calculated
512001_Hf_21_29	21	29	mantle	9.5	0.2	415	480	87	not calculated
512001_Hf_22_30	22	30	core	9.3	0.2	-	-		-
512001_Hf_23_31	23	31	core	9.0	0.2	496	557	89	+9.8
512001_Hf_18b	14	18b	mantle	5.3	0.2	-	-		-
512001_Hf_18c	14	18c	core	7.5	0.2	-	-		-
512001_Hf_18d	14	18d	rim	9.3	0.2	-	-		-
512001_Hf_18e	14	18e	mantle	5.1	0.2	-	-		-
512001_Hf_18f	14	18f	rim	9.2	0.2	-	-		-
512001_Hf_23_32	23	32	rim	8.2	0.2	436	592	74	-
512001_Hf_24_33	24	33	core	8.6	0.2	451	498	91	not calculated
512001_Hf_24_34	24	34	mantle	8.9	0.2	-	-		-
Sample 512001, Sabot Amphibolite felsic layer, quartz multi-grain separate									
512001qtz	-	-	-	12.3	0.17				

[a]Zircon crystallization age of 1035 Ma used to calculate ε_{Hf} for this analysis.

Table S4. Application of multidimensional diagrams to 11 felsic rocks from the State Farm Gneiss.

Figure name	Figure type	Total number of samples	Number of discriminated samples			
			Arc			CR+OI [x ± s] [p_CR+OI] Θ
			IA+CA [x ± s] [p_IA+CA] Θ	IA [x ± s] [p_IA] Θ	CA [x ± s] [p_CA] Θ	
Verma et al. (2012); log-ratios of all major elements	(IA+CA–CR–Col)	11	0 (0)	n/a	n/a	9 [0.859±0.179] (0.5192-0.9849)
	(IA–CA–CR)	11	n/a	0 (0)	1(0.5766)	10 [0.854±0.152] (0.5183-0.9828)
	(IA–CA–Col)	11	n/a	0 (0)	8 [0.882±0.161] (0.4965-0.9790)	n/a
	(IA–CR–Col)	11	n/a	0 (0)	n/a	8 [0.942±0.095] (0.7104-0.9932)
	(CA–CR–Col)	11	n/a	n/a	0 (0)	9 [0.866±0.141] (0.5879-0.9870)
Diagrams based on log-ratios of major elements	***{Σn} {Σprob} [%prob]***	**55**	**{0} {0} [0%]**	**{0} {0} [0%]**	**{9} {7.6338} [16%]**	**{36} {31.6106} [66%]**
Verma et al. (2013); log-ratios of all major elements	(IA+CA-CR+OI-Col)	11	1(0.4030)	n/a	n/a	9 [0.935±0.131] (0.5901-0.9952)
	(IA-CA-CR+OI)	11	n/a	0 (0)	1(0.6444)	10 [0.968±0.059] (0.8129-0.9997)
	(IA-CA-Col)	11	n/a	8 [0.900±0.166] (0.4926-0.9893)	1(0.8424)	n/a
	(IA-CR+OI-Col)	11	n/a	0 (0)	n/a	10 [0.868±0.165] (0.5561-0.9897)
	(CA-CR+OI-Col)	11	n/a	n/a	0 (0)	10 [0.879±0.225] (0.3746-0.9952)
Diagrams based on log-ratios of major elements	***{Σn} {Σprob} [%prob]***	**55**	**{1} {0.4030} [---]**	**{8} {7.1983} [15%]**	**{2} {1.4868} [3%]**	**{39} {35.5664} [73%]**
Verma et al. (2013); log-ratios of immobile major and trace elements	(IA+CA-CR+OI-Col)	11	4 [0.584±0.141] (0.4399-0.7610)	n/a	n/a	6 [0.577±0.170] (0.4777-0.9215)
	(IA-CA-CR+OI)	11	n/a	2 [0.9945±0.0065] (0.9899, 0.9991)	4 [0.611±0.094] (0.5088-0.7356)	5 [0.561±0.204] (0.3383-0.8600)
	(IA-CA-Col)	11	n/a	2 [0.9957±0.0048] (0.9923, 0.9992)	4 [0.609±0.072] (0.5421-0.6916)	n/a
	(IA-CR+OI-Col)	11	n/a	2 [0.99874±0.00160] (0.9976, 0.9999)	n/a	7 [0.630±0.166] (0.4263-0.9378)
	(CA-CR+OI-Col)	11	n/a	n/a	8 [0.653±0.144] (0.4303-0.8720)	2 [0.654±0.228] (0.4928, 0.8156)
Diagrams based on log-ratios of immobile major and trace elements	***{Σn} {Σprob} [%prob]***	**55**	**{4} {2.3349} [---]**	**{6} {5.9780} [19%]**	**{16} {10.1035} [33%]**	**{20} {11.9869} [34%]**

IA−island arc; CA−continental arc; IA+CA–combined island and continental arcs, i.e., arc setting; CR−continental rift; OI−ocean island; CR+OI –com and ocean island, i.e., within-plate (WP) setting; Col−collision; Θ the probability values for samples from a given locality are represented by (pIA+CA combined island and continental arc setting in the first diagram; [pIA] – probability for the island arc setting in the diagrams; [pCA] – probability for the in the diagrams; [pCR+OI] – probability for the combined continental rift and ocean island setting in all diagrams; [pCol] – probability for the collision s − mean ± 1SD (standard deviation) of the probability estimates for all samples discriminated in a given tectonic setting; these are reported in [], the va mostly following the indications put forth by Verma (2005); the final rows give a synthesis of results as {Σn} {Σprob} [%prob], where {Σn} is the total n data points plotting in all five diagrams is reported in the column of total number of samples, whereas the sum of samples plotting in a given tectonic fi respective tectonic field column; {Σprob} is the sum of probability values for all samples plotting in a given tectonic field is reported in the respective te and [%prob] is the total probability of a given tectonic setting expressed in percent after assigning the probability of IA + CA to IA and CA (using weighi Verma and Verma, 2013).

n/a: not applicable

References not cited in main text:

Verma, S.P., 2005, Estadistica basica para el manejo de datos experimentales: aplicacion en la geoquimica (geoquimioemetria). Universidad Nacior Mexico press, Mexico D.F., 186p.

Verma, S.K., Pandarinath, K., and Verma, S.P., 2012, Statistical evaluation of tectonomagmatic discrimination diagrams for granitic rocks and propos function-based multi-dimensional diagrams for acid rocks: International Geology Review, v. 54, p.325-347, doi:10.1080/00206814.2010.543784.

Discrimanant Functions for Figure 5A

DF1 = (–0.091×ln(MgO/TiO2)adj) + (–0.228×ln(P2O5/ TiO2)adj) + (0.729×ln(Nb/ TiO2)adj) + (– 0.237×ln(Y/ TiO2)adj) + (0.577×ln(Zr/ TiO2)adj)

DF2 = (–0.268×ln(MgO/TiO2)adj) + (–1.253×ln(P2O5/ TiO2)adj) + (–0.476×ln(Nb/ TiO2)adj) + (0.209×ln(Y/ TiO2)adj) + (–0.082×ln(Zr/ TiO2)adj)

Col [x ± s] [p_Col] Θ
2 [0.879±0.085] (0.8188, 0.9393)
n/a
3 [0.880±0.168] (0.6876-0.9992)
3 [0.850±0.113] (0.7312-0.9554)
2 [0.797±0.056] (0.7577, 0.8362)
{10} {8.5418} [18%]
1(0.8994)
n/a
2 [0.9919±0.0106] (0.9844, 0.9994)
1(0.8355)
1(0.8203)
{5} {4.5389} [9%]
1(0.6024)
n/a
5 [0.558±0.078] (0.4723-0.6789)
2 [0.478±0.120] (0.3939, 0.5629)
1(0.4879)
{9} {4.8353} [14%]

bined continental rift
.) – probability for the
continental arc setting
etting in the diagrams;
lues are rounded
umber of samples or
eld is reported in the
ectonic field column;
ng factors explained in

nal Autonoma de

al of new discriminant-

+ 4.704.
– 3.709.

Table S5. Application of multidimensional diagrams to 4 intermediate rocks from the State Farm Gneiss.

Figure name	Figure type	Total number of samples	Number of discriminated samples: Arc: IA+CA [x ± s] [p_IA+CA] Θ	Arc: IA [x ± s] [p_IA] Θ	Arc: CA [x ± s] [p_CA] Θ	CR+OI [x ± s] [p_CR+OI] Θ
Verma and Verma (2013); log-ratios of all major elements	(IA+CA-CR+OI-Col)	4	0 (0)	n/a	n/a	4 [0.9963±0.0073] (0.9854-1.0000)
	(IA-CA-CR+OI)	4	n/a	0 (0)	0 (0)	4 [0.99920±0.00028] (0.9989-0.9996)
	(IA-CA-Col)	4	n/a	3 [0.99996±0.00002] (0.9999-1.0000)	0 (0)	n/a
	(IA-CR+OI-Col)	4	n/a	0 (0)	n/a	4 [0.9944±0.0056] (0.9859-0.9977)
	(CA-CR+OI-Col)	4	n/a	n/a	0 (0)	4 [0.9972±0.0057] (0.9886-1.0000)
Diagrams based on log-ratios of major elements	***{Σn} {Σprob} [%prob]***	**20**	**{0} {0} [0%]**	**{3} {2.9999} [15%]**	**{0} {0} [0%]**	**{16} {15.9483} [80%]**
Verma and Verma (2013); log-ratios of immobile major and trace elements	(IA+CA-CR+OI-Col)	1	0 (0)	n/a	n/a	1(0.9872)
	(IA-CA-CR+OI)	1	n/a	0 (0)	0 (0)	1(0.9984)
	(IA-CA-Col)	1	n/a	0 (0)	0 (0)	n/a
	(IA-CR+OI-Col)	1	n/a	0 (0)	n/a	1(0.9847)
	(CA-CR+OI-Col)	1	n/a	n/a	0 (0)	1(0.9955)
Diagrams based on log-ratios of major elements	***{Σn} {Σprob} [%prob]***	**5**	**{0} {0} [0%]**	**{0} {0} [0%]**	**{0} {0} [0%]**	**{4} {3.9658} [81%]**

IA−island arc; CA−continental arc; IA+CA–combined island and continental arcs, i.e., arc setting; CR−continental rift; OI−ocean island; CR+O
continental rift and ocean island, i.e., within-plate (WP) setting; Col−collision; Θ the probability values for samples from a given locality are rep
(pIA+CA) – probability for the combined island and continental arc setting in the first diagram; [pIA] – probability for the island arc setting in the
[pCA] – probability for the continental arc setting in the diagrams; [pCR+OI] – probability for the combined continental rift and ocean island setti
diagrams; [pCol] – probability for the collision setting in the diagrams; − mean ± 1SD (standard deviation) of the probability estimates for all sa
discriminated in a given tectonic setting; these are reported in [], the values are rounded mostly following the indications put forth by Verma (20
rows give a synthesis of results as {Σn} {Σprob} [%prob], where {Σn} is the total number of samples or data points plotting in all five diagrams i
the column of total number of samples, whereas the sum of samples plotting in a given tectonic field is reported in the respective tectonic field c
is the sum of probability values for all samples plotting in a given tectonic field is reported in the respective tectonic field column; and [%prob] is
probability of a given tectonic setting expressed in percent after assigning the probability of IA + CA to IA and CA (using weighing factors explai
and Verma, 2013).

n/a: not applicable

References not cited in main text:

Verma, S.P., 2005, Estadistica basica para el manejo de datos experimentales: aplicacion en la geoquimica (geoquimioemetria). Universidad
Autonoma de Mexico press, Mexico D.F., 186p.

Discriminant Functions for Figure 5B

DF1 = (–2.45605×ln(TiO2/SiO2)adj) + (1.11985×ln(Al2O3/SiO2)adj) + (–2.22475×ln(Fe2O3/SiO2)adj) + (2.48861×ln(FeO/SiO2)adj) + (–0.21

$$DF2 = (-0.57759 \times \ln(TiO_2/SiO_2)_{adj}) + (-0.01121 \times \ln(Al_2O_3/SiO_2)_{adj}) + (0.69125 \times \ln(Fe_2O_3/SiO_2)_{adj}) + (-1.99798 \times \ln(FeO/SiO_2)_{adj}) + (-1.7$$

Col [x ± s] [p_Col] Θ
0 (0)
n/a
1(0.9022)
0 (0)
0 (0)
{1} {0.9022} [5%]
0 (0)
n/a
1(0.9600)
0 (0)
0 (0)
{1} {0.9600} [19%]

l –combined
ɔresented by
diagrams;
ng in all
ımples
05); the final
is reported in
ɔolumn; {Σprob}
ꞩ the total
ned in Verma

Nacional

2024×ln(MnO/SiO2)adj) + (–0.06661×ln(MgO/SiO2)adj) + (1.29066×ln(CaO/SiO2)adj) + (–0.28377×ln(Na2O/SiO2)adj) + (–0.40211×ln(K2O/S

'2014×ln(MnO/SiO2)adj) + (0.305275×ln(MgO/SiO2)adj) + (0.816018×ln(CaO/SiO2)adj) + (–1.791727×ln(Na2O/SiO2)adj) + (0.871298×ln(K2(

SiO2)adj) + (0.030635×ln(P2O5/SiO2)adj) – 11.43097347.

$O/SiO_2)_{adj}) + (0.335479 \times \ln(P_2O_5/SiO_2)_{adj}) - 12.20158596.$

Table S6. Application of multidimensional diagrams to 11 felsic rocks from the Neoproterozoic granitoid.

Figure name	Figure type	Total number of samples	Number of discriminated samples			
			Arc			CR+OI [x ± s] [p_CR+OI] Θ
			IA+CA [x ± s] [p_IA+CA] Θ	IA [x ± s] [p_IA] Θ	CA [x ± s] [p_CA] Θ	
Verma et al. (2012); log-ratios of all major elements	(IA+CA–CR–Col)	11	0 (0)	n/a	n/a	8 [0.9600±0.0392] (0.8684-0.9879)
	(IA–CA–CR)	11	n/a	0 (0)	3 [0.747±0.169] (0.5969-0.9300)	8 [0.9881±0.0092] (0.9711-0.9979)
	(IA–CA–Col)	11	n/a	0 (0)	8 [0.771±0.131] (0.5311-0.9496)	n/a
	(IA–CR–Col)	11	n/a	0 (0)	n/a	8 [0.933±0.069] (0.7766-0.9830)
	(CA–CR–Col)	11	n/a	n/a	0 (0)	8 [0.922±0.065] (0.7770-0.9815)
Diagrams based on log-ratios of major elements	***{Σn} {Σprob} [%prob]***	**55**	**{0} {0} [0%]**	**{0} {0} [0%]**	**{11} {8.4102} [17%]**	**{32} {30.4255} [62%]**
Verma et al. (2013); log-ratios of all major elements	(IA+CA-CR+OI-Col)	11	0 (0)	n/a	n/a	9 [0.875±0.120] (0.6129-0.9878)
	(IA-CA-CR+OI)	11	n/a	0 (0)	0 (0)	11 [0.9871±0.0122] (0.9628-0.9990)
	(IA-CA-Col)	11	n/a	3 [0.622±0.088] (0.5551-0.7216)	5 [0.755±0.154] (0.5009-0.8936)	n/a
	(IA-CR+OI-Col)	11	n/a	0 (0)	n/a	9 [0.856±0.118] (0.6041-0.9759)
	(CA-CR+OI-Col)	11	n/a	n/a	0 (0)	9 [0.834±0.122] (0.6440-0.9728)
Diagrams based on log-ratios of major elements	***{Σn} {Σprob} [%prob]***	**55**	**{0} {0} [0%]**	**{3} {1.8672} [4%]**	**{5} {3.7754} [8%]**	**{38} {33.9400} [72%]**
Verma et al. (2013); log-ratios of immobile major and trace elements	(IA+CA-CR+OI-Col)	11	0 (0)	n/a	n/a	10 [0.877±0.122] (0.6154-0.9948)
	(IA-CA-CR+OI)	11	n/a	0 (0)	0 (0)	11 [0.9944±0.0069] (0.9765-1.0000)
	(IA-CA-Col)	11	n/a	0 (0)	0 (0)	n/a
	(IA-CR+OI-Col)	11	n/a	0 (0)	n/a	10 [0.860±0.112] (0.6421-0.9892)
	(CA-CR+OI-Col)	11	n/a	n/a	0 (0)	10 [0.864±0.128] (0.5921-0.9888)

Diagrams based on log-ratios of immobile major and trace elements	***{Σn} {Σprob} [%prob]***	**55**	**{0} {0} [0%]**	**{0} {0} [0%]**	**{0} {0} [0%]**	**{41} {36.9469} [75%]**

IA−island arc; CA−continental arc; IA+CA–combined island and continental arcs, i.e., arc setting; CR−continental rift; OI−ocean island; CR+OI –
rift and ocean island, i.e., within-plate (WP) setting; Col−collision; Θ the probability values for samples from a given locality are represented by (
for the combined island and continental arc setting in the first diagram; [pIA] – probability for the island arc setting in the diagrams; [pCA] – probab
arc setting in the diagrams; [pCR+OI] – probability for the combined continental rift and ocean island setting in all diagrams; [pCol] – probability fo
in the diagrams; − mean ± 1SD (standard deviation) of the probability estimates for all samples discriminated in a given tectonic setting; these ar
values are rounded mostly following the indications put forth by Verma (2005); the final rows give a synthesis of results as {Σn} {Σprob} [%prob],
number of samples or data points plotting in all five diagrams is reported in the column of total number of samples, whereas the sum of samples
tectonic field is reported in the respective tectonic field column; {Σprob} is the sum of probability values for all samples plotting in a given tectonic
respective tectonic field column; and [%prob] is the total probability of a given tectonic setting expressed in percent after assigning the probability
CA (using weighing factors explained in Verma and Verma, 2013).

n/a: not applicable

References not cited in main text:

Verma, S.P., 2005, Estadistica basica para el manejo de datos experimentales: aplicacion en la geoquimica (geoquimioemetria). Universidad N
Mexico press, Mexico D.F., 186p.

Verma, S.K., Pandarinath, K., and Verma, S.P., 2012, Statistical evaluation of tectonomagmatic discrimination diagrams for granitic rocks and pr
discriminant-function-based multi-dimensional diagrams for acid rocks: International Geology Review, v. 54, p.325-347, doi:10.1080/00206814.2

Col [x ± s] [p_Col] Θ
3 [0.867±0.134] (0.7135-0.9605)
n/a
3 [0.916±0.058] (0.8532-0.9663)
3 [0.910±0.052] (0.8508-0.9417)
3 [0.756±0.150] (0.6490-0.9269)
{12} {10.3482} [21%]
2 [0.856±0.125] (0.7677, 0.9449)
n/a
3 [0.865±0.131] (0.7145-0.9499)
2 [0.822±0.116] (0.7401, 0.9042)
2 [0.798±0.166] (0.6804, 0.9157)
{9} {7.5474} [16%]
1(0.6571)
n/a
11 [0.9704±0.0392] (0.8654-1.0000)
1(0.5792)
1(0.6249)

{14} {12.5353} [25%]

combined continental
pIA+CA) – probability
ility for the continental
r the collision setting
e reported in [], the
where {Σn} is the total
plotting in a given
field is reported in the
of IA + CA to IA and

acional Autonoma de

posal of new
10.543784.

Table S7. Application of multidimensional diagrams to 2 intermediate rocks from the Neoproterozoic granito

Figure name	Figure type	Total number of samples	Number of discriminated samples			
			Arc			CR+OI [x ± s] [p_CR+OI] Θ
			IA+CA [x ± s] [p_IA+CA] Θ	IA [x ± s] [p_IA] Θ	CA [x ± s] [p_CA] Θ	
Verma and Verma (2013); log-ratios of all major elements	(IA+CA-CR+OI-Col)	2	0 (0)	n/a	n/a	2 [0.820±0.190] (0.6857, 0.9543)
	(IA-CA-CR+OI)	2	n/a	0 (0)	0 (0)	2 [0.698±0.290] (0.4926, 0.9028)
	(IA-CA-Col)	2	n/a	2 [0.8994±0.0299] (0.8782, 0.9205)	0 (0)	n/a
	(IA-CR+OI-Col)	2	n/a	0 (0)	n/a	2 [0.783±0.213] (0.6329, 0.9334)
	(CA-CR+OI-Col)	2	n/a	n/a	0 (0)	2 [0.922±0.091] (0.8576, 0.9862)
Diagrams based on log-ratios of major elements	***{Σn} {Σprob} [%prob]***	**10**	**{0} {0} [0%]**	**{2} {1.7988} [22%]**	**{0} {0} [0%]**	**{8} {6.4454} [78%]**

IA−island arc; CA−continental arc; IA+CA–combined island and continental arcs, i.e., arc setting; CR−continental rift; OI−ocean island; CR· continental rift and ocean island, i.e., within-plate (WP) setting; Col−collision; Θ the probability values for samples from a given locality are (pIA+CA) – probability for the combined island and continental arc setting in the first diagram; [pIA] – probability for the island arc setting in t [pCA] – probability for the continental arc setting in the diagrams; [pCR+OI] – probability for the combined continental rift and ocean island s diagrams; [pCol] – probability for the collision setting in the diagrams; − mean ± 1SD (standard deviation) of the probability estimates for all discriminated in a given tectonic setting; these are reported in [], the values are rounded mostly following the indications put forth by Verma (rows give a synthesis of results as {Σn} {Σprob} [%prob], where {Σn} is the total number of samples or data points plotting in all five diagran the column of total number of samples, whereas the sum of samples plotting in a given tectonic field is reported in the respective tectonic fie {Σprob} is the sum of probability values for all samples plotting in a given tectonic field is reported in the respective tectonic field column; an total probability of a given tectonic setting expressed in percent after assigning the probability of IA + CA to IA and CA (using weighing factor Verma and Verma, 2013).

n/a: not applicable

References not cited in main text:

Verma, S.P., 2005, Estadistica basica para el manejo de datos experimentales: aplicacion en la geoquimica (geoquimioemetria). Universic Autonoma de Mexico press, Mexico D.F., 186p.

id.

Col [x ± s] [p_Col] Θ
0 (0)
n/a
0 (0)
0 (0)
0 (0)
{0} {0} [0%]

+OI –combined
represented by
he diagrams;
etting in all
l samples
2005); the final
ns is reported in
ld column;
d [%prob] is the
s explained in

lad Nacional

Table S8. Application of multidimensional diagrams to 8 mafic rocks from the Sabot Amphibolite

Discrimination Figure Type	Number of samples					Percentage of samples				
	IAB	CRB+OIB	CRB	OIB	MORB	IAB	CRB+OIB	CRB	OIB	MORB
Agrawal et al. (2008)										
MORB-IAB-CRB+OIB	1	0	n/a	n/a	7	13	0	n/a	n/a	88
IAB-OIB-CRB	1	n/a	3	4	n/a	13	n/a	38	50	n/a
MORB-IAB-CRB	1	n/a	1	n/a	6	13	n/a	13	n/a	75
MORB-IAB-OIB	1	n/a	n/a	0	7	13	n/a	n/a	0	88
MORB-OIB-CRB	n/a	n/a	2	0	6	n/a	n/a	25	0	75
Verma and Agrawal (2011)										
MORB-IAB-CRB+OIB	1	2	n/a	n/a	5	13	25	n/a	n/a	63
IAB-OIB-CRB	4	n/a	2	2	n/a	50	n/a	25	25	n/a
MORB-IAB-CRB	2	n/a	2	n/a	4	25	n/a	25	n/a	50
MORB-IAB-OIB	0	n/a	n/a	3	5	0	n/a	n/a	38	63
MORB-OIB-CRB	n/a	n/a	1	2	5	n/a	n/a	13	25	63

IAB-Island Arc Basalt, CRB-Continental Rift Basalt, OIB-Ocean Island Basalt, MORB-Mid-ocean Ridge Basalt
n/a: not applicable
Reference not cited in main text:

Verma, S.P. and Agrawal, S., 2011. New tectonic discrimination diagrams for basic and ultrabasic volcanic rocks through log-transformed ratios of high field strength elements and implications for petrogenetic processes: Revista Mexicana de Ciencias Geologicas, v.28, p. 24-44.

Discriminant functions for Figure 5C

$DF1 = -0.5558\times\ln(La/Th) - 1.4260\times\ln(Sm/Th) + 2.2935\times\ln(Yb/Th) - 0.6890\times\ln(Nb/Th) + 4.1422.$

$DF2 = -0.9207\times\ln(La/Th) + 3.6520\times\ln(Sm/Th) - 1.9866\times\ln(Yb/Th) + 1.0574\times\ln(Nb/Th) - 4.4283.$

TABLE S9: SABOT1 ZIRCON U-Pb GEOCHRONOLOGIC A

				Isotope ratios								
Analysis	U conc	206Pb	U	206Pb*	±	207Pb*	±	206Pb*	±	error	206Pb*	±
	(ppm)	204Pb	Th	207Pb*	(%)	235U	(%)	238U	(%)	corr.	238U	(Ma)
Sample Sabot1: Sabot Amphibolite												
SABOT_23R	474	58838	37.2	17.9536	0.7	0.4911	3.2	0.0640	3.1	0.98	400	12
SABOT_27C	261	46277	68.8	17.8460	0.9	0.5119	1.9	0.0663	1.6	0.87	414	7
SABOT_4RTOP	273	41255	15.3	18.1093	0.6	0.5053	3.7	0.0664	3.7	0.99	414	15
SABOT_32RNORTH	689	113986	51.2	18.0178	0.9	0.5088	3.0	0.0665	2.9	0.96	415	12
SABOT_26C	117	27348	98.6	17.8605	1.5	0.5177	4.5	0.0671	4.3	0.94	418	17
SABOT_7CRIGHT	957	179202	3.7	17.8937	1.2	0.5169	3.9	0.0671	3.7	0.95	419	15
SABOT_28RLEFT	327	72433	34.3	17.9474	1.1	0.5211	3.3	0.0678	3.1	0.94	423	13
SABOT_32RSOUTH	510	66601	48.7	17.9758	0.8	0.5230	2.8	0.0682	2.7	0.96	425	11
SABOT_26R	147	30641	114.9	17.6739	0.9	0.5413	4.0	0.0694	3.9	0.97	432	16
SABOT_15R	421	86159	49.0	17.7857	0.8	0.5405	3.4	0.0697	3.3	0.97	434	14
SABOT_24C	914	140651	8.7	17.8605	0.7	0.5409	2.8	0.0701	2.7	0.97	437	11
SABOT_29R	655	149791	37.1	17.9653	1.0	0.5386	3.3	0.0702	3.2	0.96	437	13
SABOT_32C	322	98660	29.7	17.9046	1.0	0.5466	2.8	0.0710	2.6	0.93	442	11
SABOT_1R	811	352284	39.6	18.0059	0.6	0.5467	2.8	0.0714	2.7	0.98	445	12
SABOT_5R	654	163994	57.6	17.9615	1.0	0.5493	2.9	0.0716	2.7	0.94	446	12
SABOT_7CLEFT	910	389377	6.9	17.7907	1.0	0.5591	3.2	0.0721	3.1	0.95	449	13
SABOT_18R	849	150355	31.2	17.9972	0.7	0.5546	3.1	0.0724	3.0	0.97	451	13
SABOT_32CLEFT	1228	375056	1.4	17.3415	0.6	0.5789	2.9	0.0728	2.8	0.98	453	12
SABOT_18CNORTH	594	180733	2.9	17.4905	1.4	0.6041	1.7	0.0766	1.0	0.56	476	4
SABOT_10C	540	111407	2.6	17.4736	1.8	0.6195	2.6	0.0785	1.9	0.73	487	9
SABOT_9R	186	43387	0.8	16.8970	1.0	0.6497	3.6	0.0796	3.5	0.96	494	17
SABOT_20CLEFT	279	46663	1.7	17.0319	0.8	0.6651	2.5	0.0822	2.4	0.95	509	12
SABOT_20CRIGHT	286	84374	1.5	17.0847	0.7	0.6797	2.8	0.0842	2.7	0.97	521	14
SABOT_2C	691	135951	0.8	17.1052	0.6	0.7028	3.6	0.0872	3.6	0.99	539	18
SABOT_16C	622	206885	2.0	17.2203	1.6	0.7048	2.3	0.0880	1.7	0.73	544	9
SABOT_23C	838	203148	1.7	17.0316	0.8	0.7143	3.0	0.0882	2.9	0.96	545	15
SABOT_22	559	162563	2.1	17.2705	1.0	0.7104	1.2	0.0890	0.7	0.56	550	4
SABOT_17C	207	92597	4.3	17.2809	1.3	0.7110	2.4	0.0891	2.0	0.84	550	11
SABOT_29C	1057	367657	1.5	17.0325	0.6	0.7246	2.7	0.0895	2.7	0.97	553	14
SABOT_4C	714	207711	1.6	17.0338	0.6	0.7281	2.5	0.0899	2.4	0.97	555	13
SABOT_6C	95	33842	1.9	16.9634	1.3	0.7352	2.3	0.0904	1.9	0.82	558	10
SABOT_12C	338	139859	1.3	16.9958	1.0	0.7405	2.5	0.0913	2.3	0.92	563	12
SABOT_19C	483	169181	1.4	17.1510	1.0	0.7391	3.5	0.0919	3.4	0.96	567	18
SABOT_18CSOUTH	1065	345799	0.9	17.0609	0.7	0.7441	2.7	0.0921	2.6	0.97	568	14
SABOT_27CRIGHT	1348	562719	0.8	17.0680	0.8	0.7533	2.9	0.0933	2.8	0.96	575	15
SL-1	517	88955	4.7	16.9732	0.8	0.7295	2.6	0.0898	2.5	0.95	554	13
SL-2	535	168988	4.9	16.9720	0.8	0.7443	3.1	0.0916	3.0	0.96	565	16
SL-3	545	213580	4.7	16.9209	0.6	0.7493	3.6	0.0920	3.6	0.99	567	19
SL-4	602	311133	3.4	16.9503	0.6	0.6990	2.6	0.0859	2.5	0.97	531	13
SL-5	521	149791	4.6	16.9430	0.9	0.7344	3.1	0.0902	3.0	0.96	557	16
SL-6	563	145589	5.0	16.9884	0.7	0.7268	2.6	0.0895	2.5	0.96	553	13
SL-7	515	143722	4.9	17.0360	0.7	0.7203	2.5	0.0890	2.4	0.96	550	13
SL-8	513	192850	4.7	16.9686	0.7	0.7777	2.6	0.0957	2.5	0.96	589	14
SL-9	567	166608	4.2	17.0331	0.5	0.7565	3.4	0.0935	3.3	0.99	576	18

SL-10	466	148522	5.1	16.9089	0.7	0.7566	2.1	0.0928	1.9	0.93	572	10
SL-11	527	287548	4.6	16.9730	0.5	0.7619	3.8	0.0938	3.8	0.99	578	21
SL-12	528	271828	4.4	16.9075	0.8	0.7686	2.9	0.0942	2.8	0.96	581	15
SL-13	583	137406	3.4	16.9518	0.8	0.7096	2.8	0.0872	2.7	0.96	539	14
SL-14	554	83775	4.1	17.1175	0.9	0.7457	3.1	0.0926	3.0	0.96	571	16
SL-15	601	238531	4.4	17.0362	0.7	0.7455	3.4	0.0921	3.3	0.98	568	18
SL-16	506	372883	4.8	16.9831	0.7	0.7546	2.3	0.0930	2.2	0.96	573	12
SL-17	504	280293	4.9	16.9330	0.7	0.7225	3.3	0.0887	3.3	0.98	548	17
SL-18	533	293166	3.5	16.8847	0.9	0.7361	3.7	0.0901	3.6	0.97	556	19
SL-19	488	201353	4.5	17.1048	1.0	0.7377	2.1	0.0915	1.9	0.89	564	10
SL-20	537	211802	5.0	16.8819	0.5	0.7623	2.7	0.0933	2.6	0.98	575	14
SL-21	423	145043	4.8	16.9887	0.6	0.7612	2.6	0.0938	2.5	0.97	578	14
SL-22	528	111855	4.6	16.9399	1.1	0.7668	3.0	0.0942	2.8	0.93	580	16
SL-23	560	131619	4.7	17.0045	1.2	0.7162	3.4	0.0883	3.1	0.93	546	16
SL-24	570	115497	3.4	17.0101	0.8	0.7112	2.9	0.0877	2.8	0.96	542	14
SL-25	474	110203	4.9	17.0689	0.6	0.7026	3.9	0.0870	3.8	0.99	538	20
SL-26	476	122629	4.4	16.9622	0.8	0.7594	3.0	0.0934	2.9	0.96	576	16
SL-27	502	87944	4.8	16.9513	0.7	0.7532	2.9	0.0926	2.8	0.97	571	15
SL-28	493	167499	4.8	16.9500	0.7	0.7488	2.9	0.0920	2.8	0.97	568	15
SL-29	511	80010	4.6	16.9813	0.7	0.7515	3.0	0.0925	2.9	0.97	571	16
SL-30	531	124510	3.3	16.9351	0.9	0.7555	3.1	0.0928	3.0	0.96	572	17
SL-31	530	106359	4.3	17.0474	0.5	0.7272	2.6	0.0899	2.6	0.98	555	14
SL-32	511	446256	5.0	16.8728	0.9	0.7402	2.8	0.0906	2.7	0.95	559	14
SL-33	496	151939	4.9	16.9780	0.8	0.7448	3.5	0.0917	3.4	0.98	566	18
SL-34	413	130260	4.8	16.8934	0.5	0.7446	2.2	0.0912	2.1	0.97	563	12
SL-35	501	205284	4.5	16.9965	0.5	0.7655	3.7	0.0944	3.7	0.99	581	20
SL-36	514	190177	3.5	16.9487	1.0	0.7454	3.1	0.0916	2.9	0.95	565	16
SL-37	445	112940	5.0	17.0999	0.7	0.7122	2.7	0.0883	2.6	0.97	546	14
SL-38	525	118038	5.1	16.9928	1.0	0.7340	2.6	0.0905	2.4	0.92	558	13
SL-39	475	168655	4.8	17.0638	0.7	0.7568	3.2	0.0937	3.1	0.98	577	17
SL-40	527	132908	4.7	16.9466	0.7	0.7307	3.6	0.0898	3.6	0.98	554	19
SL-41	501	127068	4.5	16.9434	1.0	0.7540	3.1	0.0927	3.0	0.95	571	16
SL-42	541	184749	3.3	16.9339	0.7	0.7406	2.9	0.0910	2.9	0.97	561	15

*=radiogenic lead.

Notes:

1. Analyses with >5% uncertainty (1-sigma) in 206Pb/238U age or >5% uncertainty (1-sigma) in 206Pb/207Pb age are not included.
2. Concordance is 206Pb/238U age / 206Pb/207Pb age.
3. Analysis with >20% discordance (<80% concordance) are not included.
4. Analyses with >5% reverse discordance (>105% concordance) are not included.
5. Analyses were conducted by LA-MC-ICPMS, as described by Gehrels and Pecha (2014).
6. Uncertainties for individual analyses are reported at the 1-sigma level, and include only measurement errors.
7. Systematic errors for 206Pb/238U and 206Pb/207Pb ages were 1.7% and 0.8% (2-sigma), respectively.
8. U concentration and U/Th are calibrated relative to Sri Lanka zircon standard, and are accurate to about 20%.
9. Common Pb correction is from measured 204Pb.
10. Common Pb composition interpreted from Stacey and Kramers (1975).
11. Common Pb composition assigned uncertainties of 1.5 for 206Pb/204Pb, 0.3 for 207Pb/204Pb, and 2.0 for 208Pb/204Pb.
12. U/Pb and 206Pb/207Pb fractionation is calibrated relative to fragments of a large Sri Lanka zircon with age 563.5 ± 3.2 Ma (2-sigma).
13. U decay constants and composition as follows: 238U = 9.8485 x 10-10, 235U =1.55125 x 10-10, 238U/235U = 137.88.
14. Best age is 206Pb/207Pb age for zircon older than 700 Ma and 206Pb/238U age for younger grains.

15. Analyses labeled with 'C' or 'R' refer to the core and rim of the grain respectively.
16. Analyses colored red and blue were used to date crystallization of igneous and metamorphic zircon, respectively.
17. Analyses labeled "SL" were of the Sri Lanka zircon standard.

NALYSES

Apparent ages (Ma)						
207Pb*	±	206Pb*	±	Best age	±	Concor
235U	(Ma)	207Pb*	(Ma)	(Ma)	(Ma)	(%)
406	11	440	16	400	12	90.7
420	6	454	20	414	7	91.1
415	13	421	13	414	15	98.4
418	10	432	19	415	12	96.0
424	16	452	33	418	17	92.6
423	14	448	26	419	15	93.5
426	12	441	24	423	13	95.9
427	10	438	18	425	11	97.2
439	14	475	20	432	16	91.0
439	12	461	17	434	14	94.2
439	10	452	16	437	11	96.6
438	12	439	21	437	13	99.6
443	10	446	22	442	11	99.0
443	10	434	13	445	12	102.5
445	10	439	21	446	12	101.4
451	12	461	22	449	13	97.5
448	11	435	16	451	13	103.6
464	11	517	14	453	12	87.6
480	6	498	31	476	4	95.5
490	10	500	40	487	9	97.4
508	14	574	21	494	17	86.1
518	10	556	17	509	12	91.5
527	11	550	15	521	14	94.8
540	15	547	12	539	18	98.5
542	10	532	35	544	9	102.1
547	13	557	18	545	15	97.9
545	5	526	22	550	4	104.5
545	10	525	29	550	11	104.9
553	12	556	14	553	14	99.3
555	11	556	14	555	13	99.8
560	10	565	29	558	10	98.8
563	11	561	21	563	12	100.4
562	15	541	21	567	18	104.8
565	12	553	15	568	14	102.7
570	13	552	18	575	15	104.1
556	11	564	18	554	13	98.3
565	13	564	18	565	16	100.2
568	16	571	13	567	19	99.4
538	11	567	14	531	13	93.7
559	14	568	19	557	16	98.1
555	11	562	16	553	13	98.4
551	11	556	16	550	13	98.9
584	12	565	16	589	14	104.4
572	15	556	11	576	18	103.5

572	9	572	16	572	10	99.9
575	17	564	12	578	21	102.5
579	13	572	17	581	15	101.4
544	12	567	16	539	14	95.1
566	13	546	20	571	16	104.6
566	15	556	16	568	18	102.2
571	10	563	14	573	12	101.8
552	14	569	15	548	17	96.3
560	16	575	19	556	19	96.7
561	9	547	21	564	10	103.2
575	12	576	12	575	14	99.9
575	11	562	14	578	14	102.8
578	13	568	23	580	16	102.1
548	14	560	27	546	16	97.4
545	12	559	17	542	14	96.9
540	16	552	14	538	20	97.4
574	13	565	17	576	16	101.8
570	13	567	14	571	15	100.7
568	13	567	16	568	15	100.1
569	13	563	15	571	16	101.4
571	14	569	19	572	17	100.5
555	11	554	11	555	14	100.1
563	12	577	20	559	14	96.9
565	15	563	17	566	18	100.4
565	10	574	11	563	12	98.0
577	16	561	12	581	20	103.6
566	13	567	21	565	16	99.6
546	11	548	15	546	14	99.6
559	11	562	22	558	13	99.4
572	14	552	15	577	17	104.5
557	16	567	14	554	19	97.7
571	14	568	21	571	16	100.6
563	13	569	15	561	15	98.6

TABLE S10. SABOT AMPHIBOLITE WHOLE ROCK Sm-Nd ISOTOPE DATA

Sample number	Sm (ppm)	Nd (ppm)	Sm/Nd	$^{147}Sm/^{144}Nd$	$^{143}Nd/^{144}Nd$	± 2σ[a]	ε_{Nd} today	ε_{Nd} at 550 Ma
1994	5.05	16.7	0.302	0.1823	0.512828	4	+3.9	+4.8
SA-001	5.46	22.5	0.243	0.1468	0.512605	5	-0.5	+3.0
GT98-005	2.69	8.11	0.332	0.2003	0.512826	6	+3.8	+3.5
SA-007	4.01	13.7	0.293	0.1765	0.512819	4	+3.7	+5.1
GT98-012	1.26	3.45	0.365	0.2207	0.513008	7	+7.4	+5.6
GT98-013	0.564	1.39	0.406	0.2452	0.512885	9	+5.0	+1.5
GT99-014	2.76	7.97	0.346	0.2093	0.512998	5	+7.2	+6.3

[a]Uncertainty on the least significant digit in the measured $^{143}Nd/^{144}Nd$ ratio.

Table S11: Zircon spot O isotope data

File	Sample Number	$d^{18}O$_VSMOW	Error (2S)	Bias	$d^{18}O$_m	$d^{18}O$-2SE	^{16}O(E9 cps)	IP(nA)
20121203@1.asc	WI-STD-12 KIM-5 Center g1				5.803	0.272	2.487	1.630
20121203@2.asc	WI-STD-12 KIM-5 Center g2				5.649	0.232	2.515	1.649
20121203@3.asc	WI-STD-12 KIM-5 Center g3				5.892	0.239	2.544	1.657
20121203@4.asc	WI-STD-12 KIM-5 Center g4				5.826	0.275	2.553	1.671
					5.793	**0.206**		
20121203@5.asc	WI-STD-12 KIM-5 North g1				5.961	0.265	2.526	1.686
20121203@6.asc	WI-STD-12 KIM-5 North g2				5.765	0.272	2.539	1.691
20121203@7.asc	WI-STD-12 KIM-5 North g3				5.779	0.223	2.515	1.690
20121203@8.asc	WI-STD-12 KIM-5 North g4				5.828	0.256	2.522	1.686
					5.833	**0.179**		
20121203@9.asc	WI-STD-12 KIM-5 East g1				5.903	0.258	2.550	1.663
20121203@10.asc	WI-STD-12 KIM-5 East g2				5.935	0.209	2.567	1.661
20121203@11.asc	WI-STD-12 KIM-5 East g3				5.941	0.187	2.561	1.671
20121203@12.asc	WI-STD-12 KIM-5 East g4				5.808	0.221	2.557	1.672
					5.897	**0.123**		
20121203@13.asc	WI-STD-12 KIM-5 Center				5.758	0.280	2.556	1.682
20121203@14.asc	WI-STD-12 KIM-5 Center				5.801	0.166	2.554	1.680
20121203@15.asc	WI-STD-12 KIM-5 Center				5.878	0.263	2.559	1.681
20121203@16.asc	WI-STD-12 KIM-5 Center				5.940	0.244	2.544	1.679
					5.844	**0.162**		
	bracket average and 2SD	**5.09**		**0.72**	**5.818**	**0.180**		
20121203@17.asc	WI-STD-12 KIM-5 South				6.067	0.197	2.539	1.678
20121203@18.asc	WI-STD-12 KIM-5 South				6.015	0.227	2.545	1.680
20121203@19.asc	WI-STD-12 KIM-5 South				6.062	0.234	2.542	1.685
20121203@20.asc	WI-STD-12 KIM-5 South				5.788	0.208	2.548	1.691
					5.983	**0.264**		
20121203@21.asc	WI-STD-12 KIM-5 West				5.791	0.258	2.556	1.696
20121203@22.asc	WI-STD-12 KIM-5 West				5.755	0.227	2.558	1.699
20121203@23.asc	WI-STD-12 KIM-5 West				6.086	0.220	2.571	1.701
20121203@24.asc	WI-STD-12 KIM-5 West				5.782	0.258	2.546	1.707
					5.854	**0.312**		
20121203@25.asc	WI-STD-12 KIM-5 Center				5.916	0.296	2.551	1.695
20121203@26.asc	WI-STD-12 KIM-5 Center				5.990	0.212	2.574	1.687
20121203@27.asc	WI-STD-12 KIM-5 Center				5.961	0.200	2.557	1.696
20121203@28.asc	WI-STD-12 KIM-5 Center				5.960	0.178	2.559	1.707
					5.957	**0.061**		
	bracket average and 2SD	**5.09**		**0.82**	**5.911**	**0.130**		
	all spot average and 2SD				**5.880**	**0.221**		
20121204@29.asc	WI-STD-12 KIM-5 Center				5.545	0.240	2.507	1.641
20121204@30.asc	WI-STD-12 KIM-5 Center				5.546	0.232	2.521	1.646
20121204@31.asc	WI-STD-12 KIM-5 Center				5.473	0.169	2.531	1.651
20121204@32.asc	WI-STD-12 KIM-5 Center				5.672	0.290	2.536	1.666
					5.559	**0.165**		
20121204@33.asc	UMD_037 KIM-5 A				5.811	0.265	2.553	1.639
20121204@34.asc	UMD_037 KIM-5 A				5.471	0.247	2.552	1.645
20121204@35.asc	UMD_037 KIM-5 A				5.637	0.264	2.551	1.650

20121204@36.asc	UMD_037 KIM-5 A				5.544	0.206	2.549	1.650
					5.616	**0.294**		
20121204@37.asc	511001_big_1_1	**6.57**	**0.29**		7.133	0.230	2.543	1.650
20121204@38.asc	511001_big_1_2	**6.75**	**0.29**		7.311	0.233	2.560	1.652
20121204@39.asc	511001_big_1_3	**6.61**	**0.29**		7.175	0.240	2.521	1.653
20121204@40.asc	511001_big_2_4	**6.27**	**0.29**		6.829	0.178	2.550	1.623
20121204@41.asc	511001_big_4_5	**7.10**	**0.29**		7.665	0.224	2.534	1.656
20121204@42.asc	511001_big_5_6	**6.92**	**0.29**		7.479	0.222	2.547	1.649
20121204@43.asc	511001_big_5_7	**6.70**	**0.29**		7.263	0.223	2.532	1.640
20121204@44.asc	511001_big_6_8	**6.98**	**0.29**		7.540	0.249	2.529	1.644
20121204@45.asc	511001_big_6_9	**6.86**	**0.29**		7.425	0.225	2.540	1.643
20121204@46.asc	511001_big_7_10	**7.02**	**0.29**		7.582	0.194	2.532	1.665
20121204@47.asc	511001_big_7_11	**7.05**	**0.29**		7.607	0.265	2.531	1.667
20121204@48.asc	UMD_037 KIM-5 A				5.853	0.269	2.555	1.653
20121204@49.asc	UMD_037 KIM-5 A				5.590	0.244	2.549	1.656
20121204@50.asc	UMD_037 KIM-5 A				5.528	0.272	2.551	1.656
20121204@51.asc	UMD_037 KIM-5 A				5.772	0.187	2.555	1.662
					5.686	**0.304**		
	bracket average and 2SD	**5.09**		**0.56**	**5.651**	**0.287**		
20121204@52.asc	511001_big_8_12	**6.52**	**0.28**		7.178	0.271	2.564	1.668
20121204@53.asc	511001_big_8_13	**6.21**	**0.28**		6.867	0.201	2.541	1.664
20121204@54.asc	511001_big_9_14	**6.67**	**0.28**		7.325	0.240	2.564	1.670
20121204@55.asc	511001_big_9_15	**6.68**	**0.28**		7.329	0.240	2.565	1.669
20121204@56.asc	511001_big_9_16	**6.73**	**0.28**		7.387	0.251	2.569	1.671
20121204@57.asc	511001_big_9_17	**6.42**	**0.28**		7.070	0.262	2.565	1.680
20121204@58.asc	511001_big_10_18	**6.78**	**0.28**		7.437	0.288	2.583	1.680
20121204@59.asc	511001_big_11_19	**6.75**	**0.28**		7.402	0.182	2.562	1.694
20121204@60.asc	511001_big_11_20	**6.58**	**0.28**		7.238	0.264	2.573	1.686
20121204@61.asc	511001_big_11_21	**6.86**	**0.28**		7.518	0.222	2.565	1.683
20121204@62.asc	511001_big_11_22	**6.60**	**0.28**		7.250	0.220	2.560	1.686
20121204@63.asc	511001_big_12_23	**6.53**	**0.28**		7.186	0.287	2.591	1.687
20121204@64.asc	511001_big_12_24	**6.65**	**0.28**		7.307	0.230	2.574	1.691
20121204@65.asc	511001_big_13_25	**6.34**	**0.28**		6.997	0.222	2.557	1.680
20121204@66.asc	511001_big_14_26	**6.80**	**0.28**		7.453	0.292	2.579	1.701
20121204@67.asc	511001_big_14_27	**6.76**	**0.28**		7.412	0.203	2.595	1.710
20121204@68.asc	UMD_037 KIM-5 A				5.708	0.317	2.595	1.682
20121204@69.asc	UMD_037 KIM-5 A				5.909	0.229	2.597	1.689
20121204@70.asc	UMD_037 KIM-5 A				5.695	0.210	2.596	1.688
20121204@71.asc	UMD_037 KIM-5 A				5.887	0.247	2.583	1.688
					5.800	**0.228**		
	bracket average and 2SD	**5.09**		**0.65**	**5.743**	**0.277**		
20121204@72.asc	511001_big_15_28	**6.65**	**0.22**		7.387	0.242	2.574	1.716
20121204@73.asc	511001_big_16_29	**8.16**	**0.22**		8.903	0.199	2.602	1.716
20121204@74.asc	511001_big_16_30	**6.91**	**0.22**		7.653	0.215	2.559	1.715
20121204@75.asc	511001_big_17_31	**7.81**	**0.22**		8.549	0.205	2.577	1.700
20121204@76.asc	511005_big_2_1	**7.68**	**0.22**		8.422	0.224	2.594	1.630
20121204@77.asc	511005_big_3_2	**7.63**	**0.22**		8.373	0.237	2.542	1.655
20121204@78.asc	511005_big_3_3	**7.82**	**0.22**		8.562	0.248	2.599	1.661
20121204@79.asc	511005_big_4_4	**9.69**	**0.22**		10.434	0.237	2.613	1.668
20121204@80.asc	511005_big_5_5	**8.32**	**0.22**		9.061	0.226	2.610	1.694
20121204@81.asc	511005_big_5_6	**8.16**	**0.22**		8.904	0.202	2.624	1.691
20121204@82.asc	511005_big_6_7	**9.04**	**0.22**		9.781	0.255	2.620	1.684
20121204@83.asc	511005_big_6_8	**7.90**	**0.22**		8.641	0.265	2.600	1.727
20121204@84.asc	511005_big_7_9	**7.66**	**0.22**		8.405	0.209	2.615	1.728
20121204@85.asc	511005_big_7_10	**8.22**	**0.22**		8.957	0.222	2.627	1.712

20121204@86.asc	511005_big_7_11	**8.26**	**0.22**		9.000	0.333	2.627	1.709
20121204@87.asc	511005_big_8_12	**8.27**	**0.22**		9.009	0.191	2.639	1.721
20121204@88.asc	511005_big_8_13	**8.23**	**0.22**		8.967	0.248	2.645	1.720
20121204@89.asc	UMD_037 KIM-5 A				5.916	0.200	2.640	1.728
20121204@90.asc	UMD_037 KIM-5 A				5.716	0.233	2.637	1.727
20121204@91.asc	UMD_037 KIM-5 A				5.829	0.289	2.638	1.730
20121204@92.asc	UMD_037 KIM-5 A				5.970	0.245	2.640	1.734
					5.858	**0.222**		
	bracket average and 2SD	**5.09**		**0.74**	**5.829**	**0.217**		
20121204@93.asc	511005_big_9_14	**7.55**	**0.28**		8.225	0.235	2.609	1.729
20121204@94.asc	511005_big_9_15	**7.56**	**0.28**		8.234	0.251	2.628	1.719
20121204@95.asc	511005_big_10_16	**7.52**	**0.28**		8.196	0.144	2.639	1.723
20121204@96.asc	511005_big_10_17	**7.24**	**0.28**		7.921	0.181	2.640	1.730
20121204@97.asc	511005_big_11_18	**7.70**	**0.28**		8.380	0.241	2.626	1.749
20121204@98.asc	511005_big_12_19	**7.65**	**0.28**		8.324	0.233	2.648	1.729
20121204@99.asc	511005_big_12_20	**7.57**	**0.28**		8.252	0.268	2.648	1.740
20121204@100.asc	511005_big_13_21	**7.43**	**0.28**		8.105	0.338	2.636	1.753
20121204@101.asc	511005_big_14_22	**6.80**	**0.28**		7.483	0.246	2.625	1.764
20121204@102.asc	511005_big_15_23	**7.63**	**0.28**		8.305	0.207	2.673	1.716
20121204@103.asc	511005_big_16_24	**7.51**	**0.28**		8.187	0.235	2.663	1.723
20121204@104.asc	511005_big_17_25	**7.65**	**0.28**		8.329	0.200	2.667	1.726
20121204@105.asc	511005_big_18_26	**7.71**	**0.28**		8.391	0.197	2.662	1.730
20121204@106.asc	511005_big_18_27	**7.80**	**0.28**		8.483	0.205	2.643	1.761
20121204@107.asc	511005_big_19_28	**7.91**	**0.28**		8.589	0.238	2.660	1.730
20121204@108.asc	511005_big_19_29	**6.57**	**0.28**		7.248	0.241	2.653	1.746
20121204@109.asc	UMD_037 KIM-5 A				5.699	0.203	2.671	1.744
20121204@110.asc	UMD_037 KIM-5 A				5.518	0.249	2.669	1.739
20121204@111.asc	UMD_037 KIM-5 A				5.728	0.236	2.661	1.740
20121204@112.asc	UMD_037 KIM-5 A				5.759	0.220	2.680	1.749
					5.676	**0.216**		
	bracket average and 2SD	**5.09**		**0.67**	**5.767**	**0.281**		
20121204@113.asc	511005_big_20_30	**6.93**	**0.22**		7.587	0.225	2.693	1.743
20121204@114.asc	511005_big_21_31	**7.89**	**0.22**		8.546	0.257	2.623	1.761
20121204@115.asc	511005_big_22_32	**7.47**	**0.22**		8.129	0.227	2.670	1.756
20121204@116.asc	511005_big_23_33	**7.98**	**0.22**		8.632	0.238	2.666	1.744
20121204@117.asc	511005_big_23_34	**8.02**	**0.22**		8.679	0.230	2.664	1.748
20121204@118.asc	511005_big_24_35	**7.49**	**0.22**		8.147	0.201	2.679	1.730
20121204@119.asc	511005_big_24_36	**7.47**	**0.22**		8.123	0.205	2.617	1.742
20121204@120.asc	511005_big_25_37	**8.73**	**0.22**		9.391	0.235	2.635	1.749
20121204@121.asc	UMD_037 KIM-5 A				5.768	0.216	2.688	1.750
20121204@122.asc	UMD_037 KIM-5 A				5.766	0.248	2.682	1.751
20121204@123.asc	UMD_037 KIM-5 A				5.861	0.310	2.680	1.751
20121204@124.asc	UMD_037 KIM-5 A				5.858	0.288	2.687	1.759
					5.813	**0.107**		
	bracket average and 2SD	**5.09**		**0.65**	**5.745**	**0.216**		
20121204@125.asc	UMD_039 KIM-5				5.694	0.232	2.646	1.790
20121204@126.asc	UMD_039 KIM-5				5.461	0.188	2.654	1.791
20121204@127.asc	UMD_039 KIM-5				5.590	0.227	2.657	1.796
20121204@128.asc	UMD_039 KIM-5				5.571	0.217	2.658	1.798
					5.579	**0.191**		
20121204@129.asc	512001_Hf_1_1	**7.21**	**0.22**		7.652	0.237	2.650	1.822
20121204@130.asc	512001_Hf_2_2	**8.43**	**0.22**		8.868	0.279	2.642	1.809
20121204@131.asc	512001_Hf_3_3	**8.54**	**0.22**		8.984	0.225	2.649	1.793

20121204@132.asc	512001_Hf_4_4	**8.29**	**0.22**		8.728	0.147	2.635	1.778
20121204@133.asc	512001_Hf_4_5	**9.17**	**0.22**		9.615	0.216	2.642	1.794
20121204@134.asc	512001_Hf_5_6	**8.34**	**0.22**		8.777	0.244	2.650	1.780
20121204@135.asc	512001_Hf_6_7	**8.69**	**0.22**		9.132	0.195	2.645	1.789
20121204@136.asc	512001_Hf_7_8	**8.85**	**0.22**		9.296	0.220	2.637	1.787
20121204@137.asc	512001_Hf_7_9	**8.17**	**0.22**		8.615	0.249	2.637	1.794
20121204@138.asc	512001_Hf_8_10	**8.27**	**0.22**		8.711	0.212	2.634	1.804
20121204@139.asc	512001_Hf_9_11	**7.81**	**0.22**		8.251	0.233	2.647	1.791
20121204@140.asc	512001_Hf_9_12	**8.64**	**0.22**		9.083	0.259	2.616	1.793
20121204@141.asc	512001_Hf_10_13	**8.55**	**0.22**		8.989	0.208	2.650	1.799
20121204@142.asc	512001_Hf_11_14	**9.12**	**0.22**		9.559	0.171	2.645	1.799
20121204@143.asc	512001_Hf_11_15	**9.46**	**0.22**		9.901	0.296	2.647	1.791
20121204@144.asc	UMD_039 KIM-5				5.587	0.286	2.676	1.805
20121204@145.asc	UMD_039 KIM-5				5.474	0.282	2.671	1.807
20121204@146.asc	UMD_039 KIM-5				5.323	0.275	2.680	1.809
20121204@147.asc	UMD_039 KIM-5				5.536	0.209	2.679	1.811
					5.480	**0.229**		
	bracket average and 2SD	**5.09**		**0.44**	**5.530**	**0.222**		
20121204@148.asc	512001_Hf_12_16	**8.82**	**0.21**		9.159	0.209	2.654	1.813
20121204@149.asc	512001_Hf_13_17	**8.21**	**0.21**		8.546	0.292	2.697	1.808
20121204@150.asc	512001_Hf_14_18	**5.57**	**0.21**		5.902	0.227	2.661	1.787
20121204@151.asc	512001_Hf_15_19	**9.39**	**0.21**		9.726	0.264	2.658	1.799
20121204@152.asc	512001_Hf_16_20	**9.32**	**0.21**		9.657	0.154	2.670	1.799
20121204@153.asc	512001_Hf_17_21	**9.29**	**0.21**		9.626	0.187	2.667	1.817
20121204@154.asc	512001_Hf_17_22	**9.33**	**0.21**		9.664	0.254	2.692	1.820
20121204@155.asc	512001_Hf_18_23	**9.33**	**0.21**		9.667	0.164	2.656	1.819
20121204@156.asc	512001_Hf_19_24	**8.68**	**0.21**		9.013	0.257	2.669	1.811
20121204@157.asc	512001_Hf_20_25	**7.86**	**0.21**		8.194	0.167	2.679	1.813
20121204@158.asc	512001_Hf_20_26	**9.10**	**0.21**		9.437	0.239	2.688	1.801
20121204@159.asc	512001_Hf_20_27	**8.85**	**0.21**		9.185	0.235	2.626	1.795
20121204@160.asc	512001_Hf_21_28	**8.59**	**0.21**		8.925	0.229	2.671	1.807
20121204@161.asc	512001_Hf_21_29	**9.48**	**0.21**		9.814	0.146	2.687	1.806
20121204@162.asc	512001_Hf_22_30	**9.27**	**0.21**		9.611	0.225	2.649	1.819
20121204@163.asc	512001_Hf_23_31	**8.96**	**0.21**		9.297	0.246	2.669	1.833
20121204@164.asc	UMD_039 KIM-5				5.430	0.255	2.703	1.823
20121204@165.asc	UMD_039 KIM-5				5.429	0.251	2.692	1.822
20121204@166.asc	UMD_039 KIM-5				5.296	0.228	2.699	1.824
20121204@167.asc	UMD_039 KIM-5				5.329	0.241	2.697	1.824
					5.371	**0.138**		
	bracket average and 2SD	**5.09**		**0.33**	**5.426**	**0.210**		
20121204@168.asc	512001_Hf_18b	**5.31**	**0.21**		5.635	0.235	2.690	1.806
20121204@169.asc	512001_Hf_18c	**7.52**	**0.21**		7.843	0.237	2.686	1.815
20121204@170.asc	512001_Hf_18d	**9.27**	**0.21**		9.597	0.253	2.695	1.821
20121204@171.asc	512001_Hf_18e	**5.12**	**0.21**		5.447	0.253	2.666	1.813
20121204@172.asc	512001_Hf_18f	**9.24**	**0.21**		9.569	0.150	2.685	1.823
20121204@173.asc	512001_Hf_23_32	**8.16**	**0.21**		8.491	0.192	2.677	1.847
20121204@174.asc	512001_Hf_24_33	**8.59**	**0.21**		8.913	0.184	2.702	1.830
20121204@175.asc	512001_Hf_24_34	**8.90**	**0.21**		9.226	0.204	2.675	1.839
20121204@176.asc	UMD_039 KIM-5				5.282	0.191	2.720	1.843
20121204@177.asc	UMD_039 KIM-5				5.501	0.185	2.723	1.847
20121204@178.asc	UMD_039 KIM-5				5.553	0.271	2.726	1.848
20121204@179.asc	UMD_039 KIM-5				5.504	0.252	2.732	1.850
					5.460	**0.242**		
	bracket average and 2SD	**5.09**		**0.32**	**5.416**	**0.206**		

20121205@180.asc	WI-STD-12 KIM-5 Center				6.010	0.200	2.697	1.748
20121205@181.asc	WI-STD-12 KIM-5 Center				6.118	0.291	2.702	1.747
20121205@182.asc	WI-STD-12 KIM-5 Center				5.933	0.244	2.704	1.746
20121205@183.asc	WI-STD-12 KIM-5 Center				6.177	0.223	2.685	1.749
20121205@184.asc	UMD_38 KIM-5 A				6.071	0.326	2.677	1.759
20121205@185.asc	UMD_38 KIM-5 A				6.145	0.229	2.659	1.760
20121205@186.asc	UMD_38 KIM-5 A				6.011	0.222	2.662	1.760
20121205@187.asc	UMD_38 KIM-5 A				6.139	0.214	2.651	1.759
					6.092	**0.127**		
20121205@188.asc	mont1_flu_1_1	**8.04**	**0.26**		9.005	0.238	2.618	1.723
20121205@189.asc	mont1_flu_2_2	**7.60**	**0.26**		8.572	0.216	2.625	1.723
20121205@190.asc	mont1_flu_3_3	**7.69**	**0.26**		8.658	0.240	2.553	1.742
20121205@191.asc	mont1_flu_4_4	**8.28**	**0.26**		9.250	0.221	2.589	1.745
20121205@192.asc	mont1_flu_4_5	**8.24**	**0.26**		9.212	0.210	2.610	1.753
20121205@193.asc	mont1_flu_4_6	**7.95**	**0.26**		8.923	0.238	2.579	1.751
20121205@194.asc	mont1_flu_4_7	**8.40**	**0.26**		9.368	0.267	2.581	1.764
20121205@195.asc	mont1_flu_5_8	**8.20**	**0.26**		9.172	0.218	2.562	1.745
20121205@196.asc	mont1_flu_6_9	**8.00**	**0.26**		8.971	0.227	2.562	1.749
20121205@197.asc	mont1_flu_7_10	**8.31**	**0.26**		9.276	0.230	2.558	1.752
20121205@198.asc	mont1_flu_8_11	**8.31**	**0.26**		9.275	0.238	2.571	1.740
20121205@199.asc	mont1_flu_8_13	**8.28**	**0.26**		9.249	0.154	2.577	1.727
20121205@200.asc	mont1_flu_9_14	**8.28**	**0.26**		9.245	0.257	2.578	1.727
20121205@201.asc	mont1_flu_10_15	**7.78**	**0.26**		8.753	0.290	2.574	1.733
20121205@202.asc	mont1_flu_10_16	**7.86**	**0.26**		8.833	0.174	2.531	1.733
20121205@203.asc	mont1_flu_10_17	**7.64**	**0.26**		8.613	0.229	2.548	1.733
20121205@204.asc	mont1_flu_11_18	**8.26**	**0.26**		9.232	0.238	2.551	1.723
20121205@205.asc	umd_038 KIM-5A				6.251	0.281	2.590	1.726
20121205@206.asc	umd_038 KIM-5A				5.907	0.252	2.598	1.728
20121205@207.asc	umd_038 KIM-5A				5.861	0.198	2.591	1.729
20121205@208.asc	umd_038 KIM-5A				6.068	0.215	2.586	1.728
					6.022	**0.353**		
	bracket average and 2SD	**5.09**		**0.96**	**6.057**	**0.257**		
~~20121205@209.asc~~	~~511004_1_1~~	~~**5.96**~~	~~**0.33**~~		~~6.965~~	~~0.770~~	~~2.474~~	~~1.761~~
20121205@210.asc	511004_1_2	**5.17**	**0.33**		6.168	0.254	2.531	1.739
20121205@211.asc	511004_3_3	**6.17**	**0.33**		7.172	0.228	2.527	1.753
20121205@212.asc	511004_3_4	**6.06**	**0.33**		7.064	0.216	2.529	1.713
20121205@213.asc	511004_3_5	**3.73**	**0.33**		4.733	0.240	2.491	1.725
20121205@214.asc	511004_4_6	**4.72**	**0.33**		5.724	0.263	2.564	1.746
20121205@215.asc	511004_4_7	**2.05**	**0.33**		3.045	0.167	2.538	1.714
20121205@216.asc	511004_5_8	**1.79**	**0.33**		2.793	0.238	2.529	1.728
20121205@217.asc	511004_6_9	**6.04**	**0.33**		7.046	0.208	2.554	1.736
20121205@218.asc	511004_6_10	**5.10**	**0.33**		6.104	0.265	2.529	1.717
20121205@219.asc	511004_7_11	**3.94**	**0.33**		4.944	0.239	2.508	1.750
20121205@220.asc	511004_7_12	**3.10**	**0.33**		4.099	0.259	2.559	1.727
20121205@221.asc	511004_8_13	**3.58**	**0.33**		4.578	0.197	2.530	1.723
20121205@222.asc	511004_8_14	**1.93**	**0.33**		2.927	0.234	2.506	1.723
20121205@223.asc	511004_9_15	**4.27**	**0.33**		5.270	0.217	2.533	1.747
20121205@224.asc	umd_038 KIM-5A				6.407	0.219	2.575	1.720
20121205@225.asc	umd_038 KIM-5A				6.075	0.213	2.579	1.723
20121205@226.asc	umd_038 KIM-5A				6.038	0.270	2.569	1.723
20121205@227.asc	umd_038 KIM-5A				6.072	0.144	2.576	1.726
20121205@228.asc	umd_038 KIM-5A				6.154	0.283	2.565	1.723
					6.149	**0.301**		
	bracket average and 2SD	**5.09**		**1.00**	**6.093**	**0.332**		
20121205@229.asc	511004_9_16	**2.16**	**0.26**		3.165	0.294	2.554	1.717

20121205@230.asc	511004_10_17	3.89	0.26		4.890	0.221	2.520	1.746
20121205@231.asc	511004_10_18	2.16	0.26		3.166	0.211	2.494	1.721
20121205@232.asc	511004_11_19	4.91	0.26		5.913	0.179	2.527	1.718
~~20121205@233.asc~~	~~511004_12_20~~	2.79	0.26		~~3.787~~	~~0.238~~	~~2.493~~	~~1.749~~
20121205@234.asc	511004_12_21	6.31	0.26		7.319	0.181	2.547	1.729
20121205@235.asc	511004_13_22	6.45	0.26		7.454	0.264	2.546	1.711
20121205@236.asc	511004_14_23	2.19	0.26		3.189	0.243	2.537	1.747
20121205@237.asc	511004_14_24	4.74	0.26		5.745	0.237	2.524	1.712
20121205@238.asc	511004_15_25	5.05	0.26		6.051	0.191	2.565	1.735
20121205@239.asc	511004_15_26	5.30	0.26		6.308	0.281	2.511	1.725
20121205@240.asc	511004_16_27	6.20	0.26		7.210	0.255	2.566	1.734
20121205@241.asc	511004_16_28	4.90	0.26		5.902	0.173	2.526	1.728
20121205@242.asc	511004_17_29	5.68	0.26		6.687	0.215	2.528	1.700
20121205@243.asc	511004_18_30	5.97	0.26		6.972	0.269	2.547	1.730
20121205@244.asc	umd_038 KIM-5A				6.234	0.226	2.581	1.725
20121205@245.asc	umd_038 KIM-5A				6.280	0.238	2.569	1.730
20121205@246.asc	umd_038 KIM-5A				5.859	0.204	2.571	1.722
20121205@247.asc	umd_038 KIM-5A				6.040	0.300	2.562	1.726
					6.103	0.386		
	bracket average and 2SD	5.09		1.00	6.094	0.262		
20121205@248.asc	511004_18_31	5.38	0.27		6.354	0.284	2.512	1.708
20121205@249.asc	511004_18_32	2.16	0.27		3.133	0.203	2.463	1.708
20121205@250.asc	511004_19_33	2.10	0.27		3.070	0.142	2.531	1.708
20121205@251.asc	511004_20_34	4.28	0.27		5.249	0.215	2.551	1.749
20121205@252.asc	511004_20_35	1.89	0.27		2.856	0.266	2.572	1.740
20121205@253.asc	511004_21_36	3.62	0.27		4.593	0.217	2.545	1.740
20121205@254.asc	511004_22_37	3.80	0.27		4.774	0.155	2.511	1.735
20121205@255.asc	511004_22_38	4.54	0.27		5.517	0.248	2.525	1.707
20121205@256.asc	511004_22_39	4.82	0.27		5.794	0.249	2.578	1.705
20121205@257.asc	511004_22_40	2.85	0.27		3.821	0.232	2.534	1.722
20121205@258.asc	511004_23_41	6.56	0.27		7.537	0.234	2.534	1.733
20121205@259.asc	511004_24_42	2.12	0.27		3.087	0.243	2.522	1.732
20121205@260.asc	511004_24_43	5.91	0.27		6.888	0.198	2.566	1.735
20121205@261.asc	511004_25_44	1.79	0.27		2.761	0.204	2.573	1.751
20121205@262.asc	511004_25_45	1.78	0.27		2.752	0.240	2.553	1.736
20121205@263.asc	UMD-038 KIM-5A				6.010	0.228	2.610	1.746
20121205@264.asc	UMD-038 KIM-5A				5.983	0.239	2.599	1.746
20121205@265.asc	UMD-038 KIM-5A				6.033	0.207	2.602	1.745
20121205@266.asc	UMD-038 KIM-5A				6.065	0.183	2.601	1.744
					6.023	0.070		
	bracket average and 2SD	5.09		0.97	6.063	0.271		
20121205@267.asc	511004_26_46	6.66	0.21		7.678	0.244	2.545	1.764
20121205@268.asc	511004_26_47	6.68	0.21		7.699	0.186	2.556	1.746
20121205@269.asc	511004_27_48	2.73	0.21		3.748	0.242	2.516	1.757
20121205@270.asc	511001_med_1_1	6.81	0.21		7.826	0.185	2.569	1.761
20121205@271.asc	511001_med_1_2	8.29	0.21		9.317	0.218	2.542	1.719
20121205@272.asc	511001_med_3_3	6.24	0.21		7.259	0.204	2.576	1.736
20121205@273.asc	511001_med_3_4	6.51	0.21		7.533	0.264	2.570	1.727
20121205@274.asc	511001_med_5_5	6.24	0.21		7.261	0.251	2.576	1.739
20121205@275.asc	511001_med_5_6	6.53	0.21		7.553	0.272	2.581	1.739
20121205@276.asc	511001_med_6_7	6.78	0.21		7.797	0.255	2.564	1.737
20121205@277.asc	511001_med_10_8	6.57	0.21		7.588	0.318	2.590	1.738
20121205@278.asc	511001_med_13_9	6.58	0.21		7.600	0.213	2.538	1.743
20121205@279.asc	511001_med_17_10	6.54	0.21		7.561	0.243	2.574	1.752

20121205@280.asc	umd_038 KIM-5A				6.124	0.252	2.608	1.748
20121205@281.asc	umd_038 KIM-5A				6.181	0.253	2.597	1.749
20121205@282.asc	umd_038 KIM-5A				6.207	0.306	2.585	1.754
20121205@283.asc	umd_038 KIM-5A				6.271	0.251	2.606	1.757
					6.196	**0.122**		
	bracket average and 2SD	**5.09**		**1.01**	**6.109**	**0.207**		
20121205@284.asc	511005_med_1_1	**7.28**	**0.14**		8.340	0.242	2.598	1.753
20121205@285.asc	511005_med_5_2	**8.23**	**0.14**		9.285	0.223	2.562	1.761
20121205@286.asc	511005_med_5_3	**8.15**	**0.14**		9.210	0.207	2.609	1.744
20121205@287.asc	511005_med_6_4	**7.86**	**0.14**		8.915	0.214	2.585	1.736
20121205@288.asc	511005_med_6_5	**7.82**	**0.14**		8.881	0.225	2.573	1.732
20121205@289.asc	511005_med_8_6	**7.30**	**0.14**		8.358	0.248	2.582	1.762
20121205@290.asc	511005_med_8_7	**7.19**	**0.14**		8.247	0.286	2.612	1.735
20121205@291.asc	511005_med_10_8	**7.89**	**0.14**		8.951	0.272	2.585	1.749
20121205@292.asc	511005_med_10_9	**8.80**	**0.14**		9.859	0.193	2.582	1.734
20121205@293.asc	511005_med_11_10	**6.40**	**0.14**		7.456	0.222	2.614	1.732
20121205@294.asc	511005_med_11_11	**7.61**	**0.14**		8.667	0.269	2.586	1.734
20121205@295.asc	umd_038 KIM5A				6.105	0.281	2.616	1.763
20121205@296.asc	umd_038 KIM5A				6.095	0.224	2.610	1.763
20121205@297.asc	umd_038 KIM5A				6.045	0.281	2.606	1.766
20121205@298.asc	umd_038 KIM5A				6.123	0.223	2.598	1.765
					6.092	**0.067**		
	bracket average and 2SD	**5.09**		**1.05**	**6.144**	**0.143**		

Yield(E9cps/nA)	date	time	X	Y	DTFA-X	DTFA-Y	Mass	L1-bkg	H1-bkg	$^{16}O^{1}H/^{16}O$	KIM-5 mean OH/O
1.526	12/3/12	14:20	1315	326	-2	-2	898658	-2511676	-48600	0.000456	
1.525	12/3/12	14:24	1358	1031	-3	0	898658	-2511676	-48600	0.000462	
1.535	12/3/12	14:28	1476	1453	-3	2	898658	-2511676	-48600	0.000429	
1.528	12/3/12	14:32	883	1384	-1	-2	898658	-2511676	-48600	0.000396	
1.498	12/3/12	14:36	260	6754	-3	33	898658	-2511676	-48600	0.000421	
1.502	12/3/12	14:39	489	6516	-5	28	898658	-2511676	-48600	0.000386	
1.488	12/3/12	14:43	193	7133	-1	45	898658	-2511676	-48600	0.000425	
1.496	12/3/12	14:47	-101	7062	-2	43	898658	-2511676	-48600	0.000423	
1.533	12/3/12	14:51	7026	453	-2	-7	898658	-2511676	-48600	0.000359	
1.546	12/3/12	14:55	7695	435	2	-10	898658	-2511676	-48600	0.000359	
1.532	12/3/12	14:58	7088	136	3	-6	898658	-2511676	-48600	0.000372	
1.529	12/3/12	15:02	6522	213	3	-8	898658	-2511676	-48600	0.000364	
1.519	12/3/12	15:06	236	387	-10	-2	898658	-2511676	-48600	0.000418	
1.521	12/3/12	15:10	263	762	-10	-2	898658	-2511676	-48600	0.000446	
1.523	12/3/12	15:15	210	1044	-11	-3	898658	-2511676	-48600	0.000448	
1.516	12/3/12	15:18	63	1383	-8	-2	898658	-2511676	-48600	0.000434	
1.513	12/3/12	15:26	480	-6285	0	-40	898658	-2511676	-48600	0.000355	
1.514	12/3/12	15:29	1058	-6245	0	-39	898658	-2511676	-48600	0.000359	
1.508	12/3/12	15:32	1402	-6206	-1	-38	898658	-2511676	-48600	0.000353	
1.507	12/3/12	15:35	1334	-5904	0	-33	898658	-2511676	-48600	0.000354	
1.507	12/3/12	16:02	-6056	-147	-16	0	898658	-2511676	-48600	0.000386	
1.506	12/3/12	16:05	-5558	154	-17	1	898658	-2511676	-48600	0.000372	
1.512	12/3/12	16:08	-6021	675	-14	-1	898658	-2511676	-48600	0.000367	
1.492	12/3/12	16:11	-5594	862	-16	-3	898658	-2511676	-48600	0.000513	
1.505	12/3/12	16:18	1350	987	-6	-1	898658	-2511676	-48600	0.000415	
1.526	12/3/12	16:21	1421	1397	-5	-2	898658	-2511676	-48600	0.000398	
1.508	12/3/12	16:24	1350	665	-5	-3	898658	-2511676	-48600	0.000398	
1.499	12/3/12	16:28	1803	632	-7	-3	898658	-2511676	-48600	0.000410	
1.528	12/4/12	8:45	1807	579	-1	-1	898652	-2511676	-48600	0.000378	
1.532	12/4/12	8:48	1299	388	1	-2	898652	-2511676	-48600	0.000370	
1.533	12/4/12	8:52	801	533	2	-1	898652	-2511676	-48600	0.000365	
1.522	12/4/12	8:56	889	796	3	-6	898652	-2511676	-48600	0.000375	
1.558	12/4/12	9:04	-1056	796	9	-22	898652	-2511676	-48600	0.001049	
1.552	12/4/12	9:08	-1056	766	9	-22	898652	-2511676	-48600	0.001057	
1.546	12/4/12	9:11	-1056	746	9	-22	898652	-2511676	-48600	0.001078	

1.545	12/4/12	9:15	-1056	726	9	-22	898652	-2511676	-48600	0.001104	
1.541	12/4/12	9:21	-2608	1923	14	-21	898652	-2511676	-48600	0.001261	
1.550	12/4/12	9:25	-2641	2121	14	-22	898652	-2511676	-48600	0.001252	
1.525	12/4/12	9:29	-2683	2179	14	-24	898652	-2511676	-48600	0.001165	
1.572	12/4/12	9:33	-2371	2067	12	-22	898652	-2511676	-48600	0.001308	
1.530	12/4/12	9:38	-1744	2328	6	-18	898652	-2511676	-48600	0.001286	
1.545	12/4/12	9:42	-1459	2212	3	-17	898652	-2511676	-48600	0.001332	
1.544	12/4/12	9:47	-1429	2345	2	-17	898652	-2511676	-48600	0.001492	
1.538	12/4/12	9:52	-1202	2125	3	-19	898652	-2511676	-48600	0.001317	
1.546	12/4/12	9:55	-1064	2275	0	-15	898652	-2511676	-48600	0.001336	
1.521	12/4/12	10:00	-219	2470	-6	-16	898652	-2511676	-48600	0.001306	
1.518	12/4/12	10:03	-182	2558	-6	-13	898652	-2511676	-48600	0.001406	
1.546	12/4/12	10:08	-1025	807	15	-23	898652	-2511676	-48600	0.001273	
1.539	12/4/12	10:12	-1025	787	15	-23	898652	-2511676	-48600	0.001259	
1.540	12/4/12	10:15	-1025	767	15	-24	898652	-2511676	-48600	0.001261	
1.537	12/4/12	10:18	-1025	747	17	-23	898652	-2511676	-48600	0.001260	
											0.001167
1.537	12/4/12	10:24	136	2154	4	-18	898652	-2511676	-48600	0.001492	
1.528	12/4/12	10:28	187	2543	3	-15	898652	-2511676	-48600	0.001464	
1.535	12/4/12	10:32	325	2335	3	-17	898652	-2511676	-48600	0.001387	
1.537	12/4/12	10:35	372	2387	3	-16	898652	-2511676	-48600	0.001377	
1.538	12/4/12	10:39	436	2449	2	-17	898652	-2511676	-48600	0.001420	
1.527	12/4/12	10:43	447	2509	1	-15	898652	-2511676	-48600	0.001476	
1.537	12/4/12	10:47	668	2332	1	-13	898652	-2511676	-48600	0.001476	
1.512	12/4/12	10:52	901	2401	-1	-18	898652	-2511676	-48600	0.001380	
1.526	12/4/12	10:57	941	2488	0	-14	898652	-2511676	-48600	0.001417	
1.524	12/4/12	11:00	940	2558	-1	-17	898652	-2511676	-48600	0.001414	
1.519	12/4/12	11:04	988	2698	-2	-17	898652	-2511676	-48600	0.001471	
1.535	12/4/12	11:08	1248	2555	-3	-16	898652	-2511676	-48600	0.001540	
1.522	12/4/12	11:13	1322	2743	-4	-14	898652	-2511676	-48600	0.001377	
1.522	12/4/12	11:17	1565	3059	-4	-15	898652	-2511676	-48600	0.001457	
1.516	12/4/12	11:22	1524	2566	-5	-17	898652	-2511676	-48600	0.001431	
1.517	12/4/12	11:25	1595	2579	-5	-15	898652	-2511676	-48600	0.001471	
1.543	12/4/12	11:30	-1025	727	14	-27	898652	-2511676	-48600	0.001294	
1.537	12/4/12	11:34	-1024	707	15	-24	898652	-2511676	-48600	0.001319	
1.537	12/4/12	11:37	-1023	688	14	-25	898652	-2511676	-48600	0.001322	
1.530	12/4/12	11:41	-1022	666	15	-25	898652	-2511676	-48600	0.001327	
											0.001289
1.500	12/4/12	11:46	1888	2652	-7	-15	898652	-2511676	-48600	0.001419	
1.516	12/4/12	11:50	2151	2500	-7	-15	898652	-2511676	-48600	0.001331	
1.492	12/4/12	11:55	2166	2614	-7	-17	898652	-2511676	-48600	0.001398	
1.515	12/4/12	11:59	2470	2325	-7	-13	898652	-2511676	-48600	0.001304	
1.591	12/4/12	12:07	-1539	-2429	1	-33	898652	-2511676	-48600	0.001344	
1.536	12/4/12	12:12	-1281	-2500	-2	-35	898652	-2511676	-48600	0.001271	
1.565	12/4/12	12:16	-1125	-2583	-4	-35	898652	-2511676	-48600	0.001258	
1.566	12/4/12	12:20	-778	-2627	-9	-35	898652	-2511676	-48600	0.001236	
1.540	12/4/12	12:25	-702	-2310	-10	-35	898652	-2511676	-48600	0.001284	
1.552	12/4/12	12:29	-601	-2518	-11	-36	898652	-2511676	-48600	0.001245	
1.556	12/4/12	12:34	-261	-2574	-13	-37	898652	-2511676	-48600	0.001240	
1.506	12/4/12	12:38	-427	-2292	-13	-37	898652	-2511676	-48600	0.001291	
1.513	12/4/12	12:42	-139	-2249	-17	-37	898652	-2511676	-48600	0.001316	
1.534	12/4/12	12:45	-57	-2537	-16	-40	898652	-2511676	-48600	0.001234	

1.537	12/4/12	12:50	0	-2413	-14	-35	898652	-2511676	-48600	0.001260	
1.533	12/4/12	12:54	147	-2359	-16	-34	898652	-2511676	-48600	0.001275	
1.538	12/4/12	12:58	148	-2509	-16	-37	898652	-2511676	-48600	0.001232	
1.528	12/4/12	13:02	-1020	636	4	-24	898652	-2511676	-48600	0.001297	
1.527	12/4/12	13:06	-1020	613	4	-26	898652	-2511676	-48600	0.001292	
1.525	12/4/12	13:10	-1022	586	5	-24	898652	-2511676	-48600	0.001298	
1.522	12/4/12	13:14	-1022	560	5	-26	898652	-2511676	-48600	0.001299	
											0.001306
1.509	12/4/12	13:19	335	-2266	-1	-40	898652	-2511676	-48600	0.001327	
1.529	12/4/12	13:24	439	-2386	-1	-37	898652	-2511676	-48600	0.001267	
1.531	12/4/12	13:29	724	-2332	-3	-38	898652	-2511676	-48600	0.001254	
1.526	12/4/12	13:34	748	-2254	-5	-35	898652	-2511676	-48600	0.001255	
1.501	12/4/12	13:39	984	-2158	-4	-39	898652	-2511676	-48600	0.001262	
1.531	12/4/12	13:43	1178	-2178	-4	-34	898652	-2511676	-48600	0.001345	
1.522	12/4/12	13:49	1264	-2248	-7	-36	898652	-2511676	-48600	0.001233	
1.503	12/4/12	13:53	1626	-2026	-12	-33	898652	-2511676	-48600	0.001275	
1.487	12/4/12	13:58	2063	-2068	-11	-37	898652	-2511676	-48600	0.001293	
1.558	12/4/12	14:04	-405	-3116	8	-37	898652	-2511676	-48600	0.001246	
1.545	12/4/12	14:08	-98	-2900	5	-37	898652	-2511676	-48600	0.001213	
1.545	12/4/12	14:12	131	-3086	4	-40	898652	-2511676	-48600	0.001247	
1.539	12/4/12	14:16	378	-2952	2	-37	898652	-2511676	-48600	0.001235	
1.501	12/4/12	14:20	276	-2816	1	-37	898652	-2511676	-48600	0.001241	
1.538	12/4/12	14:25	668	-2862	-2	-42	898652	-2511676	-48600	0.001212	
1.519	12/4/12	14:29	733	-2960	-1	-37	898652	-2511676	-48600	0.001214	
1.532	12/4/12	14:34	-1000	807	3	-22	898652	-2511676	-48600	0.001247	
1.535	12/4/12	14:38	-1001	790	3	-24	898652	-2511676	-48600	0.001244	
1.530	12/4/12	14:42	-999	770	3	-25	898652	-2511676	-48600	0.001239	
1.532	12/4/12	14:45	-996	748	3	-24	898652	-2511676	-48600	0.001215	
											0.001266
1.545	12/4/12	14:52	782	-2733	-3	-36	898652	-2511676	-48600	0.001643	
1.489	12/4/12	14:57	926	-2671	-5	-37	898652	-2511676	-48600	0.001235	
1.520	12/4/12	15:01	1285	-2605	-6	-36	898652	-2511676	-48600	0.001222	
1.529	12/4/12	15:05	1528	-2410	-8	-39	898652	-2511676	-48600	0.001223	
1.523	12/4/12	15:10	1598	-2539	-6	-34	898652	-2511676	-48600	0.001200	
1.549	12/4/12	15:14	919	-3196	0	-36	898652	-2511676	-48600	0.001199	
1.503	12/4/12	15:18	973	-3097	-2	-37	898652	-2511676	-48600	0.001317	
1.506	12/4/12	15:22	1220	-2994	-4	-38	898652	-2511676	-48600	0.001222	
1.536	12/4/12	15:27	-996	729	3	-25	898652	-2511676	-48600	0.001191	
1.532	12/4/12	15:31	-997	709	3	-26	898652	-2511676	-48600	0.001210	
1.531	12/4/12	15:35	-999	686	3	-26	898652	-2511676	-48600	0.001201	
1.528	12/4/12	15:38	-997	665	3	-24	898652	-2511676	-48600	0.001201	
											0.001218
1.478	12/4/12	15:50	173	-765	-20	-16	898652	-2511676	-48600	0.000979	
1.482	12/4/12	15:54	174	-788	-19	-16	898652	-2511676	-48600	0.000980	
1.479	12/4/12	15:58	174	-817	-19	-14	898652	-2511676	-48600	0.000985	
1.478	12/4/12	16:01	172	-844	-19	-16	898652	-2511676	-48600	0.000992	
1.455	12/4/12	16:07	-1579	-162	-18	-10	898652	-2511676	-48600	0.001274	
1.460	12/4/12	16:11	-1507	14	-16	-15	898652	-2511676	-48600	0.001800	
1.478	12/4/12	16:16	-1296	-19	-18	-13	898652	-2511676	-48600	0.001148	

1.482	12/4/12	16:21	-1164	-61	-17	-13	898652	-2511676	-48600	0.001096		
1.473	12/4/12	16:25	-1188	-8	-17	-13	898652	-2511676	-48600	0.001127		
1.488	12/4/12	16:29	-1093	-98	-17	-13	898652	-2511676	-48600	0.001235		
1.479	12/4/12	16:33	-961	-61	-18	-16	898652	-2511676	-48600	0.001083		
1.475	12/4/12	16:38	-849	-63	-19	-16	898652	-2511676	-48600	0.001109		
1.470	12/4/12	16:43	-838	-10	-20	-14	898652	-2511676	-48600	0.001204		
1.460	12/4/12	16:47	-716	-81	-19	-13	898652	-2511676	-48600	0.001236		
1.478	12/4/12	16:51	-585	34	-20	-14	898652	-2511676	-48600	0.001202		
1.459	12/4/12	16:56	-589	66	-20	-17	898652	-2511676	-48600	0.001124		
1.473	12/4/12	17:01	-512	-44	-19	-14	898652	-2511676	-48600	0.001134		
1.471	12/4/12	17:05	-431	-91	-20	-15	898652	-2511676	-48600	0.001385		
1.478	12/4/12	17:09	-435	-47	-20	-12	898652	-2511676	-48600	0.001117		
1.483	12/4/12	17:13	199	-764	-22	-13	898652	-2511676	-48600	0.001102		
1.478	12/4/12	17:17	199	-784	-22	-16	898652	-2511676	-48600	0.001101		
1.482	12/4/12	17:20	198	-808	-22	-14	898652	-2511676	-48600	0.001096		
1.480	12/4/12	17:24	196	-828	-22	-15	898652	-2511676	-48600	0.001103		
											0.001042	
1.464	12/4/12	17:28	-284	-61	-21	-13	898652	-2511676	-48600	0.001620		
1.492	12/4/12	17:34	29	-89	-21	-14	898652	-2511676	-48600	0.001143		
1.489	12/4/12	17:38	94	-51	-20	-11	898652	-2511676	-48600	0.001288		
1.477	12/4/12	17:43	196	-3	-21	-10	898652	-2511676	-48600	0.001156		
1.484	12/4/12	17:47	292	-80	-22	-11	898652	-2511676	-48600	0.001134		
1.468	12/4/12	17:51	419	65	-24	-10	898652	-2511676	-48600	0.001175		
1.479	12/4/12	17:55	427	-88	-22	-10	898652	-2511676	-48600	0.001114		
1.461	12/4/12	18:00	463	8	-22	-10	898652	-2511676	-48600	0.001158		
1.474	12/4/12	18:05	690	166	-22	-11	898652	-2511676	-48600	0.001451		
1.478	12/4/12	18:08	778	232	-24	-12	898652	-2511676	-48600	0.001202		
1.492	12/4/12	18:12	787	180	-23	-14	898652	-2511676	-48600	0.001143		
1.463	12/4/12	18:16	789	151	-22	-11	898652	-2511676	-48600	0.001230		
1.478	12/4/12	18:20	874	188	-22	-9	898652	-2511676	-48600	0.001421		
1.488	12/4/12	18:24	893	125	-22	-11	898652	-2511676	-48600	0.001141		
1.456	12/4/12	18:27	1004	199	-24	-15	898652	-2511676	-48600	0.001175		
1.456	12/4/12	18:31	1104	288	-22	-17	898652	-2511676	-48600	0.001447		
1.483	12/4/12	18:36	217	-750	-23	-12	898652	-2511676	-48600	0.001128		
1.478	12/4/12	18:39	221	-766	-23	-13	898652	-2511676	-48600	0.001104		
1.480	12/4/12	18:43	220	-788	-24	-13	898652	-2511676	-48600	0.001101		
1.479	12/4/12	18:46	219	-807	-23	-14	898652	-2511676	-48600	0.001107		
											0.001105	
1.490	12/4/12	18:54	133	-57	-22	-13	898652	-2511676	-48600	0.001351		
1.480	12/4/12	18:59	91	-24	-22	-11	898652	-2511676	-48600	0.001414		
1.480	12/4/12	19:04	108	16	-23	-13	898652	-2511676	-48600	0.001160		
1.470	12/4/12	19:08	111	-68	-22	-13	898652	-2511676	-48600	0.001322		
1.473	12/4/12	19:13	71	-64	-21	-10	898652	-2511676	-48600	0.001097		
1.450	12/4/12	19:18	1125	365	-23	-12	898652	-2511676	-48600	0.001147		
1.476	12/4/12	19:24	1231	350	-23	-12	898652	-2511676	-48600	0.001285		
1.454	12/4/12	19:27	1231	403	-24	-13	898652	-2511676	-48600	0.001219		
1.476	12/4/12	19:32	245	-752	-24	-15	898652	-2511676	-48600	0.001098		
1.475	12/4/12	19:35	245	-784	-23	-12	898652	-2511676	-48600	0.001095		
1.475	12/4/12	19:39	248	-817	-24	-17	898652	-2511676	-48600	0.001093		
1.477	12/4/12	19:43	247	-845	-23	-13	898652	-2511676	-48600	0.001120		
											0.001106	

1.543	12/5/12	8:17	285	1023	2	-3	898652	-2529804	-49137	0.000299	
1.547	12/5/12	8:20	595	1102	3	-6	898652	-2529804	-49137	0.000274	
1.549	12/5/12	8:24	918	1479	2	0	898652	-2529804	-49137	0.000314	
1.535	12/5/12	8:27	1306	1416	0	-2	898652	-2529804	-49137	0.000275	
1.522	12/5/12	8:37	-148	948	-17	-17	898652	-2529804	-49137	0.000649	
1.511	12/5/12	8:41	-148	928	-16	-17	898652	-2529804	-49137	0.000679	
1.513	12/5/12	8:44	-148	908	-17	-18	898652	-2529804	-49137	0.000660	
1.506	12/5/12	8:47	-148	888	-17	-19	898652	-2529804	-49137	0.000690	
1.519	12/5/12	8:54	-1985	3025	-15	-19	898652	-2529804	-49137	0.000726	
1.524	12/5/12	8:59	-1993	2506	-15	-19	898652	-2529804	-49137	0.000752	
1.465	12/5/12	9:04	-1723	2521	-15	-20	898652	-2529804	-49137	0.000725	
1.484	12/5/12	9:10	-1404	2393	-16	-16	898652	-2529804	-49137	0.000878	
1.489	12/5/12	9:15	-1475	2494	-17	-16	898652	-2529804	-49137	0.000880	
1.473	12/5/12	9:20	-1462	2602	-17	-14	898652	-2529804	-49137	0.000900	
1.463	12/5/12	9:24	-1551	2594	-18	-18	898652	-2529804	-49137	0.000955	
1.468	12/5/12	9:29	-1256	2456	-19	-16	898652	-2529804	-49137	0.000762	
1.465	12/5/12	9:34	-1062	2441	-18	-16	898652	-2529804	-49137	0.000799	
1.460	12/5/12	9:39	-731	2436	-16	-15	898652	-2529804	-49137	0.000790	
1.478	12/5/12	9:44	-588	2576	-17	-16	898652	-2529804	-49137	0.000813	
1.492	12/5/12	9:49	-557	2486	-17	-11	898652	-2529804	-49137	0.000799	
1.493	12/5/12	9:53	-396	2564	-19	-16	898652	-2529804	-49137	0.000832	
1.486	12/5/12	9:57	-235	2595	-19	-16	898652	-2529804	-49137	0.001026	
1.460	12/5/12	10:01	-220	2554	-19	-17	898652	-2529804	-49137	0.000961	
1.471	12/5/12	10:06	-173	2494	-18	-15	898652	-2529804	-49137	0.000892	
1.481	12/5/12	10:10	-70	2556	-19	-16	898652	-2529804	-49137	0.000836	
1.501	12/5/12	10:15	-108	951	-19	-19	898652	-2529804	-49137	0.000860	
1.504	12/5/12	10:19	-108	928	-20	-19	898652	-2529804	-49137	0.000873	
1.499	12/5/12	10:23	-110	906	-20	-19	898652	-2529804	-49137	0.000848	
1.496	12/5/12	10:26	-116	883	-19	-19	898652	-2529804	-49137	0.000869	
											0.000766
~~1.405~~	~~12/5/12~~	~~10:33~~	~~809~~	~~2107~~	~~-21~~	~~-18~~	~~898652~~	~~-2529804~~	~~-49137~~	~~0.001033~~	
1.455	12/5/12	10:38	884	2159	-19	-16	898652	-2529804	-49137	0.001040	
1.441	12/5/12	10:42	841	1827	-22	-19	898652	-2529804	-49137	0.000884	
1.477	12/5/12	10:47	1058	1857	-23	-15	898652	-2529804	-49137	0.001069	
1.444	12/5/12	10:51	1103	1871	-22	-15	898652	-2529804	-49137	0.000996	
1.469	12/5/12	10:56	926	1646	-22	-18	898652	-2529804	-49137	0.001053	
1.481	12/5/12	11:00	1064	1673	-24	-18	898652	-2529804	-49137	0.001189	
1.463	12/5/12	11:05	1083	1590	-24	-20	898652	-2529804	-49137	0.000934	
1.471	12/5/12	11:10	993	1380	-22	-17	898652	-2529804	-49137	0.001009	
1.472	12/5/12	11:14	1065	1395	-23	-17	898652	-2529804	-49137	0.001061	
1.433	12/5/12	11:20	935	1222	-22	-21	898652	-2529804	-49137	0.000968	
1.482	12/5/12	11:24	1074	1229	-23	-20	898652	-2529804	-49137	0.001210	
1.468	12/5/12	11:30	1058	1109	-24	-19	898652	-2529804	-49137	0.001285	
1.455	12/5/12	11:34	1136	1122	-24	-19	898652	-2529804	-49137	0.001079	
1.450	12/5/12	11:39	910	978	-22	-22	898652	-2529804	-49137	0.001206	
1.497	12/5/12	11:45	-22	984	-20	-18	898652	-2529804	-49137	0.000922	
1.496	12/5/12	11:48	-82	924	-20	-19	898652	-2529804	-49137	0.000887	
1.491	12/5/12	11:52	-82	904	-20	-21	898652	-2529804	-49137	0.000894	
1.493	12/5/12	11:55	-82	884	-20	-20	898652	-2529804	-49137	0.000912	
1.488	12/5/12	11:59	-82	864	-20	-21	898652	-2529804	-49137	0.000935	
											0.000889
1.488	12/5/12	12:04	1050	996	-23	-18	898652	-2529804	-49137	0.000922	

1.443	12/5/12	12:09	934	784	-21	-23	898652	-2529804	-49137	0.001085		
1.449	12/5/12	12:14	1023	839	-23	-18	898652	-2529804	-49137	0.000921		
1.471	12/5/12	12:20	1132	748	-23	-18	898652	-2529804	-49137	0.001045		
~~1.425~~	~~12/5/12~~	~~12:26~~	~~934~~	~~582~~	~~-21~~	~~-19~~	~~898652~~	~~-2529804~~	~~-49137~~	~~0.002371~~		
1.473	12/5/12	12:30	1032	571	-21	-21	898652	-2529804	-49137	0.000940		
1.488	12/5/12	12:36	1155	505	-23	-18	898652	-2529804	-49137	0.001039		
1.452	12/5/12	12:41	985	310	-21	-23	898652	-2529804	-49137	0.001067		
1.475	12/5/12	12:45	1205	354	-23	-22	898652	-2529804	-49137	0.001043		
1.478	12/5/12	12:49	975	119	-21	-22	898652	-2529804	-49137	0.001052		
1.455	12/5/12	12:54	1318	183	-22	-23	898652	-2529804	-49137	0.001011		
1.480	12/5/12	13:00	995	-49	-20	-24	898652	-2529804	-49137	0.000981		
1.462	12/5/12	13:04	1006	9	-21	-21	898652	-2529804	-49137	0.001140		
1.487	12/5/12	13:10	1165	-138	-21	-19	898652	-2529804	-49137	0.001052		
1.473	12/5/12	13:15	1047	-322	-21	-21	898652	-2529804	-49137	0.000907		
1.496	12/5/12	13:20	7	983	-21	-21	898652	-2529804	-49137	0.000925		
1.485	12/5/12	13:23	7	963	-20	-19	898652	-2529804	-49137	0.000960		
1.493	12/5/12	13:27	38	982	-22	-19	898652	-2529804	-49137	0.000941		
1.485	12/5/12	13:31	6	939	-22	-19	898652	-2529804	-49137	0.000925		
												0.000922
1.471	12/5/12	13:39	1235	-285	-22	-21	898652	-2529804	-49137	0.001030		
1.442	12/5/12	13:44	1258	-294	-22	-21	898652	-2529804	-49137	0.000907		
1.482	12/5/12	13:48	1140	-490	-22	-24	898652	-2529804	-49137	0.001195		
1.458	12/5/12	13:52	951	-591	-20	-22	898652	-2529804	-49137	0.001142		
1.478	12/5/12	13:56	1013	-579	-20	-22	898652	-2529804	-49137	0.001183		
1.463	12/5/12	14:00	947	-734	-19	-26	898652	-2529804	-49137	0.001090		
1.447	12/5/12	14:06	1242	2129	-21	-20	898652	-2529804	-49137	0.000939		
1.479	12/5/12	14:11	1345	2129	-22	-19	898652	-2529804	-49137	0.000945		
1.512	12/5/12	14:17	1444	2118	-24	-18	898652	-2529804	-49137	0.000900		
1.472	12/5/12	14:21	1475	2192	-24	-19	898652	-2529804	-49137	0.001198		
1.462	12/5/12	14:25	1431	1945	-22	-21	898652	-2529804	-49137	0.001106		
1.456	12/5/12	14:29	1518	1773	-22	-19	898652	-2529804	-49137	0.001173		
1.479	12/5/12	14:33	1524	1731	-24	-19	898652	-2529804	-49137	0.000992		
1.470	12/5/12	14:39	1430	1620	-24	-22	898652	-2529804	-49137	0.001311		
1.471	12/5/12	14:43	1534	1635	-25	-20	898652	-2529804	-49137	0.001208		
1.495	12/5/12	14:48	-177	954	-21	-18	898652	-2529804	-49137	0.000915		
1.488	12/5/12	14:52	-176	926	-20	-19	898652	-2529804	-49137	0.000918		
1.491	12/5/12	14:56	-176	897	-22	-21	898652	-2529804	-49137	0.000893		
1.491	12/5/12	14:59	-174	873	-22	-23	898652	-2529804	-49137	0.000927		
												0.000926
1.443	12/5/12	15:05	1434	1483	-23	-23	898652	-2529804	-49137	0.001130		
1.464	12/5/12	15:11	1505	1516	-23	-17	898652	-2529804	-49137	0.001096		
1.432	12/5/12	15:16	1514	1291	-23	-19	898652	-2529804	-49137	0.000962		
1.459	12/5/12	15:24	-1665	-1280	-12	-22	898652	-2529804	-49137	0.001000		
1.479	12/5/12	15:30	-1480	-1228	-13	-28	898652	-2529804	-49137	0.000877		
1.484	12/5/12	15:34	-1232	-979	-15	-25	898652	-2529804	-49137	0.001026		
1.488	12/5/12	15:38	-1149	-1174	-15	-28	898652	-2529804	-49137	0.000987		
1.481	12/5/12	15:43	-834	-974	-15	-25	898652	-2529804	-49137	0.000986		
1.484	12/5/12	15:47	-797	-1094	-15	-24	898652	-2529804	-49137	0.001048		
1.476	12/5/12	15:51	-714	-936	-16	-26	898652	-2529804	-49137	0.001080		
1.490	12/5/12	15:57	-147	-1111	-18	-29	898652	-2529804	-49137	0.001027		
1.456	12/5/12	16:03	280	-966	-21	-25	898652	-2529804	-49137	0.001005		
1.469	12/5/12	16:07	681	-1071	-19	-27	898652	-2529804	-49137	0.001061		

1.492	12/5/12	16:12	-268	794	-20	-19	898652	-2529804	-49137	0.000917	
1.485	12/5/12	16:16	-244	781	-19	-19	898652	-2529804	-49137	0.000919	
1.474	12/5/12	16:20	-220	768	-20	-18	898652	-2529804	-49137	0.000927	
1.483	12/5/12	16:23	-198	756	-20	-19	898652	-2529804	-49137	0.000928	
											0.000918
1.482	12/5/12	16:29	-2270	1776	-15	-17	898652	-2529804	-49137	0.000876	
1.455	12/5/12	16:34	-2448	1115	-10	-22	898652	-2529804	-49137	0.000868	
1.496	12/5/12	16:38	-2361	1180	-12	-20	898652	-2529804	-49137	0.000884	
1.489	12/5/12	16:43	-2332	1014	-12	-19	898652	-2529804	-49137	0.000884	
1.485	12/5/12	16:47	-2240	1000	-13	-20	898652	-2529804	-49137	0.000882	
1.465	12/5/12	16:52	-2467	580	-12	-22	898652	-2529804	-49137	0.000860	
1.505	12/5/12	16:56	-2355	608	-12	-22	898652	-2529804	-49137	0.000950	
1.478	12/5/12	17:02	-2320	175	-12	-22	898652	-2529804	-49137	0.000858	
1.490	12/5/12	17:06	-2246	188	-12	-21	898652	-2529804	-49137	0.000871	
1.509	12/5/12	17:11	-2252	-64	-12	-24	898652	-2529804	-49137	0.000890	
1.491	12/5/12	17:17	-2217	48	-13	-21	898652	-2529804	-49137	0.000881	
1.484	12/5/12	17:21	-182	750	-21	-20	898652	-2529804	-49137	0.000892	
1.481	12/5/12	17:25	-159	735	-21	-18	898652	-2529804	-49137	0.000916	
1.476	12/5/12	17:29	-136	720	-21	-24	898652	-2529804	-49137	0.000909	
1.472	12/5/12	17:33	-118	745	-21	-22	898652	-2529804	-49137	0.000912	
											0.000915

background-corrected OH/O	Comment

9.36E-05
8.48E-05
-2.05E-06
1.41E-04
1.19E-04
1.65E-04
3.25E-04
1.50E-04
1.69E-04
1.39E-04
2.39E-04

2.03E-04
1.75E-04
9.79E-05
8.83E-05
1.31E-04
1.87E-04
1.87E-04
9.11E-05
1.28E-04
1.25E-04
1.82E-04
2.51E-04
8.84E-05
1.68E-04
1.42E-04
1.82E-04

1.13E-04
2.45E-05
9.19E-05
-2.34E-06
3.75E-05
-3.53E-05
-4.76E-05
-7.03E-05
-2.23E-05
-6.13E-05
-6.61E-05
-1.52E-05
1.01E-05
-7.21E-05

-4.61E-05
-3.13E-05
-7.36E-05

6.13E-05
1.27E-06
-1.20E-05
-1.15E-05
-3.77E-06
7.91E-05
-3.29E-05
9.07E-06
2.75E-05
-1.98E-05
-5.25E-05
-1.92E-05
-3.05E-05
-2.48E-05
-5.41E-05
-5.21E-05

4.25E-04
1.65E-05
3.66E-06
5.08E-06
-1.76E-05
-1.86E-05
9.95E-05
4.26E-06

2.32E-04
7.58E-04
1.06E-04

5.39E-05
8.46E-05
1.93E-04
4.08E-05
6.74E-05
1.62E-04
1.94E-04
1.60E-04
8.15E-05
9.25E-05
3.43E-04
7.49E-05

5.15E-04
3.85E-05
1.83E-04
5.07E-05
2.93E-05
6.96E-05
9.23E-06
5.27E-05
3.46E-04
9.71E-05
3.75E-05
1.25E-04
3.16E-04
3.56E-05
7.03E-05
3.42E-04

2.45E-04
3.08E-04
5.41E-05
2.16E-04
-9.28E-06
4.12E-05
1.79E-04
1.13E-04

-4.00E-05
-1.40E-05
-4.13E-05
1.12E-04
1.14E-04
1.34E-04
1.89E-04
-3.69E-06
3.28E-05
2.41E-05
4.72E-05
3.34E-05
6.63E-05
2.60E-04
1.95E-04
1.26E-04
7.04E-05

~~1.44E-04~~ high standard error
1.51E-04
-4.71E-06
1.80E-04
1.07E-04
1.64E-04
3.00E-04
4.53E-05
1.20E-04
1.72E-04
7.89E-05
3.21E-04
3.96E-04
1.90E-04
3.17E-04

-2.42E-07

1.63E-04
-7.55E-07
1.23E-04
~~1.45E-03~~ high OH/O
1.80E-05
1.17E-04
1.45E-04
1.21E-04
1.30E-04
8.86E-05
5.92E-05
2.18E-04
1.30E-04
-1.54E-05

1.04E-04
-1.91E-05
2.69E-04
2.16E-04
2.57E-04
1.64E-04
1.26E-05
1.93E-05
-2.59E-05
2.72E-04
1.80E-04
2.47E-04
6.62E-05
3.85E-04
2.82E-04

2.12E-04
1.78E-04
4.38E-05
8.16E-05
-4.11E-05
1.08E-04
6.95E-05
6.77E-05
1.30E-04
1.62E-04
1.09E-04
8.74E-05
1.43E-04

-3.90E-05
-4.74E-05
-3.05E-05
-3.15E-05
-3.31E-05
-5.50E-05
3.46E-05
-5.71E-05
-4.37E-05
-2.50E-05
-3.41E-05

TABLE S12. RESULTS OF QUARTZ-ZIRCON O ISOTOPE THERMOMETRY

Sample number	**Unit name**	**Quartz $\delta^{18}O$ (‰)**	**Quartz $^{18}O/^{16}O$**	**Mean Zircon $\delta^{18}O$ (‰)**	**Mean Zircon $^{18}O/^{16}O$**	**T °C**
511005	State Farm Gneiss	8.96	2023	7.8	2021	1242
511004	Neoproterozoic granitoid	5.37	2016	6.1	2017	thermometer inoperable
511001	Neoproterozoic granitoid	9.96	2025	6.5	2018	604
512001	Sabot Amphibolite[a]	12.31	2030	5.3	2016	343

Oxygen isotopes were analyzed at the University of Wisconsin Madison.

[a]Zircon and quartz were extracted from a felsic layer within the Sabot Amphibolite.